

Performance Improvement of Automotive Suspension Systems using Inerters and an Adaptive Controller

by

Ankur Agrawal

A thesis
presented to the University of Waterloo
in fulfillment of the
thesis requirement for the degree of
Master of Applied Science
in
Mechanical Engineering

Waterloo, Ontario, Canada, 2013

© Ankur Agrawal 2013

I hereby declare that I am the sole author of this thesis. This is a true copy of the thesis, including any required final revisions, as accepted by my examiners.

I understand that my thesis may be made electronically available to the public.

Abstract

The possible benefits of employing inerters in automotive suspensions are explored for passenger comfort and handling. Different suspension strut designs in terms of the relative arrangement of springs, dampers and inerters have been considered and their performance compared with that of a conventional system. An alternate method of electrically realizing complex mechanical circuits by using a linear motor (or a rotary motor with an appropriate mechanism) and a shunt circuit is then proposed and evaluated for performance. However, the performance improvement is shown from simulations to be significant only for very stiff suspensions, unlike those in passenger vehicles. Hence, the concept is not taken up for prototyping.

Variable damping can be implemented in suspension systems in various ways, for example, using magneto-rheological (MR) fluids, proportional valves, or variable shunt resistance with a linear electromagnetic motor. Hence for a generic variable damping system, a control algorithm is developed which can provide more comfort and better handling simultaneously compared to a passive system. After establishing through simulations that the proposed adaptive control algorithm can demonstrate a performance better than some controllers in prior-art, it is implemented on an actual vehicle (Cadillac STS) which is equipped with MR dampers and several sensors. In order to maintain the controller economical so that it is practically viable, an estimator is developed for variables which require expensive sensors to measure. The characteristic of the MR damper installed in the vehicle is obtained through tests as a 3-dimensional map relating suspension speed, input current and damping force and then used as a look-up table in the controller. Experiments to compare the performance of different controllers are carried out on smooth and rough roads and over speed bumps.

Acknowledgements

I would like to express my sincere gratitude to my supervisor, Dr. Amir Khajepour, for providing me this opportunity and his ample support. He has not only guided me in the project, but also encouraged me at every step and shown confidence in my efforts.

I would also like to extend my thanks to my colleagues and friends at the Mechatronic Vehicle Systems Lab., who have helped me in obtaining data from the test vehicle. Even with several projects going on simultaneously at the lab. and constrained schedules, they always tried their best to make sure that my work did not suffer any delays.

I would like to thank my friends in Waterloo for making my stay memorable, enjoyable and a learning experience. My thesis would not have been possible without their support.

It would never be sufficient to thank my parents and my sister; they have always been there for me throughout my life, and it is their success that my life is about to be adorned with a master's degree.

Table of Contents

Author's Declaration	ii
Abstract	iii
Acknowledgements	iv
List of Tables	vii
List of Figures	viii
1 Introduction	1
2 Literature Review and Background	4
2.1 Semi-active suspension system	4
2.2 Active suspension system	5
2.3 Quarter-car model	8
2.3.1 Frequency response transfer functions	8
2.3.2 Inherent trade-offs	12
2.4 Inerter	13
2.4.1 Introduction to inerter	13
2.4.2 First use of Inerters in suspension systems	13
2.5 Quarter car model with a general admittance	15
2.6 Modeling road profiles	16
2.6.1 Frequency domain (ISO classification)	16
2.6.2 Time domain	18
2.7 Semi-active and adaptive control algorithms	20
2.7.1 Control algorithms in prior-art	20
3 Suspension Employing Inerters: Design, Optimization and Results	23
3.1 Defining cost functions - Performance evaluation of a suspension system	23
3.2 Passive mechanical suspension struts	27
3.2.1 Realizing a passive mechanical inerter	27
3.2.2 Suspension configurations used in optimization	28
3.2.3 Optimization results	31

3.3	Mechatronic suspension struts	38
3.3.1	Optimization results	41
4	Adaptive Semi-Active Suspension: Modeling, Control and Simulation	
	Results	46
4.1	Effect of varying driving conditions: sprung mass m_s and vehicle speed V .	46
4.2	Effect of varying damping d_p	50
4.3	Estimation	50
4.4	Adaptive semi-active suspension control	53
4.4.1	Calculation of weighting parameter α	54
4.5	Simulation results	57
5	Experimental Validation	64
5.1	Description of the experimental setup	64
5.2	Validation of the estimator	66
5.3	Modeling the characteristics of an MR damper	68
5.4	Implementation of controllers and comparison of results	71
6	Conclusions and Future Work	78
	References	81

List of Tables

2.1	Parameters for the quarter car model	10
2.2	Mechanical and electrical component analogy	14
2.3	Mechanical admittance of common components	15
2.4	Road roughness classification proposed by ISO	17
3.1	Constants defining properties of the quarter-car model used in optimization	29
3.2	Optimization results for $k_p=40\,000\text{ N/m}$	33
3.3	Parameters (constants) of the motor and screw used	41
4.1	Quarter-car parameters used in simulation of different controllers	58
5.1	Summary of test results comparing different controllers	77

List of Figures

1.1	Conflict between safety and ride comfort	2
2.1	Instrumental panel of a vehicle showing suspension control	4
2.2	Principle of operation of MR Damper from BWI	5
2.3	CDC [®] damper from ZF with proportional valve zoomed-in	6
2.4	Bose suspension front corner module and comparison of performance with a conventional system	6
2.5	Hydraulic active suspension systems.	7
2.6	Quarter car model for vehicle suspension.	9
2.7	Frequency response functions for a typical quarter car model	11
2.8	Quarter car model with a general admittance	15
2.9	Road roughness classification proposed by ISO.	17
2.10	Modeling different road profiles in time domain	18
2.10	Modeling different road profiles in time domain	19
2.11	Model of a road bump as a function of time (for $V=10$ m/s)	19
3.1	Frequency weighting filter for human comfort proposed by ISO.	24
3.2	Schematic of an inerter using Screw mechanism.	27
3.3	Suspension with a spring and a damper in parallel (Y_1)	30
3.4	Suspension with a spring, a damper and an inerter	31
3.5	Suspension with two springs, a damper and an inerter	32
3.6	Optimization of comfort for different mechanical suspension struts and static stiffness	35
3.7	Optimization of dynamic tire loads (handling) for different mechanical sus- pension struts and static stiffness	36
3.8	Variable values for optimal performance criteria for different mechanical suspension struts and static stiffness	37
3.9	Pareto-fronts from multi-objective optimization for $k_p=40\,000$ N/m	38
3.10	Schematic of a suspension strut using a ball screw mechanism and a rotary motor with shunt impedance $Z(s)$	40

3.11	Schematic of the motor with shunt impedance $Z(s)$	40
3.12	Shunt circuits	41
3.13	Optimization of comfort for different mechatronic suspension struts and static stiffness	43
3.14	Optimization of dynamic tire loads (handling) for different mechatronic suspension struts and static stiffness	44
3.15	Pareto-fronts from multi-objective optimization for $k_p=40\,000\text{ N/m}$	45
3.16	Pareto-fronts from multi-objective optimization for $k_p=100\,000\text{ N/m}$	45
4.1	Effect of varying sprung mass on comfort and handling as a function of damping in a quarter car model (The plots are overlapping for dynamic tire force)	47
4.2	Effect of varying vehicle speed on comfort and handling as a function of damping in a quarter car model	48
4.3	Effect of varying damping in a quarter car model	49
4.4	Quarter car model with a variable damping force	51
4.5	Estimator structure for various states of the system	52
4.6	An example of probability density of F_{tire} for stochastic road profile with bounds for F_{stat} and $6\sigma_{F_{tire}}$	55
4.7	Structure of the adaptation logic to obtain scheduling parameter	56
4.8	Heuristic function $h(u)$ for calculation of fast adaptation error e_f	56
4.9	Simulation results for a transition from type-A road to type-C road at 15 m/s	59
4.10	Simulation results for over a bump at speed 10 m/s	62
5.1	Structure of the experimental setup	65
5.2	SAE Coordinate system for vehicle dynamics	66
5.3	Measured and estimated vertical tire force	67
5.4	Suspension velocity and estimated damping force for a given current and harsh pitching maneuvers	69
5.5	Characteristics of the MR damper (obtained after a smooth curve-fit) showing damping force as a function of suspension velocity at different currents	70
5.6	Characteristics of the MR damper as a 3D map	70
5.7	Inverse mapping from MR damper characteristics	71
5.8	Experimental conditions	72
5.9	Test results for a transition from smooth to rough (gravel) road at 45 km/h	73
5.10	Test results for over a bump at speed 40 km/h	75
6.1	Seven degree of freedom full car model	80

Chapter 1

Introduction

The job of the suspension system in an automobile is dual: to provide a comfortable ride to the passengers by isolating them from the road irregularities, bumps and potholes, and to improve the road holding capacity of the vehicle thereby providing safety. The use of suspension systems in vehicles is not new. In fact, they have been in use since the cars were actually horse drawn carriages [3]. But still, active research has been prevalent for the development of new and better suspension systems. One major reason for this can be attributed to the fact that the two requirements of ride comfort and handling which the suspension is expected to fulfill are conflicting. Figure 1.1 shows this conflicting nature for different suspension parameters in terms of the RMS acceleration of the chassis (comfort) and RMS dynamic tire force (handling and safety) for some particular road and driving conditions. It can be seen that for better ride comfort (as in a Limousine), a softer suspension (low k and d) is required but it leads to higher tire forces, hence, less safety. On the other hand, for better handling (as in a sports car), a stiffer suspension (high k and d) is required but it makes the ride less comfortable. A conventional suspension with a passive spring and damper is represented by a fixed point on this conflict diagram. Numerous efforts have been made by researchers to design a suspension system which caters to a wide range of performance requirements with as less compromise as possible by changing its properties during run-time like active and semi-active suspensions to give near optimal performance. Such suspensions with variable properties have led to the design of several control algorithms like skyhook, groundhook, clipped optimal, etc. [23, 38, 37] which offer better results in different aspects of suspension performance. Suspensions have also been designed by using a completely different mechanical circuit employing springs, dampers and inerters [35]. Some progress has also been made in developing regenerative suspension systems [22, 26, 20] which harness a part of the vibrational energy which otherwise goes waste as heat in conventional systems.

The possible benefits of using inerters in automotive suspension systems and different

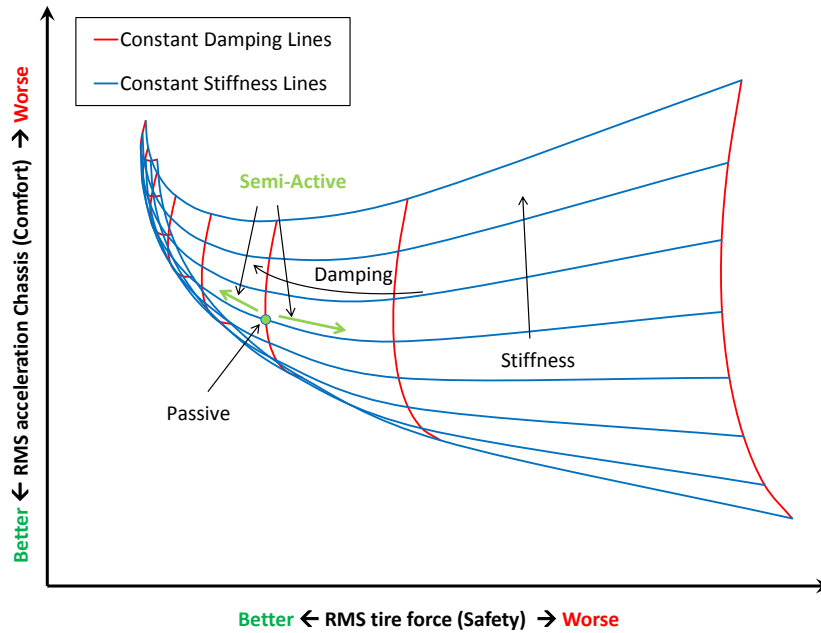


Figure 1.1: Conflict between safety and ride comfort (for some particular road and driving conditions).

methods to realize the mechanical circuit is still worth investigating. There are two elements of this thesis. The first element explores the idea of electrical realization of a complex mechanical circuit of inerters and dampers in the form of a mechatronic strut and evaluates its performance in terms of ride comfort and handling. Since one significant benefit of such a mechatronic strut is the potential for an adaptive suspension system, therefore, the second element of this thesis is the design of an adaptive controller for semi-active suspension systems. The controller is benchmarked against some well-accepted algorithms in prior-art, first through simulations and then by implementation on a fully instrumented Cadillac STS equipped with variable (MR) dampers.

The structure of this thesis is as follows: Chapter 2 is literature review and background. It reviews some of the commercially available suspension systems and then goes through the basic concepts of a quarter-car model and introduction to inerters in automotive suspensions. Then a method to model different road profiles (both frequency and time domain) is discussed. Finally, it goes over some popular control algorithms in literature for semi-active suspensions. Chapter 3 explores in detail the performance benefits and drawbacks of mechanical and electrical realization of inerters using a quarter-car model with a general admittance so as to consider complex, unconventional circuits. Chapter 4 deals with

the development of an adaptive semi-active control algorithm, which includes an estimator and a self-adjusting weighting parameter. Simulations are performed for smooth, rough, and bump profiles as road input and results are compared with skyhook and groundhook controller and passive suspension. Chapter 5 is validation of the simulation results by performing tests on an actual vehicle (Cadillac STS). Finally, a brief conclusion and scope of the future of this work is provided in Chapter 6.

Chapter 2

Literature Review and Background

This chapter will first review some commercially available suspension systems. Then, the basic theory behind a quarter-car model, inerters and semi-active control algorithms will be discussed.

2.1 Semi-active suspension system

A semi-active suspension system can change the damping characteristics during run-time but cannot provide a force input. It is represented on the conflict diagram in Figure 1.1 by a constant stiffness line. The level of damping can either be defined by the user through an instrumental panel like the one shown in Figure 2.1 or can be automatically controlled for that particular state of the vehicle by an on-board CPU that takes feedback from various sensors mounted on it.



Figure 2.1: Instrumental panel of a vehicle showing suspension control. Image reproduced from [6].

There are several ways through which the damping can be varied in a semi-active system. One popular product is MagneRideTM by BWI Group which uses Magneto-Rheological (MR) fluids [11]. An MR fluid has magnetically soft (easily, but temporarily

magnetized) iron particles suspended in a synthetic hydrocarbon base. Application of magnetic field by the electromagnetic coil contained in the piston causes the particles to align into fibrous structures thereby increasing the viscosity. Hence, varying the magnetic flux in effect controls the viscosity of the damper. The principle of operation is depicted in Figure 2.2.

Another method of varying the damping is by changing the orifice size, as is done in the CDC[®]-Continuous Damping Control by ZF [43]. The CDC has a proportional valve as shown in Figure 2.3, which offers soft damping when the opening for the oil flow is expanded and firm damping when it is restricted.

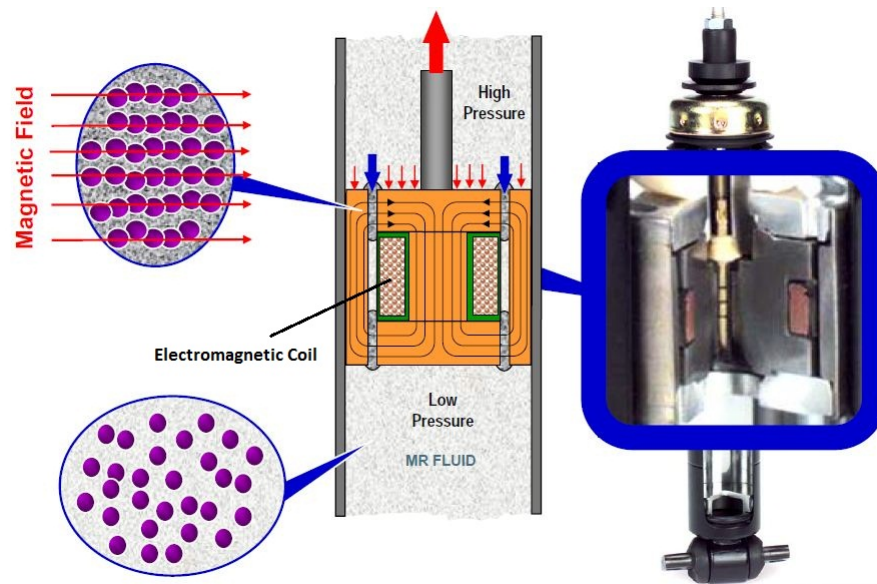


Figure 2.2: Principle of operation of MR Damper from BWI. Image reproduced from [11].

2.2 Active suspension system

Active suspension systems have been an area of immense research for more than two decades due to their far promising features. An active suspension system consists of an actuator (electric or hydraulic) which can inject as well as dissipate power. Coupled with an appropriate controller, such a system can provide a performance far better than a typical semi-active system both in terms of comfort and handling. One system developed by Bose Corporation [22] is quite famous as the company has been working on it since 1980. This system uses linear electromagnetic motors which replace the passive dampers and torsion bars to suspend the static load of the vehicle. A tuned mass damper attached to each wheel reduces the peak at the resonant frequency of the unsprung mass and keeps the

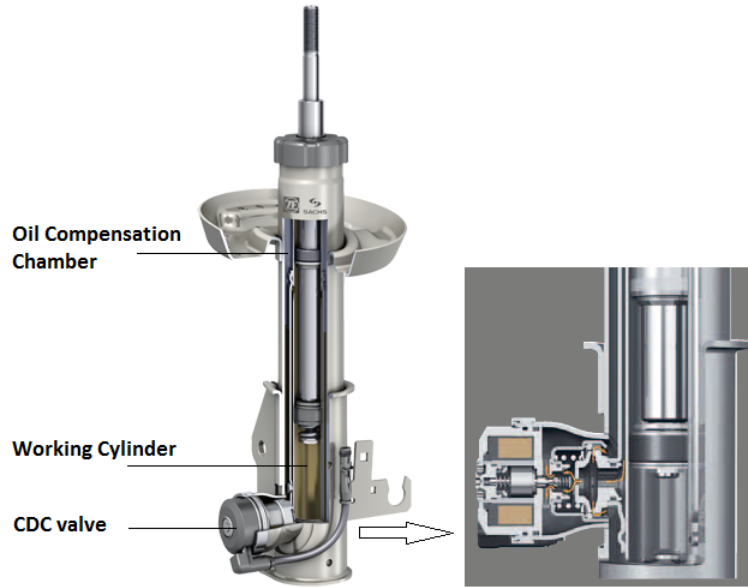


Figure 2.3: CDC[®] damper from ZF with proportional valve zoomed-in. Image reproduced from [43].

tire from bouncing and losing contact with the road. Since each corner of the vehicle can be independently controlled, the roll and pitch movements can be diminished to a great extent without using any anti-roll bars. Although the performance of this system is quite superior to that of a conventional suspension and Bose claims that the system can recover energy by driving the motors in generator mode and that it requires “less than a third of the power of a typical vehicle’s air conditioner system”, the system is yet to be integrated in a production vehicle, possibly due to high costs and power requirements.

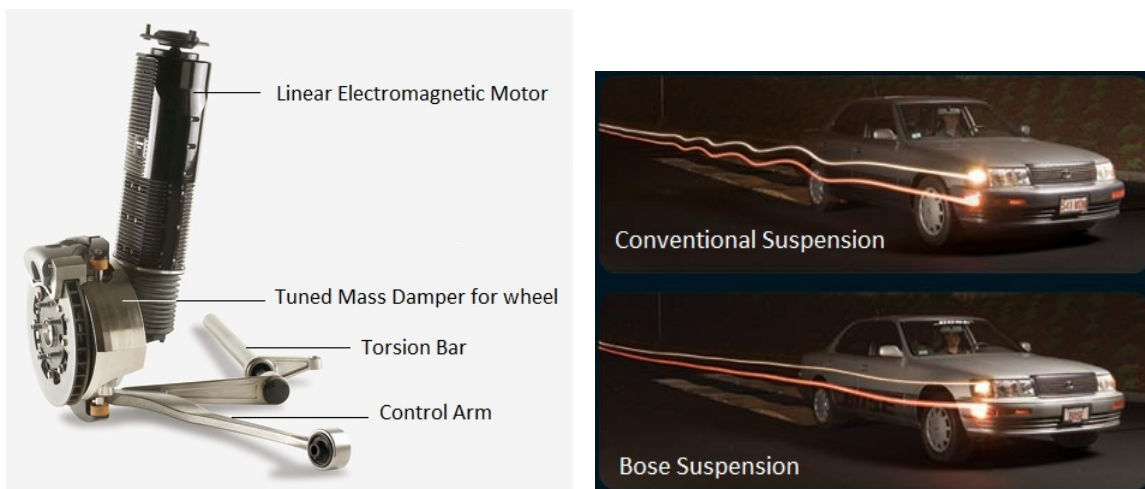


Figure 2.4: Bose suspension front corner module and comparison of performance with a conventional system. Image reproduced from [8].

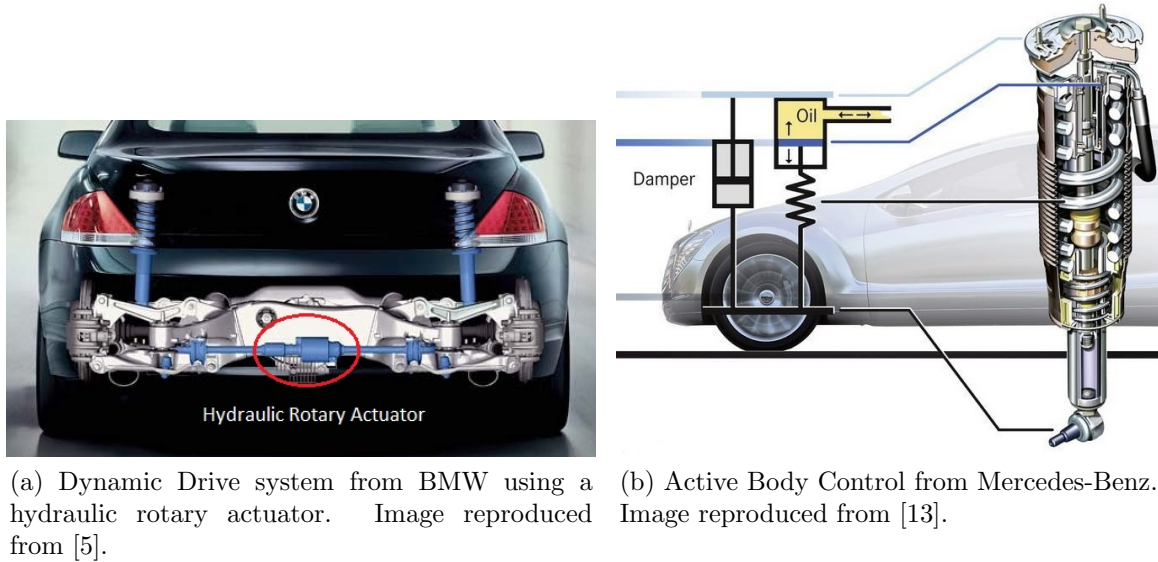


Figure 2.5: Hydraulic active suspension systems.

Most of the commercially available active suspensions as of now use hydraulic systems. For instance, the Dynamic Drive from BMW [36] is an active stabilizer bar system, which significantly reduces roll angle during cornering. The system consists of a hydraulic pump coupled to the power steering pump, a hydraulic valve block with integrated sensors and two active stabilizer bars with rotating hydraulic actuators, one of which is shown in Figure 2.5a. The control unit takes lateral acceleration and steering angle as the inputs. Mercedes-Benz has also developed a hydraulically actuated active suspension named as Active Body Control (ABC) [13]. The core of the technology is an active hydraulic cylinder mounted in series with the spring as depicted in Figure 2.5b, which can rapidly move in the vertical direction by getting energised by a high pressure hydraulic pump. As a result, ABC can change the length of each strut independently in a hundredth of a second, which generates a counter force to compensate for the forces acting on the car. The system also allows adjustment of the vehicle height for better aerodynamics and handling, as well as maintaining constant ride height in changing load conditions.

An active suspension based on a tubular permanent magnet actuator has been developed in [20]. The system is a strut for McPherson suspension system consisting of a direct drive brushless linear actuator in parallel with a passive spring and damper. Similar to the Bose suspension, their system can apply active forces by consuming power and regenerate power when acting as energy absorber. An LQR controller calculates the required amount of actuator force by either measuring or estimating the state of the system. A PWM current controlled three-phase amplifier with a dc bus voltage level of 340V ($\pm 170V$) drives the actuator. Clearly, the 12V battery of a typical passenger vehicle is not suitable for the

purpose; future hybrid and fully electric vehicles might have that level of voltage available.

To overcome the heavy weight and cost associated with a linear permanent magnet actuator, a damper and energy harvester has been developed in [26] that exploits the compact form factor and high energy density of an electromagnetic rotary motor. The system uses rack and pinion to convert the linear motion of the suspension into rotary motion of the motor with a speed reduction gearbox. An arrangement of bevel gears is used in between to transmit motion in the perpendicular direction so that the whole assembly can be made as a retrofittable shock absorber. However, due to the highly oscillatory motion of the suspension, and the backlash inherent in a geared system, the durability of such a system is worth investigating, especially at high speeds and rough roads.

2.3 Quarter-car model

The suspension system is responsible for mainly three degrees of freedom of a vehicle: heave (linear in vertical direction), pitch (rotational about lateral axis) and roll (rotational about longitudinal axis). Quarter-car is a simplified model focusing on one wheel and an equivalent sprung mass to study only the vertical dynamics of a vehicle assuming that all the four wheels are decoupled, as depicted in Figure 2.6. The sprung mass m_s is usually one-fourth of the vehicle's chassis mass, unsprung mass m_u includes the mass of the wheel and parts of suspension not resting on the spring, k_p is the passive stiffness in the suspension (which is usually from a coil spring), d_p is the passive damping in the suspension (which is usually from hydraulic or pneumatic damper) and k_t is the equivalent tire stiffness. The damping due to tire is usually small and hence neglected in most cases. z_s and z_u are the vertical displacements of the sprung mass and unsprung mass respectively from the equilibrium position. z_r represents the displacement due to road surface irregularities and it is assumed that the tire never leaves contact with the road.

2.3.1 Frequency response transfer functions

Assuming linear elements for the quarter car model, the equations of motion can be solved to obtain certain transfer functions relating the input (road displacement z_r) with variables of interest like sprung mass displacement z_s , tire deflection $z_u - z_r$ and suspension deflection $z_s - z_u$. The equation of motion of the sprung mass is given by

$$m_s \ddot{z}_s = -k_p(z_s - z_u) - d_p(\dot{z}_s - \dot{z}_u) \quad (2.1)$$

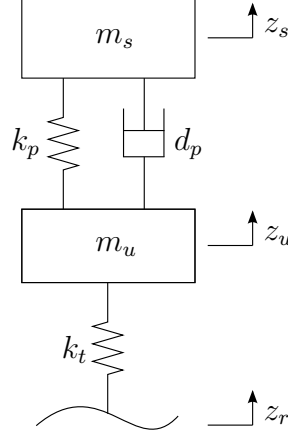


Figure 2.6: Quarter car model for vehicle suspension.

and that for the unsprung mass is given by

$$m_u \ddot{z}_u = k_p(z_s - z_u) + d_p(\dot{z}_s - \dot{z}_u) - k_t(z_u - z_r) \quad (2.2)$$

To obtain the frequency response, Laplace transformation is taken of the equations assuming zero initial conditions. If the Laplace transformed variables are \hat{z}_s , \hat{z}_u , \hat{z}_r , then Eq (2.1) and Eq (2.2) become

$$m_s s^2 \hat{z}_s = -k_p(\hat{z}_s - \hat{z}_u) - d_p s(\hat{z}_s - \hat{z}_u) \quad (2.3)$$

$$m_u s^2 \hat{z}_u = k_p(\hat{z}_s - \hat{z}_u) + d_p s(\hat{z}_s - \hat{z}_u) - k_t(\hat{z}_u - \hat{z}_r) \quad (2.4)$$

Transmissibility ratio \hat{z}_s/\hat{z}_r defines the vibration isolation property of the suspension as it is the response of the sprung mass (output) to the excitation from the road (input), and is given by

$$H_{sprung}(s) = \frac{\hat{z}_s}{\hat{z}_r} = \frac{k_t(d_p s + k_p)}{m_s m_u s^4 + d_p(m_s + m_u)s^3 + ((k_p + k_t)m_s + k_p m_u)s^2 + k_t d_p s + k_t k_p} \quad (2.5)$$

The dynamic tire deflection ratio $(\hat{z}_u - \hat{z}_r)/\hat{z}_r$ relates the road input to tire deflection, which is proportional to the dynamic tire force (assuming linear tire model) responsible for vehicle handling, and is given by

$$H_{tire}(s) = \frac{\hat{z}_u - \hat{z}_r}{\hat{z}_r} = \frac{-s^2(m_s m_u s^2 + d_p(m_s + m_u)s + k_p(m_s + m_u))}{m_s m_u s^4 + d_p(m_s + m_u)s^3 + ((k_p + k_t)m_s + k_p m_u)s^2 + k_t d_p s + k_t k_p} \quad (2.6)$$

The suspension travel ratio $(\hat{z}_s - \hat{z}_u)/\hat{z}_r$ defines the suspension deflection in response to the road excitation input, and is given by

$$H_{susp}(s) = \frac{\hat{z}_s - \hat{z}_u}{\hat{z}_r} = \frac{-m_s k_t s^2}{m_s m_u s^4 + d_p(m_s + m_u)s^3 + ((k_p + k_t)m_s + k_p m_u)s^2 + k_t d_p s + k_t k_p} \quad (2.7)$$

The frequency response plots for the above transfer functions can be plotted in the frequency range of interest (0-15 Hz) using the exemplary parameter values mentioned in Table 2.1. The three plots are shown in Figure 2.7.

Table 2.1: Parameters for the quarter car model

Parameter	Description	Value
m_s	Sprung mass	400 kg
m_u	Unsprung mass	40 kg
k_p	Spring stiffness	20 000 N/m
d_p	Damping	2000 Ns/m
k_t	Tire stiffness	180 000 N/m

Since the system has two degrees of freedom, it has two natural frequencies, which can be obtained by solving the undamped ($d_p = 0$) characteristic equation

$$m_s m_u s^4 + ((k_p + k_t)m_s + k_p m_u)s^2 + k_t k_p = 0 \quad (2.8)$$

Substituting Laplace variable s as $j\omega$,

$$m_s m_u \omega^4 - ((k_p + k_t)m_s + k_p m_u)\omega^2 + k_t k_p = 0 \quad (2.9)$$

However, in view of the fact that the sprung mass and the tire stiffness are an order of magnitude higher than the unsprung mass and spring stiffness respectively, the complicated solution to Eq (2.9) can be simplified as

$$f_{n,s} = \frac{1}{2\pi} \sqrt{\frac{k_p k_t}{(k_p + k_t)m_s}} \quad (2.10a)$$

$$f_{n,u} = \frac{1}{2\pi} \sqrt{\frac{(k_p + k_t)}{m_u}} \quad (2.10b)$$

Substituting numerical values, $f_{n,s} = 1.06$ Hz and $f_{n,u} = 11.25$ Hz. The peak due to resonance of the sprung mass is clearly visible in all the three plots between 0-2 Hz, but the peak at the natural frequency of the unsprung mass is prominent only in the dynamic

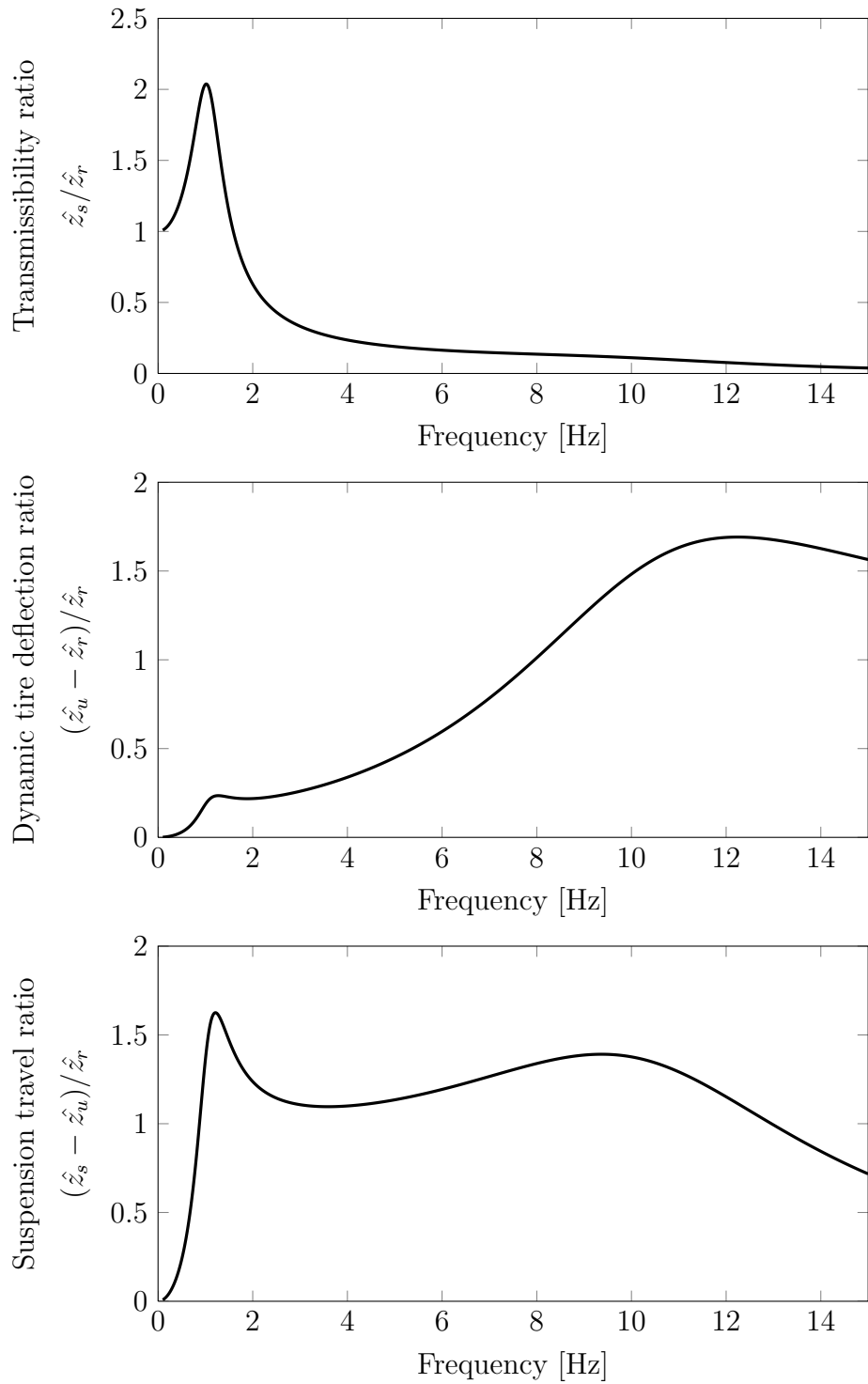


Figure 2.7: Frequency response functions for a typical quarter car model

tire deflection plot.

2.3.2 Inherent trade-offs

One very interesting property of the quarter car model described above is that the three transfer functions $H_{sprung}(s)$, $H_{tire}(s)$ and $H_{susp}(s)$ are not independent. In other words, they are related by a constraint and fixing any one determines the other two [21]. This can be mathematically observed by adding Eq (2.1) and Eq (2.2):

$$m_s \ddot{z}_s + m_u \ddot{z}_u = -k_t(z_u - z_r) \quad (2.11)$$

This is the basic invariant equation of the quarter car model as it does not depend on the active or passive forces applied by the suspension system. The Laplace transform of Eq (2.11) assuming zero initial conditions is

$$m_s s^2 \hat{z}_s + (m_u s^2 + k_t) \hat{z}_u = k_t \hat{z}_r \quad (2.12)$$

The invariant equation can be manipulated to obtain one transfer function in terms of the other. For instance, dividing Eq (2.12) by \hat{z}_r gives

$$m_s s^2 \frac{\hat{z}_s}{\hat{z}_r} + (m_u s^2 + k_t) \frac{\hat{z}_u}{\hat{z}_r} = k_t \quad (2.13)$$

which can be manipulated to express H_{sprung} in terms of H_{tire} and other system parameters as

$$H_{sprung} = -\frac{(m_u s^2 + k_t) H_{tire} + m_u s^2}{m_s s^2} \quad (2.14)$$

From the basic definitions of the three transfer functions, it can be shown that the following identity holds

$$H_{susp} = H_{sprung} - H_{tire} - 1 \quad (2.15)$$

Therefore, from Eq (2.14) and Eq (2.15), H_{susp} can be obtained in terms of H_{tire} and other system parameters as

$$H_{susp} = -\frac{((m_u + m_s) s^2 + k_t) H_{tire} + (m_u + m_s) s^2}{m_s s^2} \quad (2.16)$$

Hence, configuring one transfer function fixes the other two. This is why a suspension system has inherent trade-offs in performance, whether it is an active or passive system.

2.4 Inerter

2.4.1 Introduction to inerter

An inerter is a two-terminal mechanical device which applies force between its terminals proportional to the relative acceleration between them [35], similar to a spring and a damper which apply force proportional to respectively the relative displacement and velocity between their terminals. Inerter was first introduced by Malcom C. Smith in his paper [35] and patented [34]. The idea originated from the extension of force-current analogy [18] for mechanical and electrical circuits where an inductor is analogous to a spring, a resistor is to a damper and a capacitor is to inertia as shown in Table 2.2. But if the inertia is represented simply by a mass then the fundamental definition says that the acceleration is with respect to the mechanical ground (inertial reference frame), or, in other words, v_1 is always equal to zero. This implies that a mass is equivalent to a grounded capacitor, but there is no mechanical analogue for a general capacitor whose one terminal is not necessarily grounded. This poses a restriction if it is needed to derive an equivalent mechanical circuit from a given electrical one. Various methods have been developed [10, 14, 9] for the synthesis of an electrical network with a given admittance (or impedance), which could then be directly applied for mechanical network synthesis if there was an exact equivalent for a capacitor. This thought lead Smith to the invention of the inerter.

Although a mass is not an exact analogue for a capacitor, the crux is still the elementary property inherent in a mass - its inertia, and hence the name inerter. The governing equation is given by

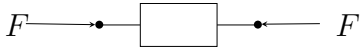

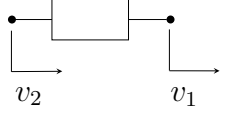
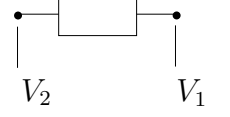
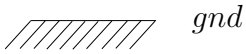
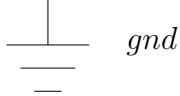
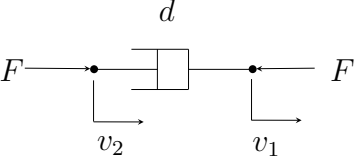
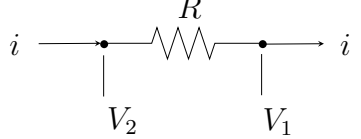
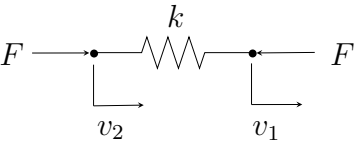
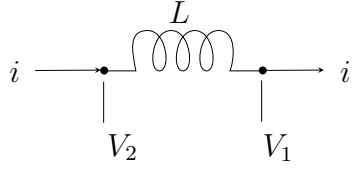
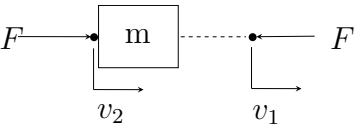
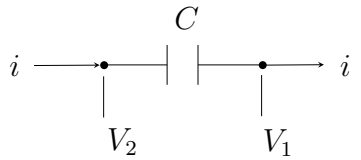
$$F = b(\ddot{x}_2 - \ddot{x}_1) \quad (2.17)$$

which represents that the force between two mechanical terminals is proportional to the relative acceleration between them and this proportionality constant is called inertance. Inertance has units of kilograms (i.e., dimensions of mass).

2.4.2 First use of Inerters in suspension systems

The principle of inerter was applied for the design of suspension systems of Formula One racing cars and first used at the 2005 Spanish Grand Prix, where it was raced by Kimi Raikkonen who achieved a victory for McLaren [12]. During that time, the inerter was codenamed “J-damper” by McLaren to keep the technology confidential from its competitors. As the “J-damper” was delivering significant performance gains in terms of handling and grip, there were many speculations throughout the racing community over the purpose and functioning of the device. Finally, two articles in the *Autosport* magazine of May 2008 revealed the truth that the J-damper was actually the inerter invented by Smith and used

Table 2.2: Mechanical and electrical component analogy

Mechanical	Electrical
Force (through variable) 	Current (through variable) 
Velocity (across variable) 	Voltage (across variable) 
Ground (reference) 	Ground (reference) 
Damping $F = d(v_2 - v_1)$ 	Resistance $i = \frac{1}{R}(V_2 - V_1)$ 
Stiffness $\frac{dF}{dt} = k(v_2 - v_1)$ 	Inductance $\frac{di}{dt} = \frac{1}{L}(V_2 - V_1)$ 
Inertia $F = m \frac{d}{dt}(v_2 - v_1)$ 	Capacitance $i = C \frac{d}{dt}(V_2 - V_1)$ 

by McLaren under a confidentiality agreement.

Inerters can effectively work as tuned mass dampers (TMDs) which were used in F1 races during 2005-06, but were banned later on due to safety issues and rules against aerodynamic effects of the suspended mass [16]. TMD (or inverter) can be tuned so as to attenuate the oscillation of the wheel at its natural frequency, thereby improving handling. The performance benefits of suspensions employing inerters have been discussed in [33]. It is observed that only using an inverter along with a damper (either in series or parallel)

does not show much gains. A little more complex configuration using multiple springs, a damper and an inerter has to be used to obtain practically useful gains. Therefore, the possibility of using inerters for passenger vehicles, which have much softer suspensions and are always under stringent cost constraints, is still open for investigation.

2.5 Quarter car model with a general admittance

Attempts have been made in literature to design suspensions with a complex mechanical network consisting of springs, dampers and inerters, as well as mechatronic suspension strut employing a rotary motor [40, 26]. In order to analyze such systems and obtain their frequency response functions, it would be easier to consider a quarter car model with a general admittance $Y(s)$ as shown in Figure 2.8. The admittance of common components is given in Table 2.3.

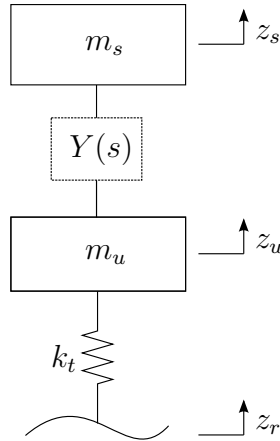


Table 2.3: Mechanical admittance of common components

Component	Admittance $Y(s)$	
Spring	k_p	$\frac{k_p}{s}$
Damper	d_p	$\frac{s}{d_p}$
Inerter	b	bs

Figure 2.8: Quarter car model with a general admittance

Given any mechanical network, the equivalent admittance can be calculated similar to an electric circuit, i.e, for components in parallel, the admittances are directly added and for components in series, the reciprocals of admittances are added.

$$Y_{parallel} = Y_1 + Y_2 \quad (2.18a)$$

$$\frac{1}{Y_{series}} = \frac{1}{Y_1} + \frac{1}{Y_2} \quad (2.18b)$$

The equations of motion, thus, can be rewritten as

$$m_s s^2 \hat{z}_s = -Y(s) (\hat{z}_s - \hat{z}_u) \quad (2.19)$$

$$m_u s^2 \hat{z}_u = Y(s) (\hat{z}_s - \hat{z}_u) - k_t (\hat{z}_u - \hat{z}_r) \quad (2.20)$$

and the transfer functions become

$$H_{sprung}(s) = \frac{\hat{z}_s}{\hat{z}_r} = \frac{k_t Y(s)}{m_s m_u s^3 + (m_s + m_u) s^2 Y(s) + k_t m_s s + k_t Y(s)} \quad (2.21)$$

$$H_{tire}(s) = \frac{\hat{z}_u - \hat{z}_r}{\hat{z}_r} = \frac{-s^2 (m_s m_u s + (m_s + m_u) Y(s))}{m_s m_u s^3 + (m_s + m_u) s^2 Y(s) + k_t m_s s + k_t Y(s)} \quad (2.22)$$

$$H_{susp}(s) = \frac{\hat{z}_s - \hat{z}_u}{\hat{z}_r} = \frac{-m_s k_t s}{m_s m_u s^3 + (m_s + m_u) s^2 Y(s) + k_t m_s s + k_t Y(s)} \quad (2.23)$$

2.6 Modeling road profiles

2.6.1 Frequency domain (ISO classification)

The disturbance arising due to road irregularities is completely random, but any random function can be characterised by its power spectral density (PSD) function [42]. Various organizations have attempted to classify roads on the basis of roughness. The International Organization for Standardization (ISO) has proposed a road roughness classification based on power spectral density, documented as ISO8608 [2]. As shown in Figure 2.9, the ISO classification approximates the relationship between the power spectral density $S_g(\Omega)$ and the spatial frequency Ω for different classes of roads by two straight lines with slopes -1.5 and -2.0 on a log-log scale. Mathematically, it can be represented as follows:

$$S_g(\Omega) = \begin{cases} S_g(\Omega_0) \left(\frac{\Omega}{\Omega_0}\right)^{-2.0} & \text{for } \Omega \leq \Omega_0 = \frac{1}{2\pi} \text{cycles/m} \\ S_g(\Omega_0) \left(\frac{\Omega}{\Omega_0}\right)^{-1.5} & \text{for } \Omega > \Omega_0 = \frac{1}{2\pi} \text{cycles/m} \end{cases} \quad (2.24)$$

where the range of values of $S_g(\Omega_0)$ for different classes of road is given in Table 2.4.

Since the vibration of a vehicle is a temporal phenomenon (function of time), the power spectral density of surface profiles are more conveniently expressed in terms of the temporal frequency f [Hz] rather than the spatial frequency Ω [cycles/m]. The speed of the vehicle V [m/s] relates the two frequencies and PSDs as:

$$f[\text{Hz}] = \Omega[\text{cycles/m}] V[\text{m/s}] \quad (2.25a)$$

$$S_g(f)[\text{m}^2/\text{cycles/m}] = \frac{S_g(\Omega)}{V} [\text{m}^2/\text{Hz}] \quad (2.25b)$$

Therefore, the power spectral density of a particular road profile while moving at a speed

Table 2.4: Road roughness classification proposed by ISO

Road Class	Degree of Roughness $S_g(\Omega_0)$, $10^{-6}\text{m}^2/\text{cycles/m}$	
	Range	Geometric Mean
A (Very Good)	< 8	4
B (Good)	8-32	16
C (Average)	32-128	64
D (Poor)	128-512	256
E (Very Poor)	512-2048	1024
F	2048-8192	4096
G	8192-32768	16384
H	> 32768	65536

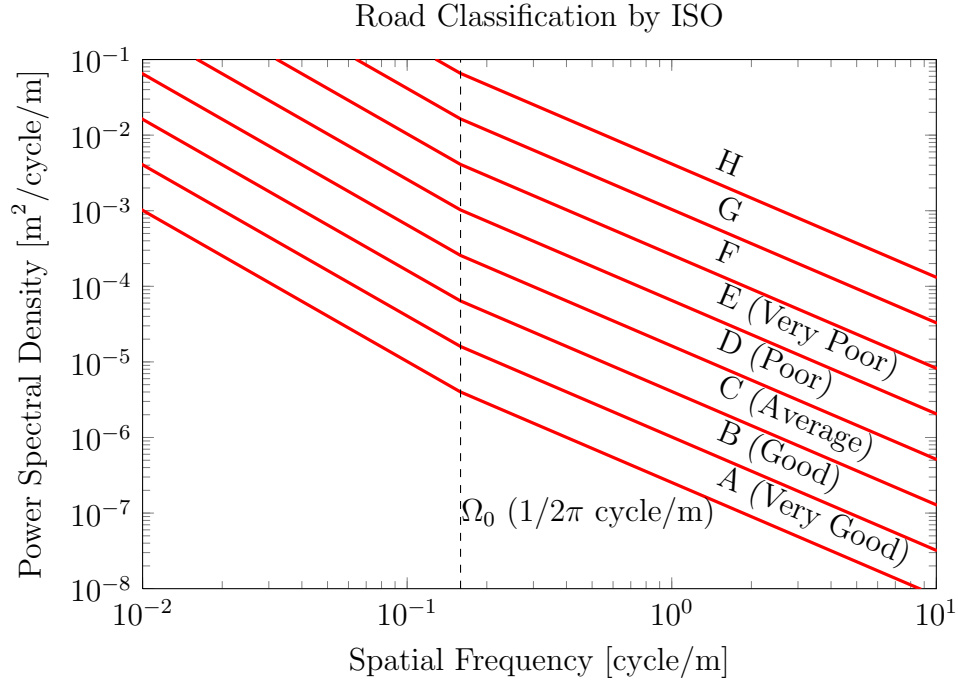


Figure 2.9: Road roughness classification proposed by ISO.

of V [m/s] can be mathematically represented as a function of temporal frequency as

$$S_g(f) = \begin{cases} \frac{S_g(\Omega_0)}{V} \left(\frac{2\pi f}{V} \right)^{-2.0} & \text{for } f \leq f_0 = \frac{V}{2\pi} \text{ Hz} \\ \frac{S_g(\Omega_0)}{V} \left(\frac{2\pi f}{V} \right)^{-1.5} & \text{for } f > f_0 = \frac{V}{2\pi} \text{ Hz} \end{cases} \quad (2.26)$$

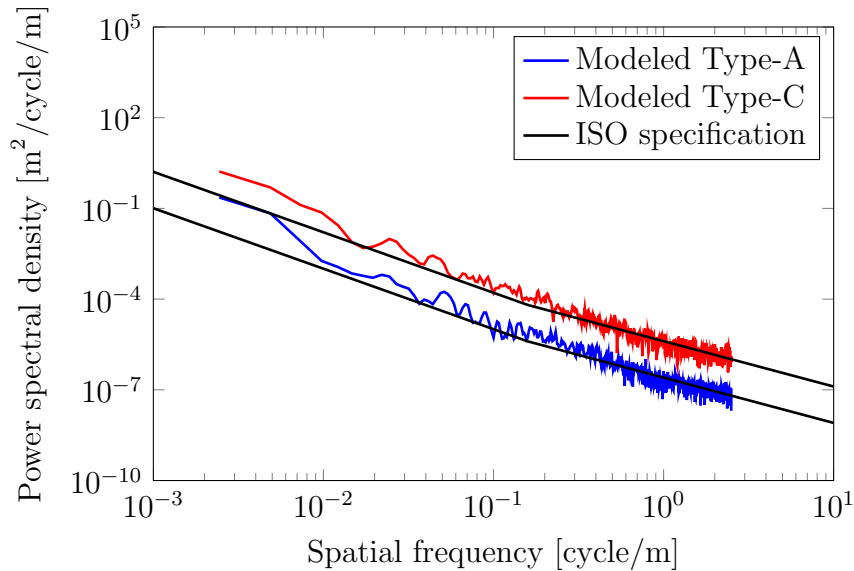
2.6.2 Time domain

For complicated systems, or switched controllers (Chapter 4) which might not have an easy closed form solution in frequency domain, it would be useful to model different road profiles (both stochastic and singular bumps) in time domain. This will later help in simulating the response of a system with different controllers using a physical modeling software like Simulink or MapleSim.

Since the road disturbance is a random process such that the relation between the power spectral density and spatial frequency on a log-log scale has slope -2 for a major part of it, it can be approximately modeled as constant K times integrated white noise. The constant parameter is assigned such that the power spectral density of the modeled signal closely resembles with that of the ISO8608 specification.

$$z_r(s) = \frac{K}{s} w(s) \quad (2.27)$$

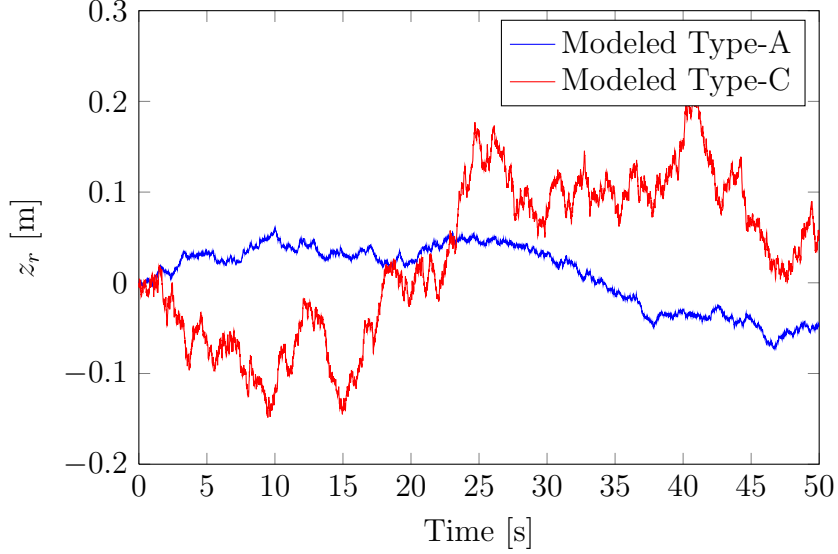
where $w(s)$ is white noise signal. If the PSD of the white noise signal is unity, then it can be shown easily that $K = \sqrt{S_g(\Omega_0)V}$.



(a) Power spectral density of two modeled road profiles with their ISO specified counterpart

Figure 2.10: Modeling different road profiles in time domain (*cont.*)

Figure 2.10a shows the PSDs of modeled type-A and type-C roads compared with their ISO specification and Figure 2.10b shows how the profiles vary as a function of time (for vehicle speed of 20 m/s).



(b) Modeled road profiles in time domain (vehicle speed=20 m/s)

Figure 2.10: Modeling different road profiles in time domain

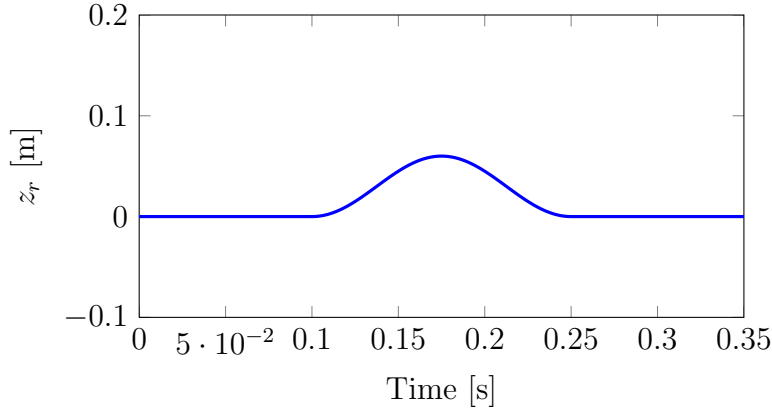


Figure 2.11: Model of a road bump as a function of time (for $V=10$ m/s)

Apart from stochastic road excitation signals, singular disturbance event like a bump is also generally used as a standard input for evaluating the performance of a suspension system. As given in [17], a simple model for a bump can be

$$z_r = \begin{cases} h_b \left(1 - \cos \left(\frac{2\pi V(t - t_0)}{L_b} \right) \right) & \text{for } t_0 \leq t \leq \frac{L_b}{V} + t_0 \\ 0 & \text{otherwise} \end{cases} \quad (2.28)$$

where h_b [m] is half the bump height, L_b [m] is the length of the bump and t_0 [s] is the time instant when the bump starts. For a vehicle speed of 10 m/s, an exemplary bump model

with height 6 cm is shown in Figure 2.11.

2.7 Semi-active and adaptive control algorithms

2.7.1 Control algorithms in prior-art

It was mentioned in Section 2.1 that semi-active active suspensions have been around for quite a while. To get the maximum benefit out of a variable damping system, various control algorithms have also been proposed. A semi-active control algorithm varies the damping in order to obtain either better comfort, or handling, or both (with weights assigned to each). An adaptive control algorithm accounts for the variation in system parameters (if it is significant, see Section 4.1) and the assignment of weights to the performance criteria. Some of the widely popular control algorithms in literature are discussed below.

Skyhook control: Introduced by Karnopp et al.[23], it is one of the most popular comfort oriented control strategies. Originally developed for a single degree of freedom quarter-car model (no unsprung mass), it tries to emulate a fictitious damper d_{sky} attached between the sprung mass and the stationary sky so that its movement is minimized thereby maximizing comfort. However, since it is practically realized by a damper mounted between the sprung and the unsprung mass which can only apply force in the direction opposite to the relative velocity between them, the damping force is assumed to be zero when the passivity constraint is violated. Mathematically, it can be expressed as

$$F_d = \begin{cases} -d_{sky}\dot{z}_s & \text{for } \dot{z}_s(\dot{z}_s - \dot{z}_u) \geq 0 \\ 0 & \text{for } \dot{z}_s(\dot{z}_s - \dot{z}_u) < 0 \end{cases} \quad (2.29)$$

Although it is a switched system, it is assumed that the damping force can take any arbitrary value within some bounds. For systems which cannot vary the damping force in a continuous manner, a simplified Skyhook strategy with on-off control is also sometimes used.

$$d = \begin{cases} d_{max} & \text{for } \dot{z}_s(\dot{z}_s - \dot{z}_u) \geq 0 \\ d_{min} & \text{for } \dot{z}_s(\dot{z}_s - \dot{z}_u) < 0 \end{cases} \quad (2.30)$$

The skyhook control strategy greatly attenuates the motion of the sprung mass. However, when implemented to a little more realistic two degree of freedom model, this technique leads to extreme vibrations of the unsprung mass (wheel hop) and high dynamic tire forces, which deteriorates vehicle stability.

Groundhook control: Analogous to the skyhook algorithm, the groundhook control algorithm [38] tries to attenuate the dynamic tire force by emulating a fictitious damper

d_{gnd} attached between the unsprung mass and a static frame on the ground.

$$F_d = \begin{cases} d_{gnd}\dot{z}_u & \text{for } \dot{z}_u(\dot{z}_s - \dot{z}_u) \leq 0 \\ 0 & \text{for } \dot{z}_u(\dot{z}_s - \dot{z}_u) > 0 \end{cases} \quad (2.31)$$

Rakheja-Sankar (R-S) control: This control strategy introduced by Rakheja and Sankar [29] is quite simple and intuitively evident from the equation of motion of the sprung mass, Eq (2.1). To reduce the acceleration of the sprung mass, which is the basic comfort criterion, the damping force must be equal and opposite to the force applied by the spring. Again, due to the passivity constraint, the damping force is assumed to be zero when the relative velocity and displacement are in the same direction. Mathematically, the control scheme can be expressed as

$$F_d = \begin{cases} k_p(z_s - z_u) & \text{for } (z_s - z_u)(\dot{z}_s - \dot{z}_u) \leq 0 \\ 0 & \text{for } (z_s - z_u)(\dot{z}_s - \dot{z}_u) > 0 \end{cases} \quad (2.32)$$

Similar to skyhook control, a simplified version of R-S control strategy is sometimes used for systems which can only have two discrete states

$$d = \begin{cases} d_{max} & \text{for } (z_s - z_u)(\dot{z}_s - \dot{z}_u) \leq 0 \\ d_{min} & \text{for } (z_s - z_u)(\dot{z}_s - \dot{z}_u) > 0 \end{cases} \quad (2.33)$$

The R-S control scheme is easy to implement as only a relative displacement sensor is required. This is also a comfort oriented strategy, and is susceptible to high dynamic tire force.

Clipped optimal control: In this control scheme, first an optimal controller is designed using techniques like LQR or LQG, to generate the optimal control force F_a which is assumed to take any arbitrary value [37], i.e, can act as an actuator as well as an energy dissipater. Then the passivity constraint is invoked to “clip” the force when it needs to inject power. It can be expressed mathematically as

$$F_d = \begin{cases} 0 & \text{if } F_a(\dot{z}_s - \dot{z}_u) > 0 \text{ (Power needs to be supplied)} \\ F_a & \text{if } F_a(\dot{z}_s - \dot{z}_u) \leq 0 \text{ (Power is dissipated)} \end{cases} \quad (2.34)$$

where F_a is the actuator force that would be optimally required if the system was fully active. It should be noted here that the term “optimal” is described in the performance index sense, which is defined by the designer as per requirement. The performance index might consist of cost on sprung mass movement, tire deflection, suspension deflection and input force, with weights assigned to each. The numerical value of the performance index,

as such, has no physical significance.

With this theoretical background at hand, the next chapter will evaluate the performance of some unconventional suspension designs. After defining cost functions for comfort and handling, the suspension parameters will be optimized to minimize those cost functions.

Chapter 3

Suspension Employing Inerters: Design, Optimization and Results

In this chapter, different suspension designs have been considered from the perspective of physical configuration of the elements like spring, damper and inerter for simple passive mechanical struts, and a motor with corresponding electronic elements for passive mechatronic struts, and then the values of those elements (effectively the admittance) have been optimized for comfort, handling and both (multi-objective optimization). But before moving on to optimization, it should be seen how the cost functions to be optimized can be defined for comfort and handling, considering a quarter car model with a general admittance (which was described in Section 2.5). Since a passive system with a known admittance $Y(s)$ offers a closed form solution for frequency response transfer functions, the cost functions will be defined using the road profile models in frequency domain (ISO8608 [2]).

3.1 Defining cost functions - Performance evaluation of a suspension system

As discussed before, the performance of a suspension system is evaluated mainly in terms of two criteria: ride comfort and handling. The third criteria, suspension travel, is more like a constraint. In other words, the suspension travel is allowed to take any value as long as it is confined within some bounds so that the hard stop bumps are not hit frequently.

The frequency response functions H_{sprung} and H_{tire} , as mentioned in previous sections, give a qualitative idea of the ride and handling. However, these performance criteria need to be defined quantitatively by some cost functions so that the suspension can be optimally designed to keep those costs minimum. Since the road excitation is a stochastic process, so

are the quantities like acceleration of the sprung mass and the dynamic tire forces. Also, the acceleration of the sprung mass needs to be related to the perception of comfort for a human body. Hence, the cost (or objective function) for handling is generally defined as the RMS tire force, and for the ride comfort is the frequency weighted RMS acceleration of the sprung mass as recommended in ISO 2631.

Human body is more sensitive to a certain frequency band, and vibrations of different frequencies produce different effects on human body. For instance, oscillations in the range of 0.1-0.5 Hz are responsible for motion sickness. Taking all these factors into account, ISO has recommended a filter which assigns weights to the RMS acceleration based on its frequency content. The filter is shown in Figure 3.1 and the details are available in [1].

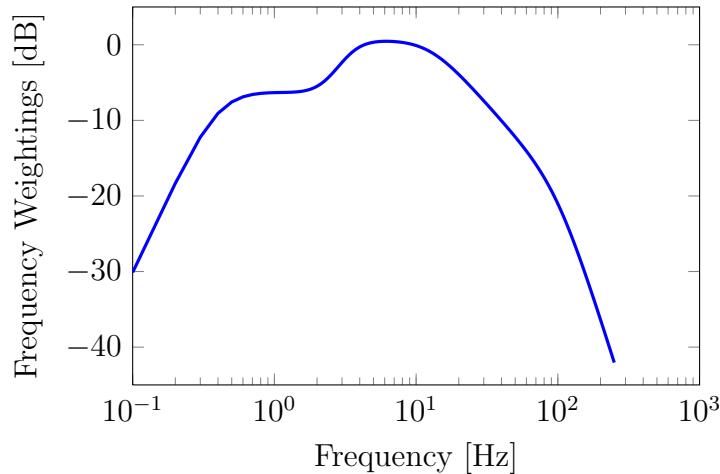


Figure 3.1: Frequency weighting filter for human comfort proposed by ISO.

In random vibrations such as road conditions, the mean square value of the amplitude is of more interest as it is associated with the average energy. If a random signal $z(x)$ has power spectral density $S(\Omega)$, then its mean square value is given by

$$\overline{z^2} = \int_0^\infty S(\Omega) d\Omega \quad (3.1)$$

and the mean square value of $z(x)$ in a particular frequency band of interest $\Omega_1 - \Omega_2$ is given by

$$\overline{z_{\Omega_1-\Omega_2}^2} = \int_{\Omega_1}^{\Omega_2} S(\Omega) d\Omega \quad (3.2)$$

It has been established before that the vehicle system is characterized by certain transfer functions (H_{sprung} , H_{tire} , etc) which relate the input representing road surface irregularities with the output representing quantities of interest in the vehicle. Given any general frequency response transfer function $H(s)$, the input $z_r(t)$ and output $z_v(t)$ which are

functions of time, are related by the modulus of the transfer function

$$z_v(t) = |H(f)|z_r(t) \quad (3.3)$$

On similar lines, the mean square values of the input and output are related as

$$\overline{z_v^2}(t) = |H(f)|^2\overline{z_r^2}(t) \quad (3.4)$$

From the definition of power spectral density and the relationship in Eq (3.4), the power spectral density of input $S_g(f)$ and of output $S_v(f)$ are related as

$$S_v(f) = |H(f)|^2S_g(f) \quad (3.5)$$

Since the power spectral density of a road with a particular roughness has been defined in ISO8608, the power spectral density of any quantity of interest can be calculated using Eq (3.5), provided an appropriate transfer function $H(f)$ is used, and then its mean square value in a particular frequency range can be obtained using Eq (3.2).

Calculating mean square dynamic tire force

The transfer function from road displacement to dynamic tire force is given by $k_t(\hat{z}_u - \hat{z}_r)/\hat{z}_r = k_tH_{tire}$. Therefore, the power spectral density of dynamic tire force as a function of temporal frequency is

$$S_{tire,F}(f) = |k_tH_{tire}(f)|^2S_g(f) \quad (3.6)$$

If the speed of the vehicle is V , the mean square tire force in the frequency range ($f_1 - f_2$) (assuming $f_1 < V/(2\pi)$ and $f_2 > V/(2\pi)$) is

$$\begin{aligned} \overline{F_{tire}^2} &= \int_{f_1}^{f_2} S_{tire,F}(f) df \\ &= \int_{f_1}^{f_2} |k_tH_{tire}(f)|^2 S_g(f) df \\ \overline{F_{tire}^2} &= \int_{f_1}^{V/(2\pi)} |k_tH_{tire}(f)|^2 \frac{S_g(\Omega_0)}{V} \left(\frac{2\pi f}{V}\right)^{-2.0} df \\ &\quad + \int_{V/(2\pi)}^{f_2} |k_tH_{tire}(f)|^2 \frac{S_g(\Omega_0)}{V} \left(\frac{2\pi f}{V}\right)^{-1.5} df \end{aligned} \quad (3.7)$$

$$\text{RMS tire force, } F_{tire,RMS} = \sqrt{\overline{F_{tire}^2}} \quad (3.8)$$

where the values of $S_g(\Omega_0)$ are available in Table 2.4 for different road conditions.

Calculating comfort weighted mean square acceleration

In the transmissibility ratio H_{sprung} , both the input and output have the same dimensions (displacement, speed or acceleration). However, generally the input from the road surface is measured in terms of displacement (road profile elevation) and the acceleration of the sprung mass is measured as output; a new transfer function from road displacement to the acceleration of the sprung mass needs to be defined as

$$\begin{aligned} H_{acc}(s) &= s^2 \frac{\hat{z}_s}{\hat{z}_r} \\ \Rightarrow H_{acc}(s) &= s^2 H_{sprung}(s) \\ \Rightarrow |H_{acc}(f)| &= (2\pi f)^2 |H_{sprung}(f)| \end{aligned} \quad (3.9)$$

If the frequency weighting filter for human comfort proposed in ISO2631 is $Q_{2631}(f)$, the transfer function from road z_r to weighted acceleration of the sprung mass (or comfort criterion) is given by

$$|H_{comf}(f)| = |Q_{2631}(f)H_{acc}(f)| \quad (3.10)$$

$$\Rightarrow |H_{comf}(f)| = (2\pi f)^2 |Q_{2631}(f)H_{sprung}(f)| \quad (3.11)$$

Similar to the calculation of mean square dynamic tire force, the mean square weighted acceleration can be calculated. The power spectral density of the weighted acceleration is

$$S_{comf}(f) = |H_{comf}(f)|^2 S_g(f) \quad (3.12)$$

So, the mean square weighted acceleration in the frequency range $(f_1 - f_2)$ [Hz] (assuming $f_1 < V/(2\pi)$ and $f_2 > V/(2\pi)$) can be calculated as

$$\begin{aligned} \overline{a_{comf}^2} &= \int_{f_1}^{f_2} S_{comf}(f) df \\ &= \int_{f_1}^{f_2} |H_{comf}(f)|^2 S_g(f) df \\ &= \int_{f_1}^{f_2} (2\pi f)^4 |Q_{2631}(f)H_{sprung}(f)|^2 S_g(f) df \\ \overline{a_{comf}^2} &= \int_{f_1}^{V/(2\pi)} (2\pi f)^4 |Q_{2631}(f)H_{sprung}(f)|^2 \frac{S_g(\Omega_0)}{V} \left(\frac{2\pi f}{V}\right)^{-2.0} df \\ &\quad + \int_{V/(2\pi)}^{f_2} (2\pi f)^4 |Q_{2631}(f)H_{sprung}(f)|^2 \frac{S_g(\Omega_0)}{V} \left(\frac{2\pi f}{V}\right)^{-1.5} df \end{aligned} \quad (3.13)$$

$$\text{Comfort weighted RMS chassis acceleration, } a_{comf,RMS} = \sqrt{a_{comf}^2} \quad (3.14)$$

Therefore, from Eq (3.7) and Eq (3.13), the two most important performance criteria for the evaluation of suspension performance have been quantified which can now be used as objective functions to optimize a given suspension design.

One interesting property which can be observed in Eq (3.7) and Eq (3.13) is that the only parameter defining road conditions is $S_g(\Omega_0)$ which can be taken out of the integral and the mean square value(s) would finally appear as a constant ($S_g(\Omega_0)$) multiple of a function of other variables like suspension admittance $Y(s)$ and speed V . This implies that the optimum value of the suspension admittance is independent of the road surface; the value of the objective function just gets scaled according to the road surface parameter. Moreover, although the speed V appears as a variable in the integral, it will be shown by numerical examples that the variation in optimum admittance for different speeds is negligible. Consequently, any typical driving and road conditions can be selected for obtaining the optimum admittance of a suspension system, without the need of considering different cases for them.

3.2 Passive mechanical suspension struts

3.2.1 Realizing a passive mechanical inerter

Any device which satisfies this mathematical property of Eq (2.17) can be termed as an inerter, but to be used in a suspension system, certain practical aspects need to be fulfilled, viz. should have small overall mass (preferably independent of the value of inertance required), finite linear travel, no attachment with the physical ground and should be compact. One simple method to accomplish that as in [34] is to convert the relative linear motion between the two terminals into the rotary motion of a flywheel by using rack-pinion or a ball screw. There may or may not be a gear assembly before the flywheel as required.

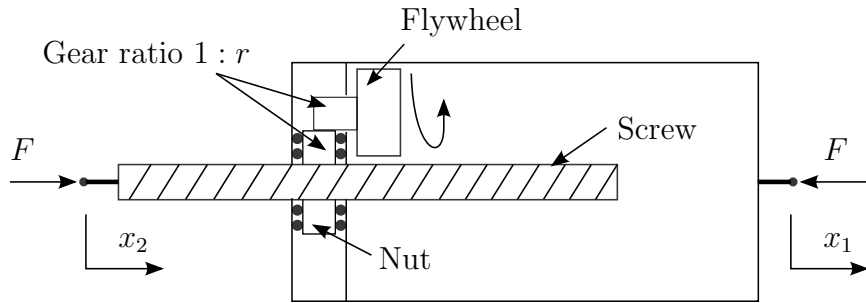


Figure 3.2: Schematic of an inerter using Screw mechanism.

A mechanism is considered that has a flywheel with rotational inertia J [kg m^2], a ball

screw with lead l [m/rev] (gear ratio l [m/rev] for rack and pinion), a gear ratio of $1 : r$ between the nut (or the pinion) and the flywheel and relative acceleration between the two terminals is $(\ddot{x}_2 - \ddot{x}_1)$ [m/s²] as depicted in Figure 3.2. Assuming that the rotational inertia of the screw and other gears is negligible compared to that of the flywheel, angular acceleration [rad/s²] and angular velocity [rad/s] of the flywheel is given by

$$\alpha = \frac{2\pi}{l}r(\ddot{x}_2 - \ddot{x}_1) \quad (3.15a)$$

$$\omega = \frac{2\pi}{l}r(\dot{x}_2 - \dot{x}_1) \quad (3.15b)$$

By conservation of energy, the power input through linear motion should be equal to the power output through rotational motion, therefore,

$$\begin{aligned} F(\dot{x}_2 - \dot{x}_1) &= T\omega \\ \Rightarrow F(\dot{x}_2 - \dot{x}_1) &= J\frac{2\pi}{l}r(\ddot{x}_2 - \ddot{x}_1)\frac{2\pi}{l}r(\dot{x}_2 - \dot{x}_1) \\ \Rightarrow F &= \left(\frac{2\pi}{l}r\right)^2 J(\ddot{x}_2 - \ddot{x}_1) \end{aligned} \quad (3.16)$$

and comparing it with Eq (2.17), inertance can be obtained as

$$b = \left(\frac{2\pi}{l}r\right)^2 J \quad (3.17)$$

Although there would be some inertial effects due to the linear motion of the masses of the flywheel and gears, that can be neglected if the inertance b is quite higher than that mass. This is also usually done in the case of spring and damper.

3.2.2 Suspension configurations used in optimization

For the purpose of evaluating the performance of a quarter car model with a complex mechanical circuit consisting of springs, dampers and inerters, an inerter can be considered as just a device with admittance bs , without going into the details of what mechanism is actually used to realize it, and using general admittance $Y(s)$ as in Section 2.5.

The stiffness of the major spring which holds the static mass of the vehicle, is varied in fixed steps, and the objective function is optimized for each value of static stiffness, the variables being rest of the components constituting the admittance. This way, a clear picture is obtained as to how a particular strut design works for different suspension stiffnesses. The static stiffness can be considered as a characterization of the type of the car; softer suspensions are found in comfortable sedans while the suspensions in sports cars are

relatively stiffer. In this study, the stiffness has been varied from 10 kN/m to 100 kN/m in steps of 10 kN/m and optimization is performed for each stiffness value. This range of stiffness encompasses a major class of road vehicles [28]. The optimization has been carried out individually for the two objective functions, viz. comfort weighted RMS acceleration of the sprung mass and RMS tire force. Practically, however, a suspension is rarely designed directed towards only one objective. To obtain an idea of the performance of the suspension over the whole span between the two extremes in the form of a pareto-front (also known as carpet plot) and visualize the conflict between ride and comfort, multi-objective optimization has been carried out. In order to avoid large number of redundant carpet plots, for multi-objective optimization, only a couple of stiffness values are considered. Other parameters are fixed to be constant as given in Table 3.1. For all the cases taken up in the following sections, the driving condition has been selected as a constant speed of $V = 25$ m/s on a type B road, unless mentioned otherwise. The frequency range (f_1, f_2) has been chosen to be 0.001 – 100 Hz. If there is no restriction on the number of components

Table 3.1: Constants defining properties of the quarter-car model used in optimization

Symbol	Description	Value
m_s	Sprung mass (quarter)	400 kg
m_u	Unsprung mass	40 kg
k_t	Tire stiffness	180 000 N/m
V	Vehicle speed	25 m/s
$S_g(\Omega_0)$	Road roughness parameter	16×10^{-6} m ² /cycle/m

used in a strut, infinitely many designs are possible. However, it is almost impractical to use multiple dampers or inerters due to their complexity, weight and cost. Using a couple of springs, on the other hand, is something which can be investigated. Therefore, to consider designs that have potential for practical implementation, the number of components in this research have been restricted to a maximum of two springs, one damper and one inerter, and a minimum of one spring and one damper. If two springs are used, then out of the two, one is responsible for providing static stiffness to the vehicle, and hence, is not considered as a variable.

One spring and one damper

The simplest and most commonly used configuration of suspension strut used in passenger cars is the parallel spring-damper, which has been discussed several times in previous

chapters. The admittance is given by

$$Y_1(s) = \frac{k_p}{s} + d_p \quad (3.18)$$

The only variable here is the damping d_p , and an optimal value exists for each performance

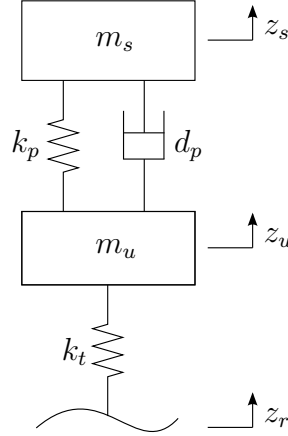


Figure 3.3: Suspension with a spring and a damper in parallel (Y_1)

criterion for a particular static stiffness k_p . The values of objective functions and the pareto-front obtained from this design will be used as references for evaluating the performance of other strut designs.

One spring, one damper and one inerter

If an inerter is also used along with a damper, then the two can either be in parallel, as shown in Figure 3.4a, and with admittance

$$Y_2(s) = \frac{k_p}{s} + d_p + b_p s \quad (3.19)$$

or in series, as shown in Figure 3.4b, and with admittance

$$Y_3(s) = \frac{k_p}{s} + \frac{1}{\frac{1}{d_p} + \frac{1}{b_p s}} \quad (3.20)$$

The variables here are damping d_p and inertance b_p , whose optimal values are found for each value of k_p to minimize a given cost function.

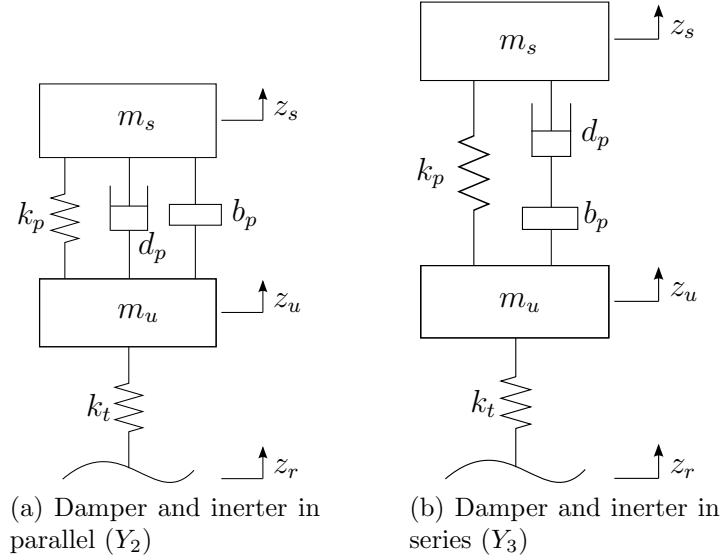


Figure 3.4: Suspension with a spring, a damper and an inerter

Two springs, one damper and one inerter

Two layouts have been considered using multiple springs - one where the second spring is in series with a parallel arrangement of a damper and an inerter as shown in Figure 3.5a, thereby having admittance

$$Y_4(s) = \frac{k_p}{s} + \frac{1}{\frac{s}{k_2} + \frac{1}{b_p s + d_p}} \quad (3.21)$$

and other where the second spring, a damper and an inerter are all in series as shown in Figure 3.5b, and thus having admittance

$$Y_5(s) = \frac{k_p}{s} + \frac{1}{\frac{s}{k_2} + \frac{1}{d_p} + \frac{1}{b_p s}} \quad (3.22)$$

The variables here are damping d_p , inertance b_p and second spring stiffness k_2 , whose optimal values are found for each value of k_p to minimize a given cost function.

3.2.3 Optimization results

Single objective optimization was done individually for comfort and handling considering weighted RMS acceleration of the spring mass and RMS dynamic tire force as the cost functions respectively, for ten values of static stiffnesses (10 kN/m to 100 kN/m). Multi-

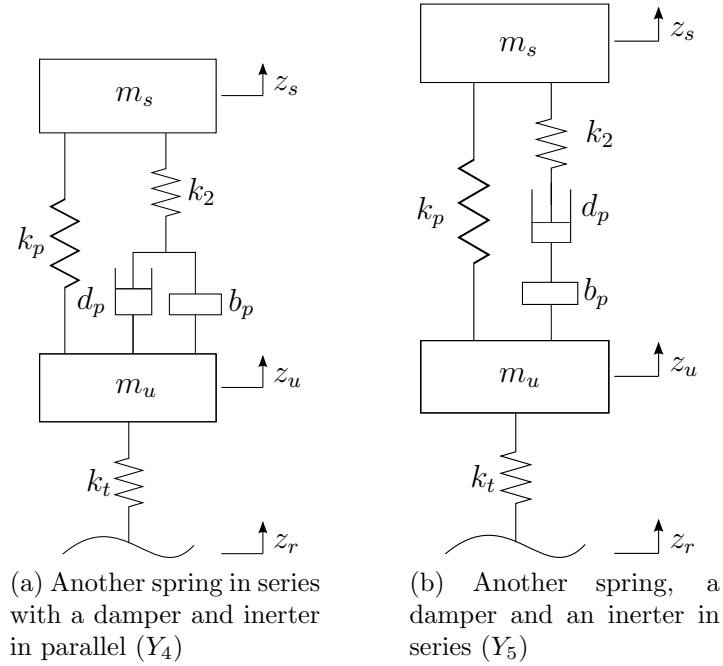


Figure 3.5: Suspension with two springs, a damper and an inerter

objective optimization, which tries to optimize both the cost functions simultaneously and eventually finds a pareto-front, was done to obtain the performance of the suspension over the whole span between the two extreme criteria.

Some predefined functions available in the Optimization Toolbox of MATLAB were utilized for optimization. The “interior point” algorithm with “fmincon” solver was used for single objective, and the “gamultiobj” solver which is based on Genetic Algorithm was used for multiple objectives.

Figure 3.6a shows the variation of optimal cost function with static stiffness when the five suspension configurations are optimized for comfort, and Figure 3.6b shows their performance in terms of the percentage improvement over the conventional spring-damper system (admittance $Y_1(s)$). It is observed that configurations Y_2 and Y_4 show around 9% improvement for lower static stiffness which is characteristic of passenger cars, while all four designs improve comfort by around 6% for higher static stiffness, which is property of sports cars. Y_3 and Y_5 don’t have a significant effect on improving comfort in softer suspensions.

The results for optimized dynamic tire loads are shown in Figure 3.7a and 3.7b. While the design Y_2 shows almost zero improvement in handling throughout the static stiffness range, Y_4 and Y_5 improve it by about 5-6% if used with a softer static stiffness. In the stiffer range, Y_5 and Y_3 respectively provide 8% and 6% better handling compared to the

baseline of Y_1 . The performance of Y_4 degrades with increase in static stiffness while Y_3 has negligible improvement in comfort for softer suspensions

Figure 3.8a shows the optimal variable values for the five suspension designs that provide maximum comfort. Only damping and inertance has been shown as the value of optimal k_2 (for Y_4 and Y_5) is of the order of 10^7 [N/m] or higher, which is practically meaningless (effectively a rigid body). It is seen that with the increase in static stiffness, the damping required to provide maximum comfort also increases for all five designs. The value of optimal inertance, also, increases with more stiffness in suspension. However, there is a huge difference in the value optimal inertance between the four designs. While Y_3 and Y_5 require inertance in the range of 250 kg to 450 kg (depending on the static stiffness), the inertance required in designs Y_2 and Y_4 is close to zero for softer springs and has a low value of less than 50 kg for stiffer ones.

The optimal variable values corresponding to minimum dynamic tire loads are shown in Figure 3.8b. After a negligible drop in the optimal damping for low static stiffness, it is generally required to increase the damping with stiffer suspensions to obtain better handling. The effect of inertance on dynamic tire load is quite interesting. While it has absolutely no effect in design Y_2 and a very low value is required in Y_4 , an arbitrarily high value of inertance is required in Y_3 and Y_5 to optimize handling for low static stiffness systems. Realistically achievable values of inertance in Y_3 and Y_5 are obtained only for medium to high static stiffness systems. The spring rate of k_2 in Y_4 and Y_5 is of the order of 10^5 [N/m], which seems to be practical.

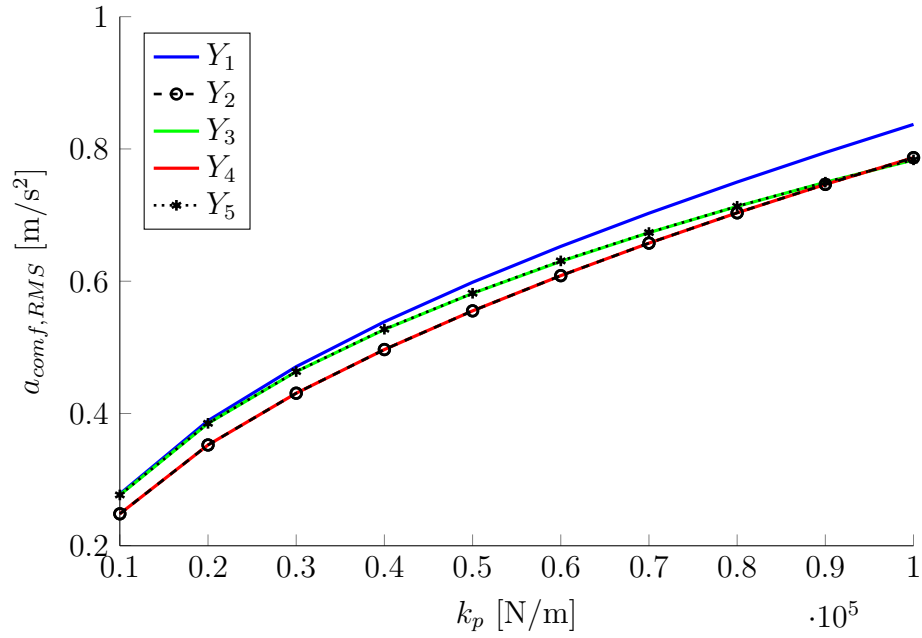
The optimization results have also been tabulated in Table 3.2 for a particular case, where static stiffness $k_p = 40\,000$ N/m.

Table 3.2: Optimization results for $k_p=40\,000$ N/m

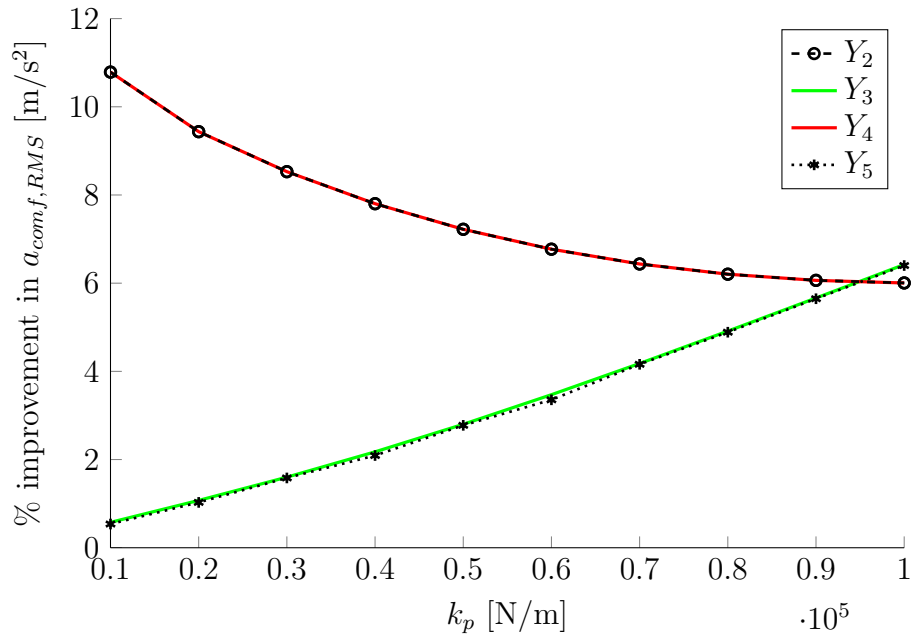
Objective function	Strut admittance	Optimal value	% improv. in obj. fn.	Optimal variables		
				[N s/m]	[kg]	[N/m]
$a_{comf,RMS}$ [m/s ²]	Y_1	0.539	-	$d_p=1080$		
	Y_2	0.497	7.8%	$d_p=866$	$b_p=10$	
	Y_3	0.527	2.2%	$d_p=1143$	$b_p=329$	
	Y_4	0.497	7.8%	$d_p=866$	$b_p=10$	$k_2 \rightarrow \infty$
	Y_5	0.528	2.1%	$d_p=1139$	$b_p=327$	$k_2=2 \times 10^7$
$F_{tire,RMS}$ [N]	Y_1	423	-	$d_p=2923$		
	Y_2	423	0%	$d_p=2923$	$b_p=0$	
	Y_3	417	1.2%	$d_p=3018$	$b_p=767$	
	Y_4	407	3.7%	$d_p=2850$	$b_p=20$	$k_2=2.8 \times 10^5$
	Y_5	398	5.8%	$d_p=3410$	$b_p=524$	$k_2=3.9 \times 10^5$

Figure 3.9 shows the performance of the different suspension designs for a particular

static stiffness of $k_p = 40\,000\text{ N/m}$ in the form of pareto-fronts obtained from multi-objective optimization. Going towards left on the x-axis implies more comfort, while moving down on the y-axis means better handling. Each point on the pareto-front corresponds to a particular set of values for the variables at hand (d_p , b_p and k_2 , depending on the strut design) which demonstrate a performance defined by the position of that point. It is observed that Y_4 can provide a wide operation range, but with improvement in comfort and handling only in the extreme cases. For a practical situation of a passenger vehicle where both the criteria are given equal weight, corresponding to the middle portion of the curve, Y_4 has similar performance as the conventional Y_1 . Likewise, Y_2 is beneficial if comfort is the only criterion. Although Y_3 and Y_5 show improvement over Y_1 throughout the range of the pareto front, it is less than 5%.

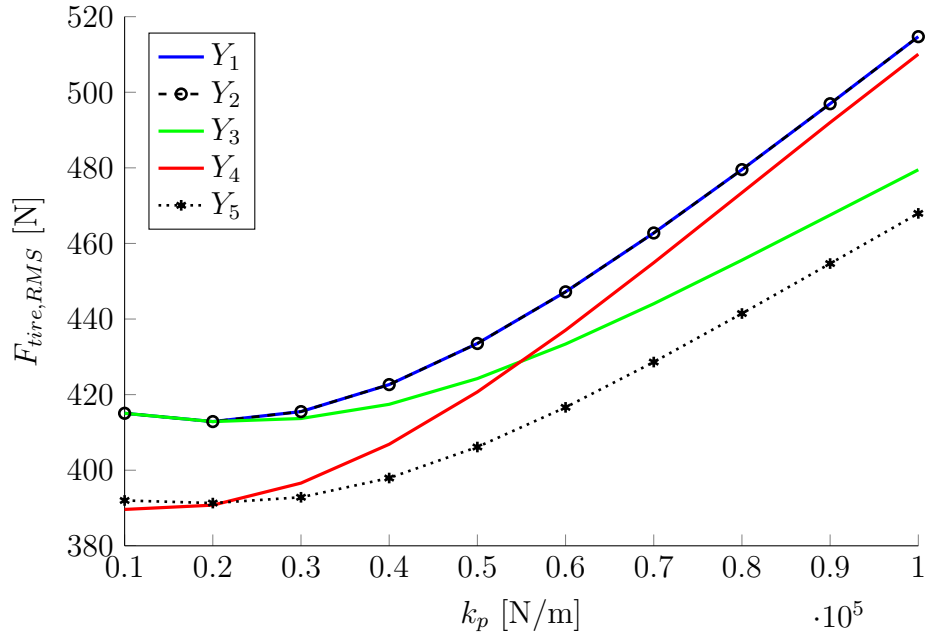


(a) Optimal cost function for comfort

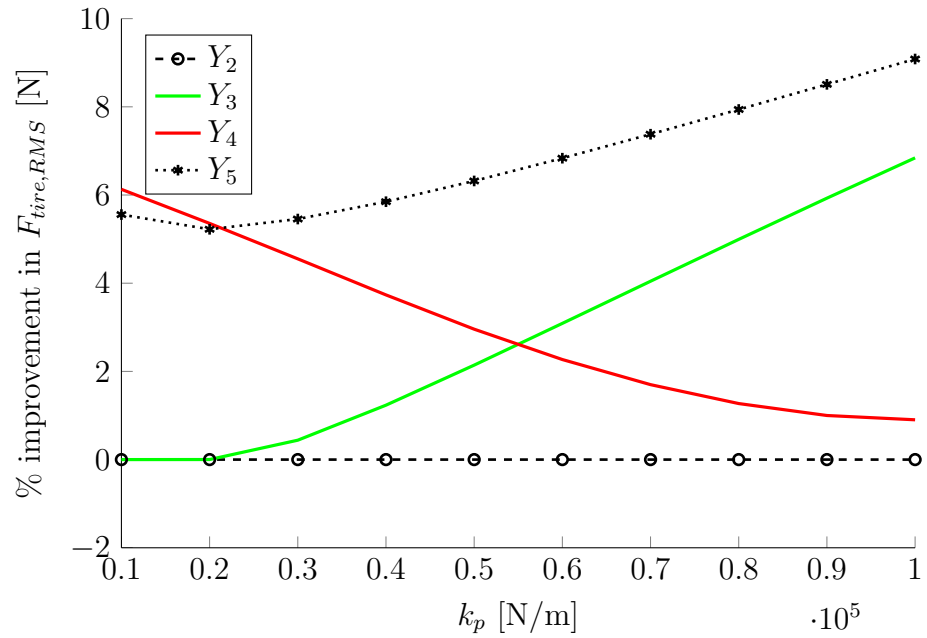


(b) Percentage improvement in comfort

Figure 3.6: Optimization of comfort for different mechanical suspension struts and static stiffness

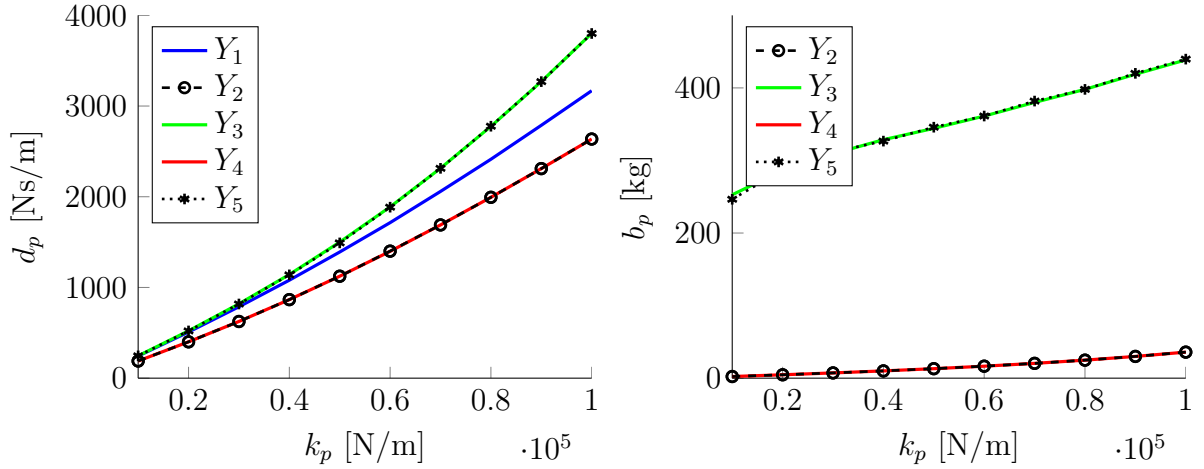


(a) Optimal cost function for dynamic tire loads

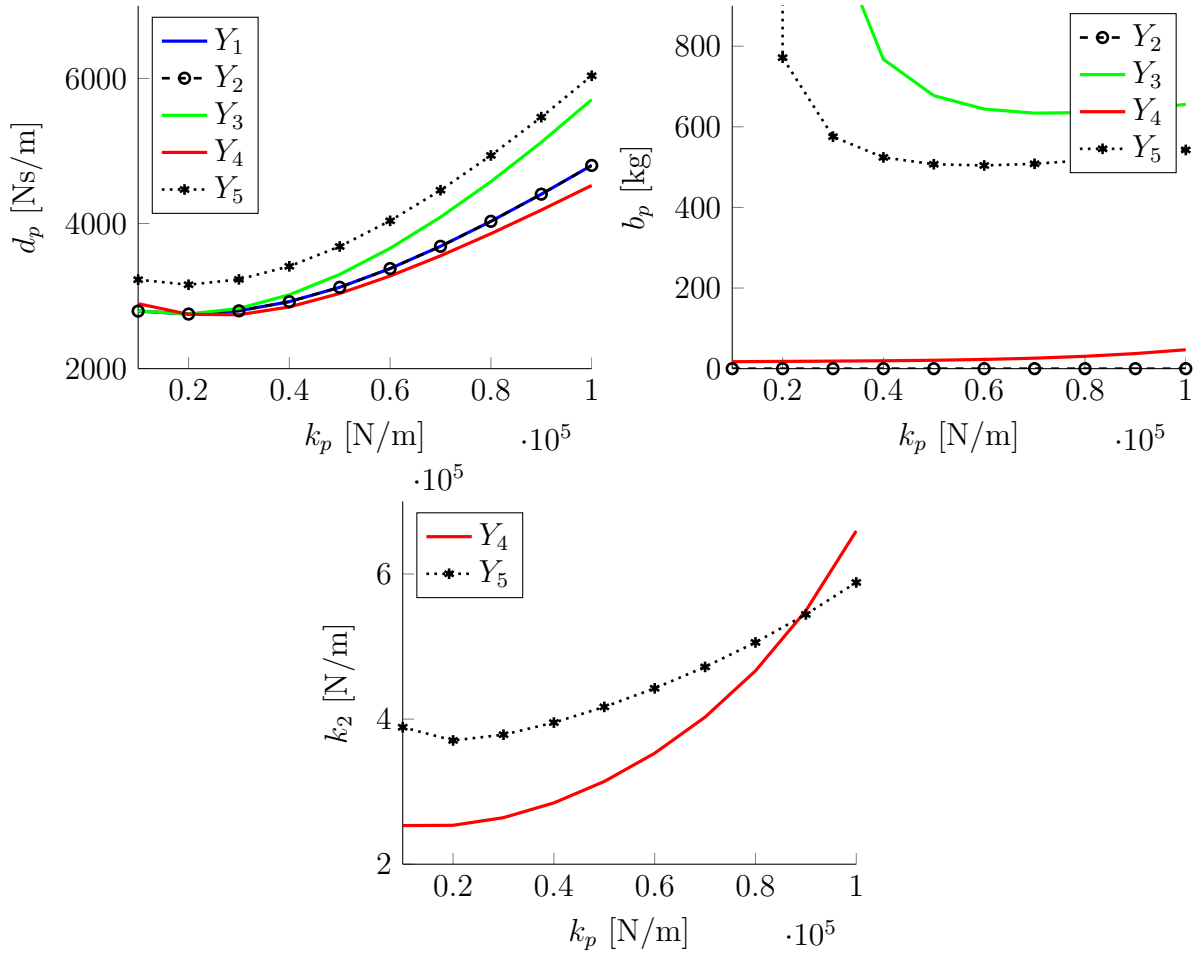


(b) Percentage improvement in dynamic tire loads

Figure 3.7: Optimization of dynamic tire loads (handling) for different mechanical suspension struts and static stiffness



(a) Variable values (damping and inertia only) for optimal comfort



(b) Variable values (damping, inertia and second spring) for optimal dynamic tire loads

Figure 3.8: Variable values for optimal performance criteria for different mechanical suspension struts and static stiffness

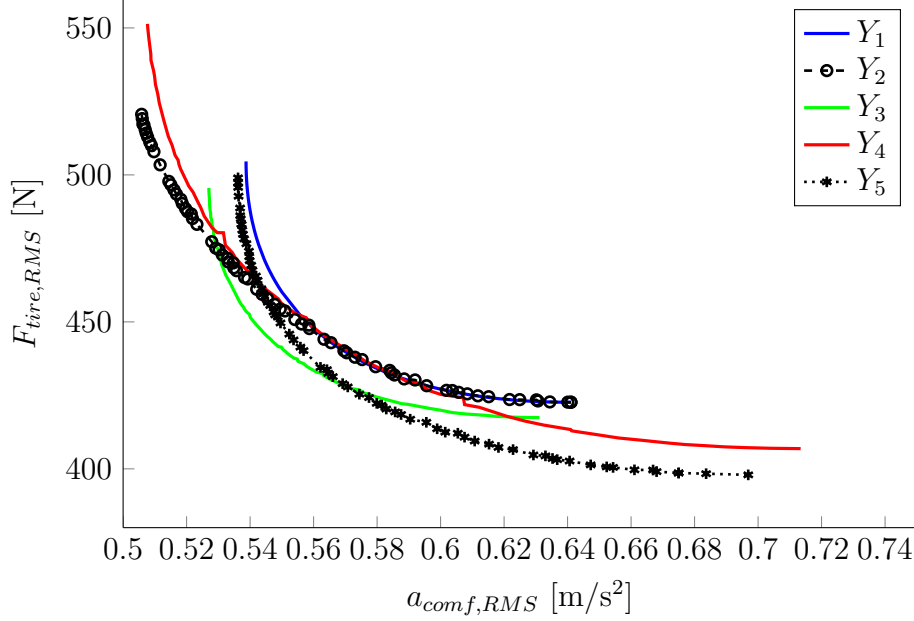


Figure 3.9: Pareto-fronts from multi-objective optimization for $k_p=40\,000\text{ N/m}$

3.3 Mechatronic suspension struts

It is evident from the previous section that better performance can be achieved from a passive suspension system by using a mechanical circuit consisting of springs, dampers and inerters. Although circuits not more complex than that with two springs, one damper and one inverter were evaluated, it has been shown in [33] that even better performance can be obtained by using more components, for instance four springs, one damper and one inverter. Hence, it is worth exploring suspension struts with more complicated admittances for possible benefits. However, it is something quite understandable that using those struts might not be practical due to increased cost and weight.

A plausible solution to realize complex mechanical admittances for suspension struts without actually using the real bulky components is to invoke the electrical-mechanical analogy (Table 2.2) again. A mechanical component can be realized by using its electrical analogue connected to a linear electromagnetic motor. This might seem bulkier for a single component, but its true potential is exploited when a complex mechanical system is replaced by an equivalent electrical circuit, which is definitely easy to construct and light weight.

For instance, a case is considered where a resistance R is connected to an ideal linear electromagnetic motor with force constant K_i [N/A] and back-emf constant K_e [V s/m]. If the relative speed between the stator and the shaft is $V_z(t)$ [m/s], then a voltage is

generated across the terminals of the motor, equal to

$$e(t) = K_e V_z(t) \quad (3.23)$$

The current through the resistor is

$$i(t) = \frac{K_e V_z(t)}{R} \quad (3.24)$$

The motor then applies a force equal to

$$F(t) = K_i i(t) = \frac{K_i K_e}{R} V_z(t) \quad (3.25)$$

Hence, comparing it with the equation of an ideal viscous damper, it can be said that the system acts like a damper with $d = K_i K_e / R$. Similar relations can be established for other components as well, and the force applied by the motor with a general impedance $Z(s)$ shunted across it terminals can be given in Laplace domain by

$$F(s) = \frac{K_i K_e}{Z(s)} \hat{V}_z(s) \quad (3.26)$$

or, in other words, the equivalent mechanical admittance obtained is

$$Y(s) = \frac{K_i K_e}{Z(s)} \quad (3.27)$$

This approach offers multiple advantages, such as

- Simpler construction compared to a system of actual mechanical components.
- Due to complexity of damper and inerter, the available literature work limits the mechanical circuits to one damper and inerter, whereas using electromagnetic actuator, any number of dampers (R) and inerters (C) can be added.
- By using variable impedance, the properties of the suspension can be easily varied online to realise an adaptive system.
- Power is regenerated
- Active force can be applied for high-end cars.

All these potential benefits seem to be quite promising. Now the crux of practical implementing the idea is realization of a linear electromagnetic motor. One solution is to simply use a commercially available linear motor. However, it has issues like high cost,

heavy weight and low energy density [26, 31]. Since rotary motor can provide more energy in a smaller form factor and is comparatively cheaper, another solution is to use a rotary motor with a mechanism like ball screw to convert the linear motion of the suspension to the motor's rotary motion as depicted in Figure 3.10. This idea will be explored in detail in the subsequent sections.

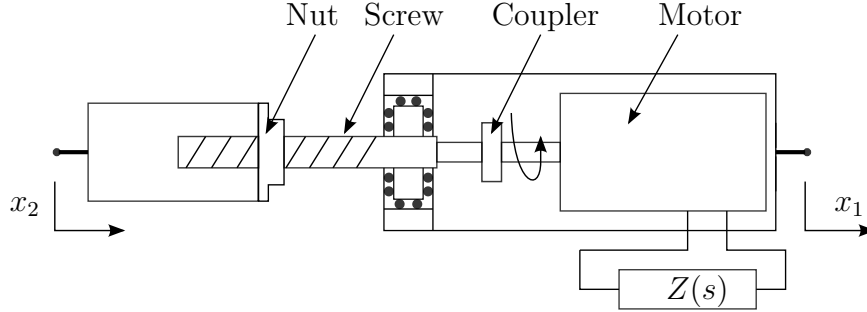


Figure 3.10: Schematic of a suspension strut using a ball screw mechanism and a rotary motor with shunt impedance $Z(s)$

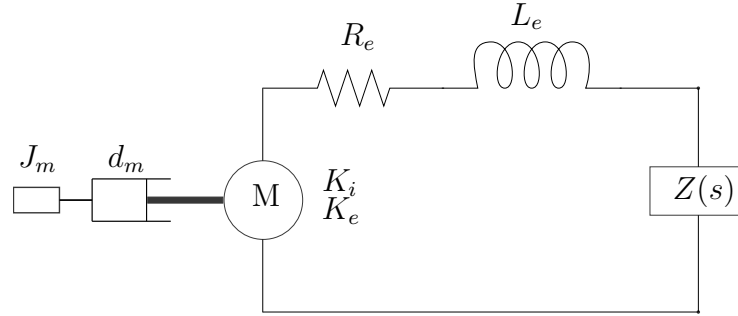


Figure 3.11: Schematic of the motor with shunt impedance $Z(s)$

Any motor has an inherent electrical resistance R_e [Ω], inductance L_e [H], viscous damping d_m [N ms/rad] and rotor inertia J_m [kg m²] (including screw). Considering the effect of these, along with that of the the ball screw mechanism of lead l [m/rev] will modify the effective mechanical admittance from that in Eq (3.27) to

$$Y(s) = \frac{k_p}{s} + \left(\frac{2\pi}{l}\right)^2 \left(J_m s + d_m + \frac{K_i K_e}{R_e + L_e s + Z(s)} \right) \quad (3.28)$$

Figure 3.11 models a simple rotary motor with shunt impedance $Z(s)$. A motor with constant parameters as in Table 3.3 has been selected for the design. Different electrical circuits with equivalent impedances $Z(s)$ as shown in Figure 3.12a and 3.12b will be evaluated for performance by optimizing the values of the electrical components and benchmarked against the simple spring-damper system ($Y_1(s)$).

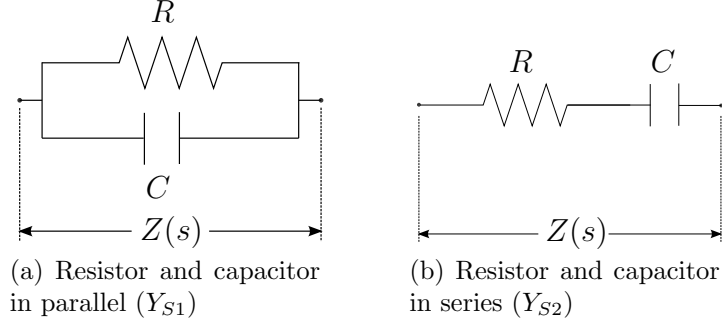


Figure 3.12: Shunt circuits

For simplicity, only two shunts circuits consisting of a resistor and a capacitor were considered just as a proof of concept. For the two in parallel, the impedance $Z(s)$ in Eq (3.28) is given by

$$Z(s) = \frac{R}{RCs + 1} \quad (3.29)$$

and for them in series,

$$Z(s) = R + \frac{1}{Cs} \quad (3.30)$$

Table 3.3: Parameters (constants) of the motor and screw used

Symbol	Description	Value
J_m	Inertia	$1.515 \times 10^{-4} \text{ kg m}^2$
K_i	Torque constant	0.214 N m/A
K_e	Back-emf constant	0.214 V s/rad
P_m	Rated power	250 W
L_e	Armature inductance	$4.58 \times 10^{-4} \text{ H}$
R_e	Armature resistance	1.06Ω
d_m	Viscous damping	$1.012 \times 10^{-4} \text{ N m s/rad}$
l	Screw lead	0.02 m/rev

3.3.1 Optimization results

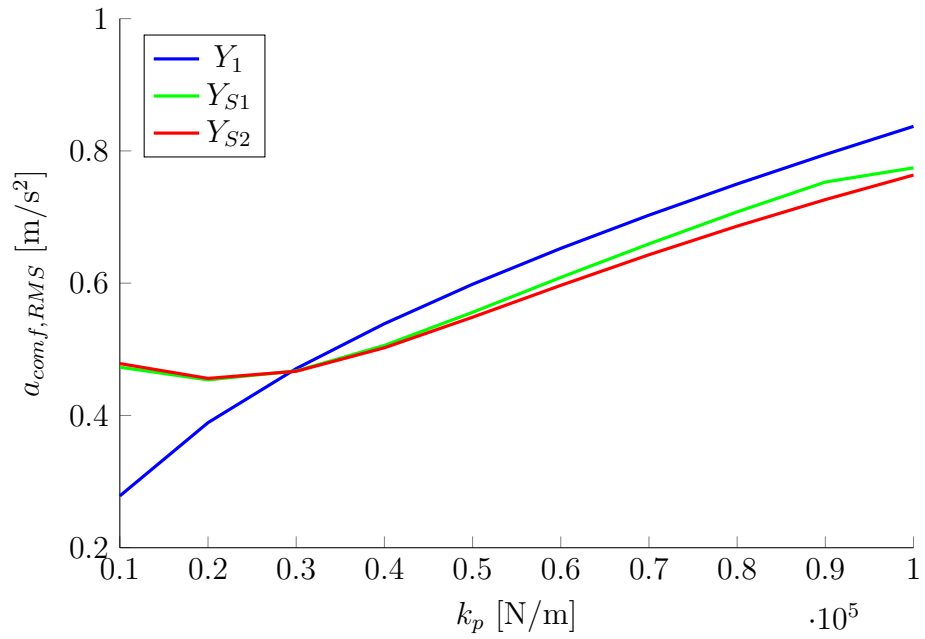
With Eq 3.28, the admittance $Y(s)$ of this mechatronic suspension strut can be calculated for a given impedance $Z(s)$. Obtaining cost functions for comfort and handling for any given admittance has already been described in Section 3.1. Using the same procedure and MATLAB functions as in Section 3.2.3, single objective optimization is performed for different static stiffness values (10 kN/m to 100 kN/m), with the variables being the electric components R and C in this case.

The results for optimized comfort are shown in Figure 3.13a. It is seen that the performance of both Y_{S1} and Y_{S2} is actually degraded compared to Y_1 if the static stiffness is less than 30 kN/m. For medium to stiffnesses, Y_{S1} can provide 6-8% improvement while Y_{S2} can show around 9% improvement in comfort. Figure 3.14a shows the results for optimized handling. It is observed that compared to Y_1 , both Y_{S1} and Y_{S2} show a degraded performance for static stiffness ranging from low to as high as 60 kN/m. Even for very high stiffnesses, the improvement is nominal at 4%, and both the circuits have almost similar performance. Hence for both the circuits, a decent improvement is obtained only in the high static stiffness region; for lower static stiffnesses similar to that found in most passenger cars, the performance can actually degrade. It is also observed that the series configuration is slightly better than the parallel one

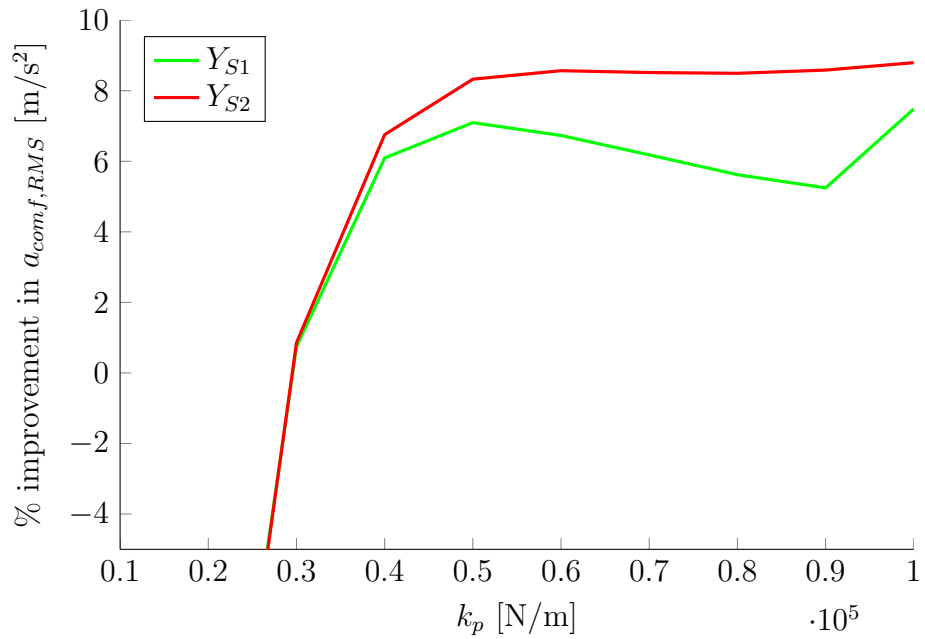
Each point on the pareto-front for Y_{S1} and Y_{S2} in Figure 3.15 and 3.16 obtained from multi-objective optimization corresponds to a particular set of values for R and C which lead to that specific $a_{comf,RMS}$ and $F_{tire,RMS}$ defined by that point's position. The pareto-fronts provide a clear comparison of the performance of the shunted system with the conventional spring-damper one. For static stiffness of $k_p = 40$ kN/m, although the shunted mechatronic struts show better comfort, but that is at the cost of very high dynamic tire force. For a major portion of the curve, their performance is worse. However, if the static stiffness is very high (for example, $k_p = 100$ kN/m), then the performance improvement of Y_{S1} and Y_{S2} over Y_1 is quite substantial.

The drastic change in the performance of this mechatronic strut compared to the ideal mechanical circuits in last section can be attributed to the inertia of the rotor and resistance of the motor coils. These values are so dominant that changing the shunt impedance circuit to a more complex one has almost negligible effect on the performance, and the optimized cost function hovers around the values obtained for simple designs Y_{S1} and Y_{S2} . The results for those complex circuits are omitted to avoid redundancy.

For stiffer suspensions, the shunted mechatronic strut provides better performance throughout the range of the pareto-front. This means that an adaptive system which maintains the operating point on the pareto-front will deliver an improved ride and handling simultaneously. However, since the results are good only for very stiff systems, a prototype was not constructed as it would not be applicable to passenger vehicles. Therefore, a generalized adaptive controller will be developed in the next chapter which can be implemented on any system with an energy dissipating device, with or without inertance.

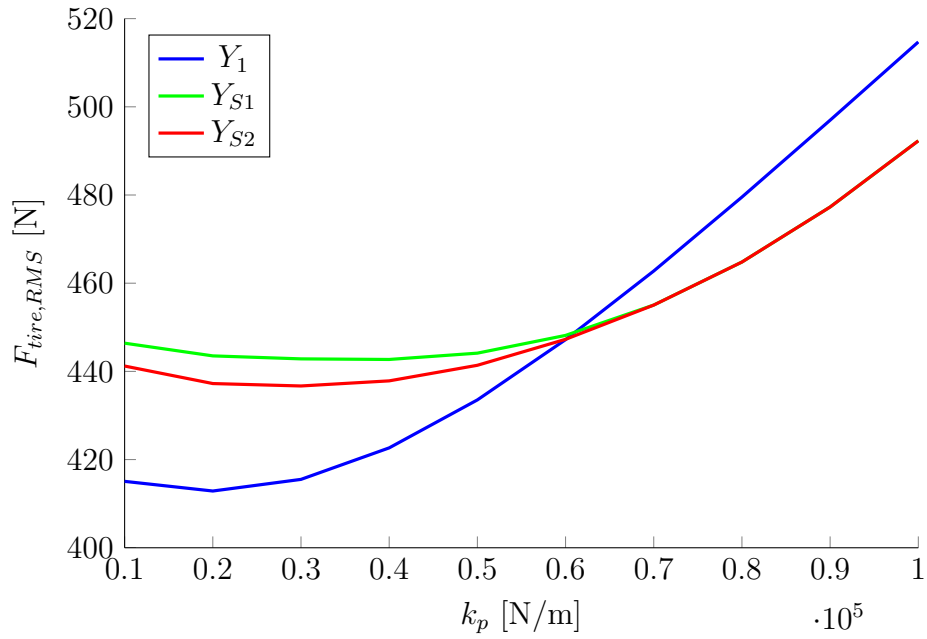


(a) Optimal cost function for comfort

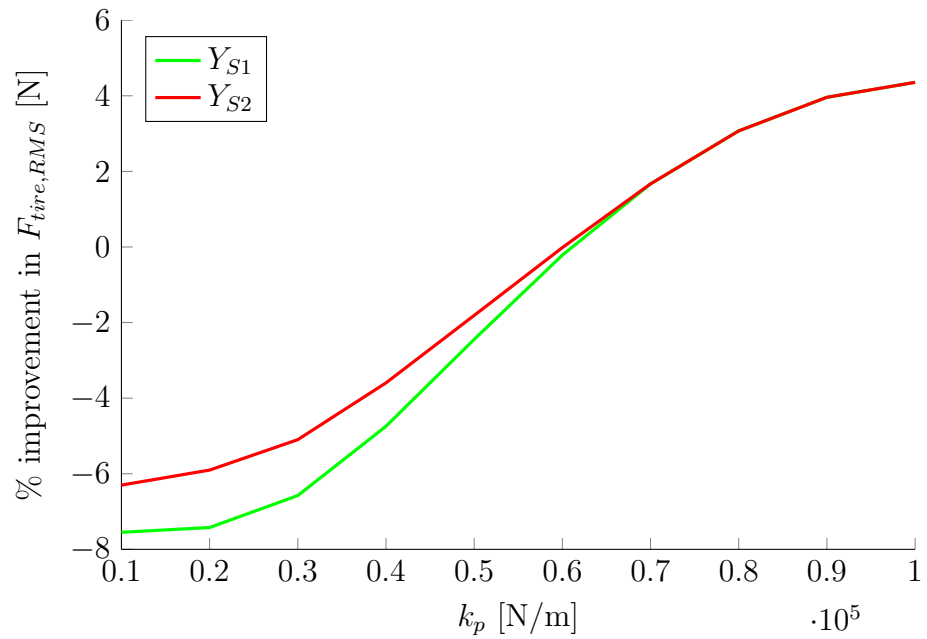


(b) Percentage improvement in comfort

Figure 3.13: Optimization of comfort for different mechatronic suspension struts and static stiffness



(a) Optimal cost function for dynamic tire loads



(b) Percentage improvement in dynamic tire loads

Figure 3.14: Optimization of dynamic tire loads (handling) for different mechatronic suspension struts and static stiffness

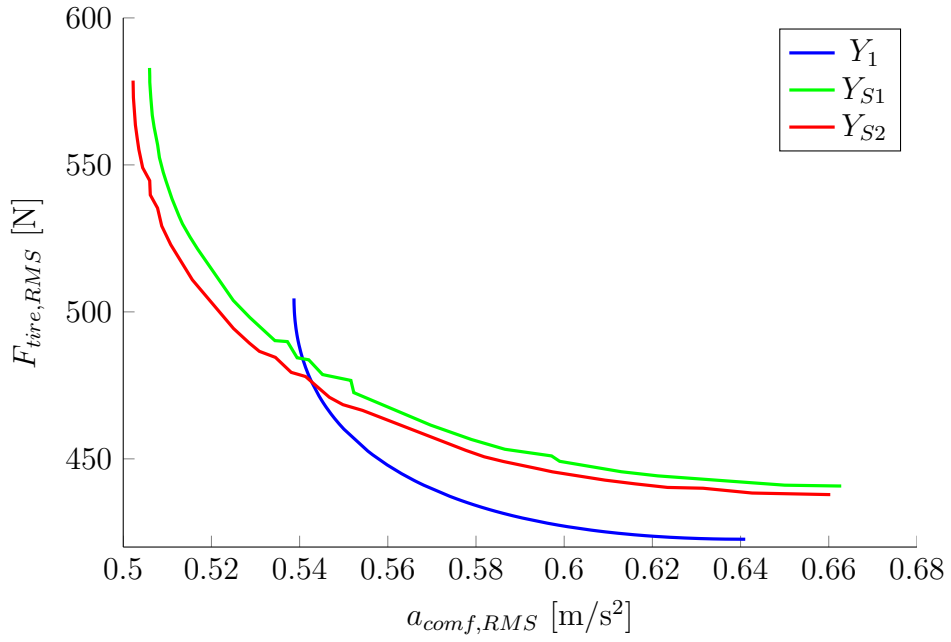


Figure 3.15: Pareto-fronts from multi-objective optimization for $k_p=40\,000$ N/m

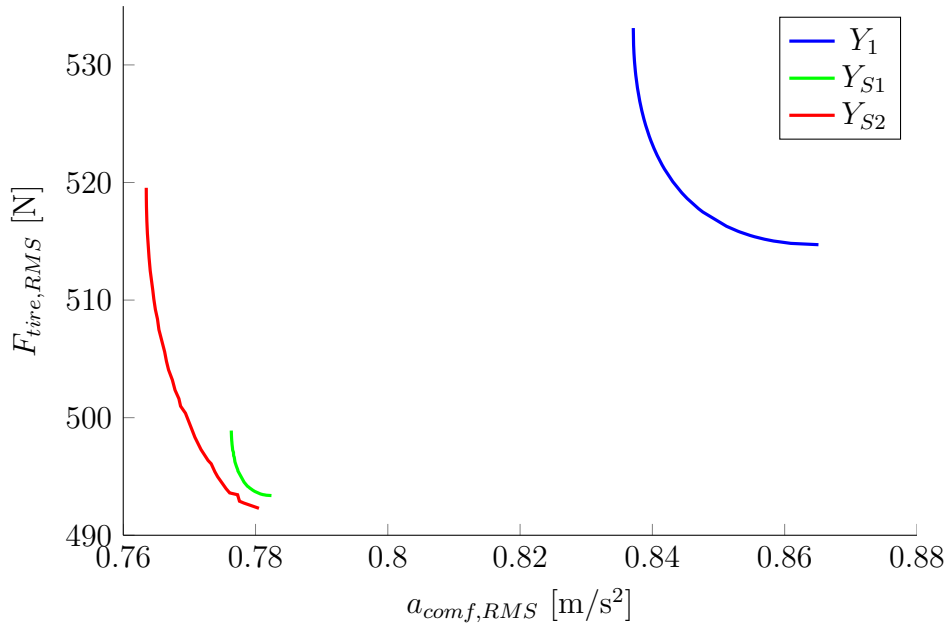


Figure 3.16: Pareto-fronts from multi-objective optimization for $k_p=100\,000$ N/m

Chapter 4

Adaptive Semi-Active Suspension: Modeling, Control and Simulation Results

As mentioned in the last chapter, the variation of damper properties by variation of the shunt impedance offers the scope of an adaptive semi-active suspension system by incorporating an appropriate control algorithm. However, since the mechatronic suspension strut is beneficial only for very stiff suspensions, constructing a prototype would not be economically fruitful as it cannot be installed on a passenger vehicle. Therefore, in this chapter, a control algorithm is developed which considers a generic passive force F_d applied between the sprung and unsprung masses. This passive force will be addressed as the damping force throughout the rest of this document, and the controller is validated through experiments on a vehicle equipped with variable dampers in Chapter 5. However, the same controller can be used for any source of passive force, including a mechatronic suspension strut with variable shunt impedance.

Before looking into the control algorithms for semi-active and adaptive suspensions, it would be worthwhile to investigate the effect of varying different parameters in a suspension.

4.1 Effect of varying driving conditions: sprung mass m_s and vehicle speed V

For a suspension system with variable damping and some fixed parameters defining the system, an optimal damping value exists for each performance criterion. However, many of the parameters vary during practical driving conditions. For example, the vehicle speed

and road type vary on the run and the vehicle sprung mass can vary from time to time depending on the number of passengers and amount of cargo. Hence, the effect of variation of these parameters on the optimal damping needs to be investigated.

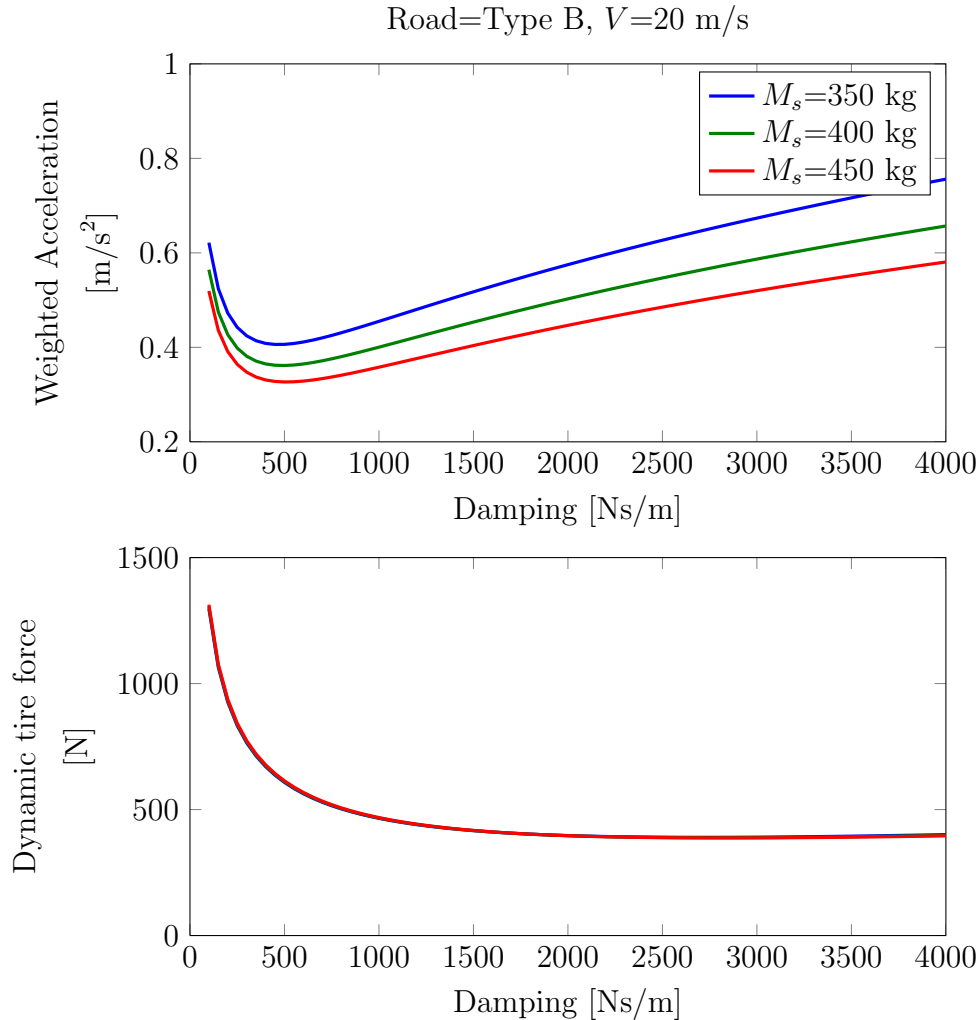


Figure 4.1: Effect of varying sprung mass on comfort and handling as a function of damping in a quarter car model (The plots are overlapping for dynamic tire force)

It was already shown analytically in Section 3.1 that the variation of road type does not affect the optimal damping values, and would therefore be omitted here. To study the effect of varying m_s and V , a numerical example is taken. Figure 4.1 and 4.2 show the effect of varying sprung mass and vehicle speed respectively on the weighted RMS sprung mass acceleration (comfort) and RMS dynamic tire force (handling). A few interesting observations can be made from these plots. First, the optimal damping values for comfort and handling do not change much with the parameters. In other words, although the optimal value for a given parameter set might not be exactly the same as that for another

parameter set, the actual change in the cost function for the ‘sub-optimal’ parameter set is not significant. Secondly, the variation of dynamic tire forces is negligible in a wide range of damping (around 2000 N s/m to 4000 N s/m). Mathematically, although, the optimal value lies around 3500 N s/m. The variation of weighted acceleration is significant enough in this region. Therefore, reducing the damping from the mathematical optimum to around 1500-2500 N s/m would improve the comfort a lot without practically affecting the handling.

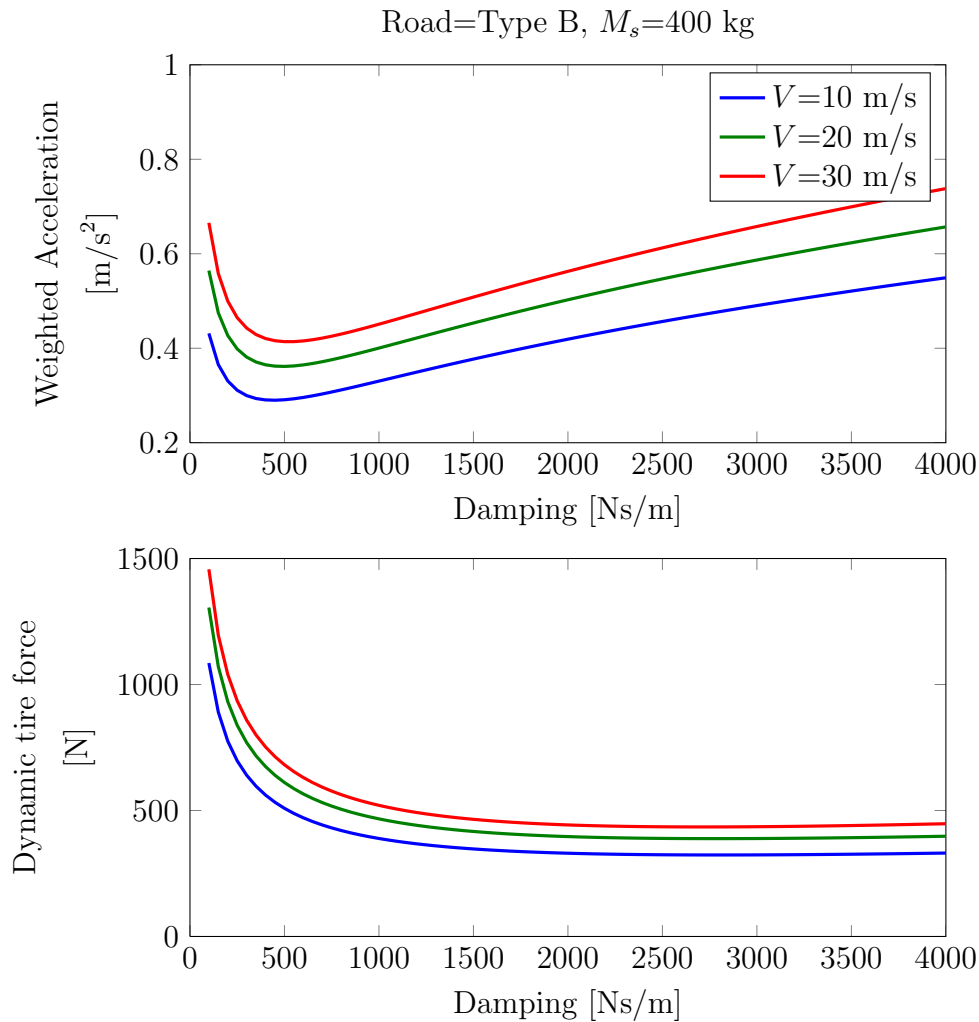


Figure 4.2: Effect of varying vehicle speed on comfort and handling as a function of damping in a quarter car model

These observations drive home the fact that the classical adaptive control techniques which are typically concerned with varying plant parameters might not be much applicable in the case of automotive suspensions. On the other hand, a control technique which is adaptive in the sense of online varying the weights assigned to the two objectives of comfort and handling is rather required.

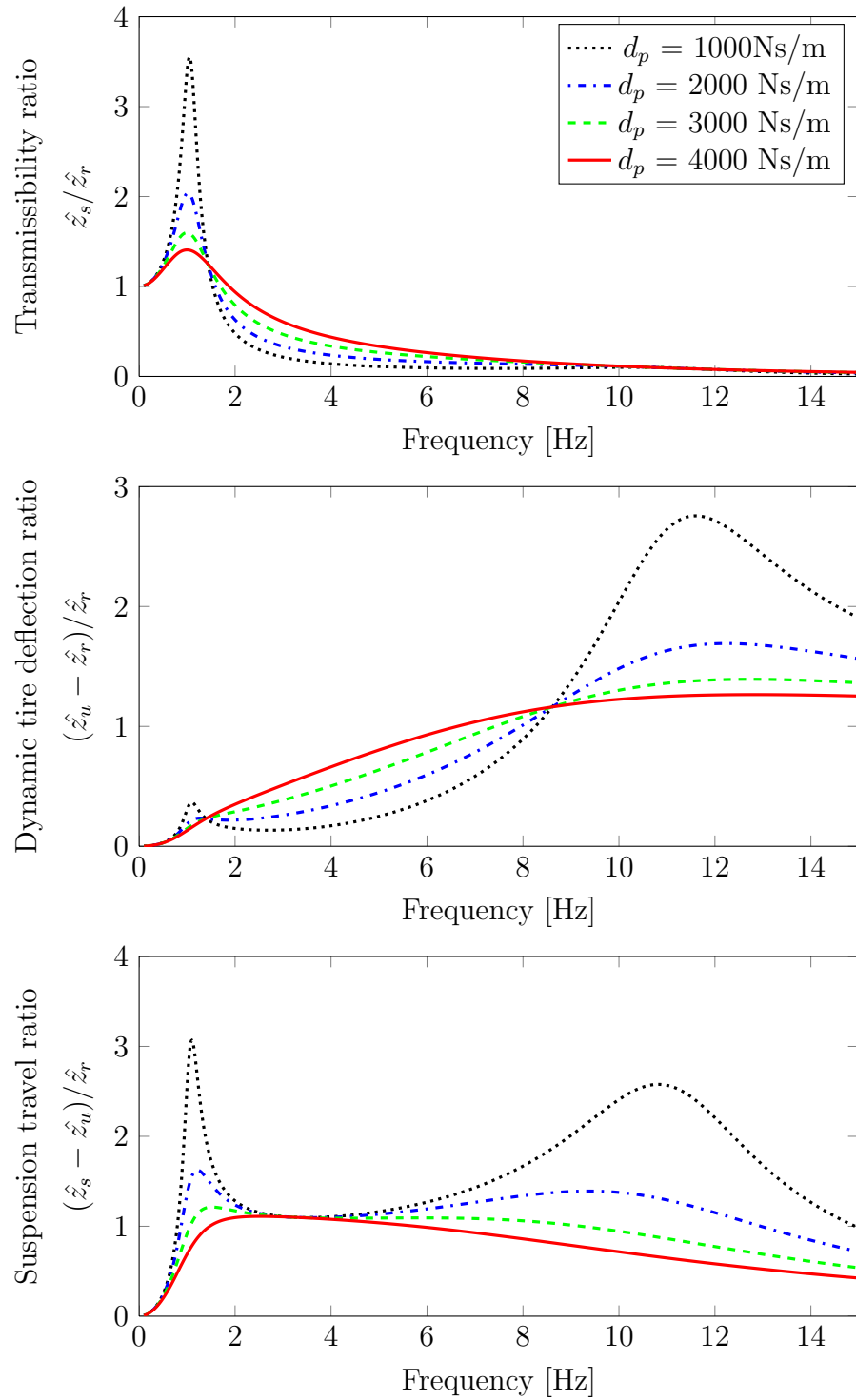


Figure 4.3: Effect of varying damping in a quarter car model

4.2 Effect of varying damping d_p

The variation of damping has an interesting effect on the frequency response functions. Keeping all other parameters same as in Table 2.1 and zero inertance, the damping is varied from 1000 N s/m to 4000 N s/m as shown in Figure 4.3. From the suspension travel ratio plot, it can be seen that more damping always leads to less suspension travel, which is also intuitive as a stiffer system would be more resistant to motion. But for the analysis of transmissibility and tire deflection, the plots can easily be divided into three frequency ranges:

1. Low frequency range (< 1.5 Hz): Both transmissibility ratio (comfort) and dynamic tire deflection ratio (handling) are low for high damping.
2. Mid frequency range (1.5 – 8.5 Hz): Low damping is favourable for both comfort and handling.
3. High frequency range (> 8.5 Hz): The effect of varying damping is negligible on the transmissibility ratio; dynamic tire deflection is lowered by higher damping.

This observation seems quite promising at first. If the damping in a suspension system can somehow be switched between two extreme values, one being very high and the other being very low (keeping the suspension deflection bounded), then by knowing the prominent frequency component in the input excitation, the suspension system can be made soft (for mid frequency range) or stiff (for low and high frequency range) to provide both comfort and handling simultaneously. Such a technique using MR damper has also been mentioned in [15]. Unfortunately, road excitation signal is never confined to a particular frequency range, and hence, it is almost impossible to tune the suspension damping through that method. This technique would, however, prove to be quite useful for systems which are excited within a certain frequency band at a time, for example, suspensions in electrical appliances, architectural suspensions, or any structure vibrating due to a rotating eccentric mass.

Tuning the damping for automotive suspensions would therefore, need more details about the system at each time step. This can be done either by measuring directly using sensors, or estimating from other measurements and a known system model.

4.3 Estimation

It was discussed that comfort and handling are two conflicting criteria for suspension design, and hence, when designing a control algorithm for a semi-active suspension (or active

suspension for that matter), it would be worthwhile to keep track of the two performance costs on-line and tune the weights assigned to the two criteria accordingly to obtain a balanced performance. Moreover, other variables like unsprung mass acceleration, suspension rattle velocity, etc. are also of interest for implementing the controller. The development of a control structure will be discussed in a later section; however, it is important to mention here that all these quantities of interest must be attainable using commonly available and economical sensors in a vehicle. Since an accelerometer on the vehicle body (sprung mass) has become almost standard equipment on all modern cars due to its use in other systems as well (like ABS and ESC), measurement of comfort objective is relatively easy. Similarly, measurement of the suspension travel (relative displacement between sprung and unsprung mass) is also possible using sensors like a potentiometer or an LVDT. On the contrary, direct measurement of tire forces requires quite expensive sensors, which are impractical for a passenger vehicle. Hence, in this chapter, a very simple filter based estimator has been designed for a quarter-car model to estimate the dynamic tire force by directly measuring two values: sprung mass acceleration \ddot{z}_s and relative displacement between sprung and unsprung mass ($z_s - z_u$) (suspension travel), the sensors for which are relatively economical and practical to mount.

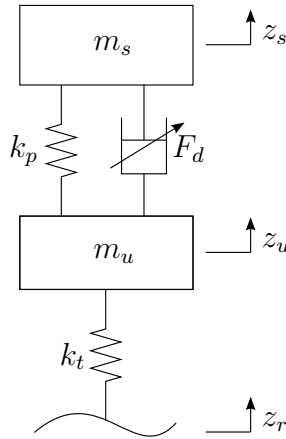


Figure 4.4: Quarter car model with a variable damping force

Ideally, the estimation of normal tire force should be quite straightforward, as can be shown by the following equation manipulations. Considering a quarter-car model with a general damping force F_d as shown in Figure 4.4, the equations of motion can be written as follows

$$m_s \ddot{z}_s = -k_p(z_s - z_u) + F_d \tag{4.1}$$

$$m_u \ddot{z}_u = k_p(z_s - z_u) - F_d - k_t(z_u - z_r) \tag{4.2}$$

Adding the above two equations,

$$m_s \ddot{z}_s + m_u \ddot{z}_u = -k_t(z_u - z_r) = F_{tire} \quad (4.3)$$

As mentioned earlier, the two outputs available are sprung mass acceleration and suspension travel. Knowing m_s and m_u , the dynamic tire force can be calculated from Eq (4.3) as

$$|F_{tire}| = \left| (m_s + m_u) \dot{z}_s - m_u \frac{d^2}{dt^2}(z_s - z_u) \right| \quad (4.4)$$

The velocity of the sprung mass \dot{z}_s (required for Skyhook control) can be directly calculated by integrating the acceleration signal \ddot{z}_s .

The suspension rattle velocity ($\dot{z}_s - \dot{z}_u$) can be calculated by differentiating the relative suspension displacement ($z_s - z_u$) and the velocity of the unsprung mass \dot{z}_u (required for Groundhook control) can then be obtained as $\dot{z}_s - (\dot{z}_s - \dot{z}_u)$.

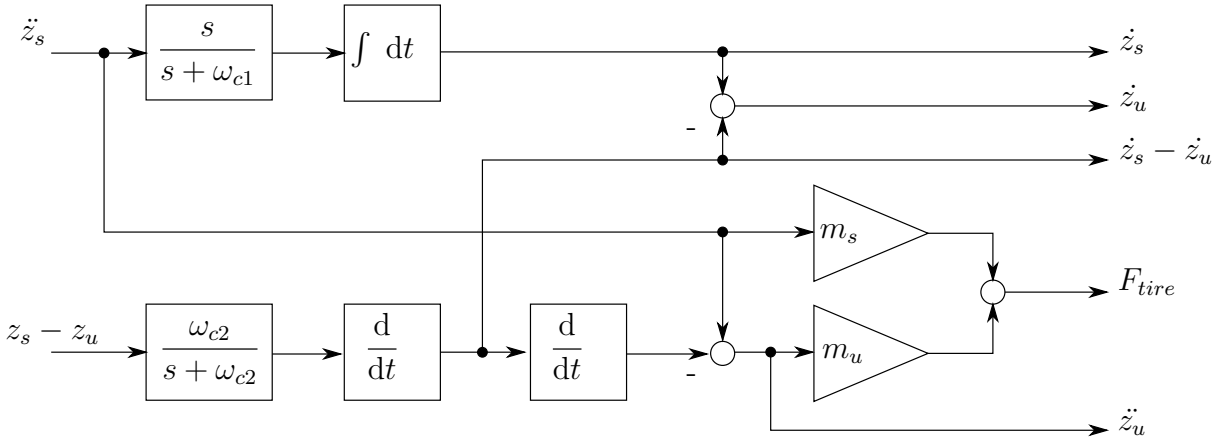


Figure 4.5: Estimator structure for various states of the system

However, these methods assume perfect measurement by the sensors. In practice, sensor values are full of noise. Differentiating those noisy signals would generate spikes and integrating it would result in drifts. Therefore, some filters need to be applied to obtain usable data. Since that noise is generally high-frequency Gaussian, a first order low-pass filter with cut-off frequency around 30 Hz before a derivative operator and a high-pass filter with cut-off frequency around 0.5 Hz before an integrator should give practically useful results. It has been mentioned before that the signal from road excitation has major content well within this frequency band. The structure of the estimator is given in Figure 4.5.

This is a very simple approach for estimation. Although more complex estimators like Extended Kalman Filter (EKF) can provide more accurate results, it gives practically useful data for the proof of concept of the controller, as shown in Section 5.2 where the

results from this estimator are compared with actual measured tire force using a wheel load sensor on a test vehicle.

4.4 Adaptive semi-active suspension control

In this section, a control algorithm for semi-active suspensions will be developed. First, a handling oriented control scheme analogous to the R-S control is proposed. Then, it is integrated with the R-S control algorithm for comfort by introducing a modification of the adaptive control structure presented in [25] to finally obtain a controller which is simple, economical to implement, and automatically distributes its priority between comfort and handling on-the-run as per the requirement.

Considering a quarter-car model with a general damping force F_d as shown in Figure 4.4, the equations of motion can be written in a modified form as follows

$$m_s \ddot{z}_s = -k_p(z_s - z_u) + F_d \quad (4.5)$$

$$-k_t(z_u - z_r) = m_u \ddot{z}_u - k_p(z_s - z_u) + F_d \quad (4.6)$$

From Eq (4.6), it can be derived that the tire force would approach to zero (thereby providing better handling) for a damping force of

$$F_d = -m_u \ddot{z}_u + k_p(z_s - z_u) \quad (4.7)$$

However, since F_d is a passive force, this rule has to be modified to accommodate the passivity constraint.

$$F_d = \begin{cases} -m_u \ddot{z}_u + k_p(z_s - z_u) & \text{for } (-m_u \ddot{z}_u + k_p(z_s - z_u))(\dot{z}_s - \dot{z}_u) \leq 0 \\ 0 & \text{for } (-m_u \ddot{z}_u + k_p(z_s - z_u))(\dot{z}_s - \dot{z}_u) > 0 \end{cases} \quad (4.8)$$

Similarly, from Eq (4.5) the acceleration of the sprung mass would approach to zero (thereby providing better comfort) for a damping force of

$$F_d = k_p(z_s - z_u) \quad (4.9)$$

which basically becomes the R-S controller after satisfying the passivity constraint (as in Eq (2.32)).

The two control schemes mentioned above cater to their own specific performance objective only. Hence, if there exists a weighting parameter $\alpha \in [0, 1]$, such that it defines the weights given to the two performance indices, and its value adapts itself online as

per the requirement from driving conditions, then a very simple yet elegant controller for semi-active suspension systems is obtained.

$$\begin{aligned} F_{adpt} &= \alpha(-m_u\ddot{z}_u + k_p(z_s - z_u)) + (1 - \alpha)(k_p(z_s - z_u)) \\ \Rightarrow F_{adpt} &= k_p(z_s - z_u) - \alpha m_u \ddot{z}_u \end{aligned} \quad (4.10)$$

The damping force is

$$F_d = \begin{cases} F_{adpt} & \text{for } F_{adpt}(\dot{z}_s - \dot{z}_u) \leq 0 \\ 0 & \text{for } F_{adpt}(\dot{z}_s - \dot{z}_u) > 0 \end{cases} \quad (4.11)$$

One interesting point to be noted here is that without the passivity constraint, Eq (4.10) gives a controller which can be applied to a fully active suspension system (like those in Section 2.2).

Hence, for one extreme value of the weighting parameter ($\alpha = 0$), the controller is purely comfort oriented, while for the other extreme value ($\alpha = 1$), the controller only focuses on handling. Now the problem has been reduced to appropriately adjusting the value of α for maximum performance improvement. An adaptive controller introduced in [39] had the basic idea that comfort is the objective, as long as the dynamic tire forces are within certain limits. The weighting parameter α varying between zero and one defines the level of this constraint violation. On similar lines but with some modifications to suit the requirements of this research, an adaptation scheme for α will be developed in the next section.

4.4.1 Calculation of weighting parameter α

From the method described in Section 4.3, the dynamic tire forces can be estimated from commonly available sensors, and thus, it can be constantly monitored for constraint violation. As discussed earlier, the RMS value is generally used to quantify a stochastic variable like tire force over time. However, during actual driving conditions, singular events like bumps and potholes suddenly change the tire forces, which might not appear in the RMS value that immediately. Hence, the absolute value also needs to be kept tracked of. The weighting parameter α , therefore, is derived from two components: slow adaptation (from RMS value $F_{tire,RMS}$) and fast adaptation (from instantaneous absolute value $|F_{tire}|$).

Assuming stochastic road input and Gaussian probability density of the dynamic tire force, its standard deviation over a time period T will be given by

$$\sigma_{F_{tire}} = \sqrt{\frac{1}{T} \int_0^T F_{tire}^2(\tau) d\tau} \quad (4.12)$$

Since the dynamic tire force has zero mean, its standard deviation is the same as its RMS value, i.e, $F_{tire,RMS} = \sigma_{F_{tire}}$. For a normally distributed zero mean stochastic signal, the 6- σ rule states that nearly all¹ of its values lie within the bounds of 6 standard deviations. Applying the 6- σ rule to dynamic tire force would mean that F_{tire} should remain within the bounds of the static tire force F_{stat} for most of the time T . In other words, the wheel almost never leaves contact with the ground. Mathematically, the constraint can be formulated as

$$F_{tire,RMS} \leq \frac{F_{stat}}{6} \quad (4.13)$$

where the static wheel load $F_{stat} = (m_s + m_u)g$.

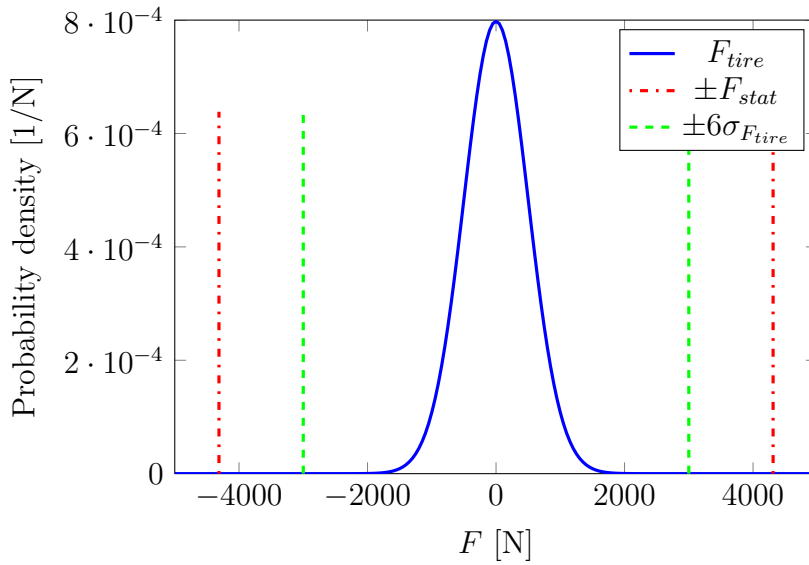


Figure 4.6: An example of probability density of F_{tire} for stochastic road profile with bounds for F_{stat} and $6\sigma_{F_{tire}}$

To also take into account the variation of F_{tire} due to singular events which might not reflect in its RMS value immediately, another constraint can be defined which takes into consideration its instantaneous value. It completely depends on the controller designer that what value of the ratio F_{tire}/F_{stat} is deemed permissible. Clearly, $F_{tire}/F_{stat} \geq -1$, with the extreme value of -1 indicating that the tire has just left contact with the ground. However, it would be too late if the controller waits for the ratio to become -1 before it changes the weighting parameter. Some buffer region is needed during which the controller can act and bring down the dynamic tire force. As an intelligent guess, a threshold of -80% is selected for the ratio of dynamic to static tire force. Mathematically,

$$F_{tire} + 0.8F_{stat} \geq 0 \Rightarrow F_{tire} \geq -0.8F_{stat} \quad (4.14)$$

¹99.999998027% of the time, to be precise

It should be noted here that only negative value of F_{tire} is responsible for leaving contact with the ground. However, since a tire has very low damping, a high positive value of F_{tire} would soon be followed by a high negative value. To avoid unnecessary chatter in the controller, the absolute value $|F_{tire}|$ can be used.

$$|F_{tire}| \leq 0.8F_{stat} \quad (4.15)$$

With the two constraint equations defined for slow and fast adaptation, a way can be developed to quantify the level of constraint violation. The adaptation structure is shown in Figure 4.7, where the input is the dynamic tire force F_{tire} (which will be the estimated tire force \hat{F}_{tire} in practice) and output is the weighting parameter α .

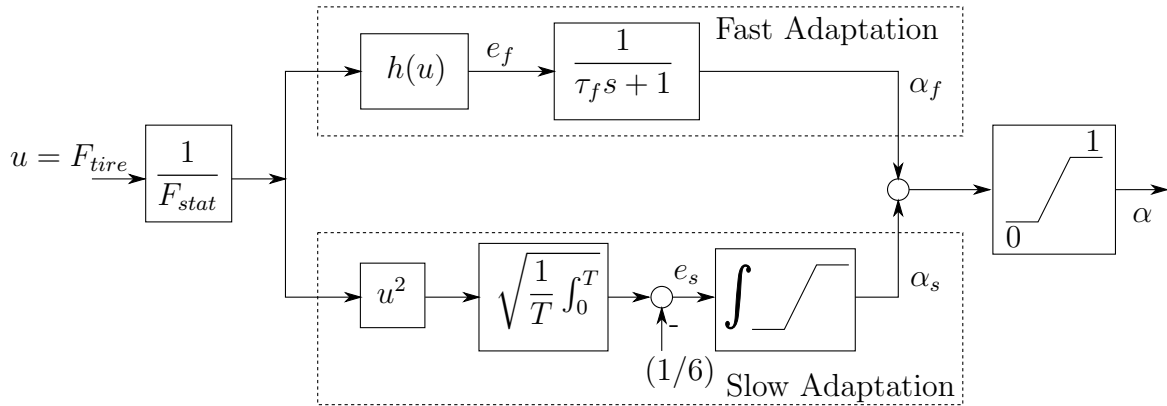


Figure 4.7: Structure of the adaptation logic to obtain scheduling parameter

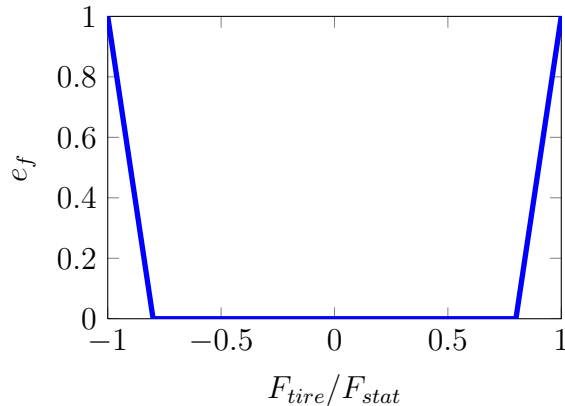


Figure 4.8: Heuristic function $h(u)$ for calculation of fast adaptation error e_f

The upper branch of the structure is responsible for fast adaptation. The ratio of dynamic to static tire force is input to a heuristic function $h(u)$ (Figure 4.8) which increases steeply from zero to one for input greater than 0.8. Just like the threshold value of 0.8,

the selection of heuristic function $h(u)$ is also based on intuitive guess. The only basic requirement for $h(u)$ is that it should increase sharply to one for input greater than 0.8. Although it can be considered as a parameter which can alter the performance of the controller, sufficiently good results are obtained in simulations and experiments (shown in later sections) for the shown linear curve, and hence, not changed. Since the absolute value of F_{tire} is considered, $h(u)$ is symmetric about y-axis. The output from $h(u)$ is error e_f which is then passed through a low pass filter with time constant τ_f to reduce the chatter and rapid variations in fast adaptation parameter α_f . The lower branch of the structure outputs the slow adaptation parameter α_s . The amount by which the RMS of the ratio of static to dynamic tire force deviates from the predefined threshold of 1/6, designated as slow adaptation error e_s , is integrated with output limited between zero and one. Finally, the two parameters from slow and fast adaptation are added, and the minimum of the sum $\alpha_f + \alpha_s$ and unity gives the final value of the weighting parameter α .

It should be noted here that since the final weighting parameter α appears in the expression for the controller in Eq (4.11), and it does not matter what are the individual contributions of the slow and fast adaptations. In other words, a positive value of α ensures that the tire does not leave contact with the ground, whether it is due to a bump (fast) or a rough road (slow). This might let one think that the controller performs the same in all conditions for a given value of the final weighting parameter α . However, it is not the case, as can be explained by this numerical example. Two scenarios are considered with same α values: $\alpha_f = 0.5, \alpha_s = 0$ ($\alpha = 0.5$) and $\alpha_f = 0, \alpha_s = 0.5$ ($\alpha = 0.5$). Clearly, the first scenario involves a bump on an otherwise smooth road, while the other is a rough road profile, like gravel. Although the controller will perform the same for the two scenarios, but it is true only for that particular time instant. Since α_f changes quite fast compared to α_s , at the next time step, the value of the two α 's will be completely different. Hence, the controller, on the whole, will perform completely different on a bump and on gravel.

4.5 Simulation results

A two degree-of-freedom (dof) quarter car model was modeled in MapleSim and simulated with different road profiles (rough, smooth, bump) as input (modeled in time domain as described in Section 2.6.2) and with different controllers. Assuming that the damping force can be varied to any arbitrary value within some bounds and all the required variables are either measured or estimated (Section 4.3), the proposed adaptive controller was then benchmarked against passive damping, skyhook and groundhook controllers. A passive damping of 1500 N s/m has been selected which provides a really good compromise between comfort and handling for quarter car parameters shown in Table 4.1, which are very close

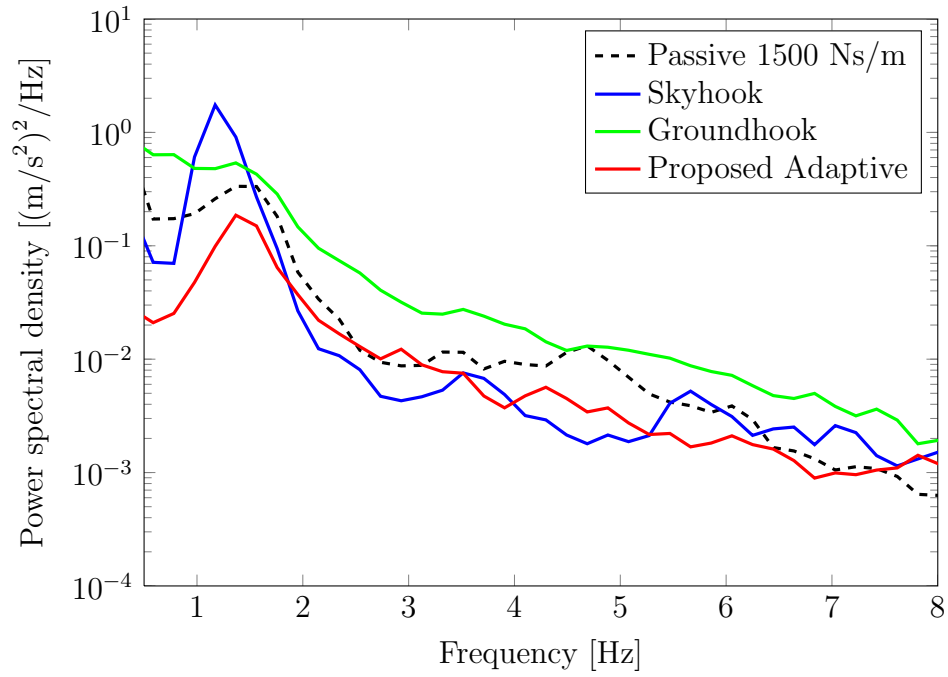
to that of the front-left suspension of a Cadillac STS (used for experimental verification in the next chapter).

Table 4.1: Quarter-car parameters used in simulation of different controllers

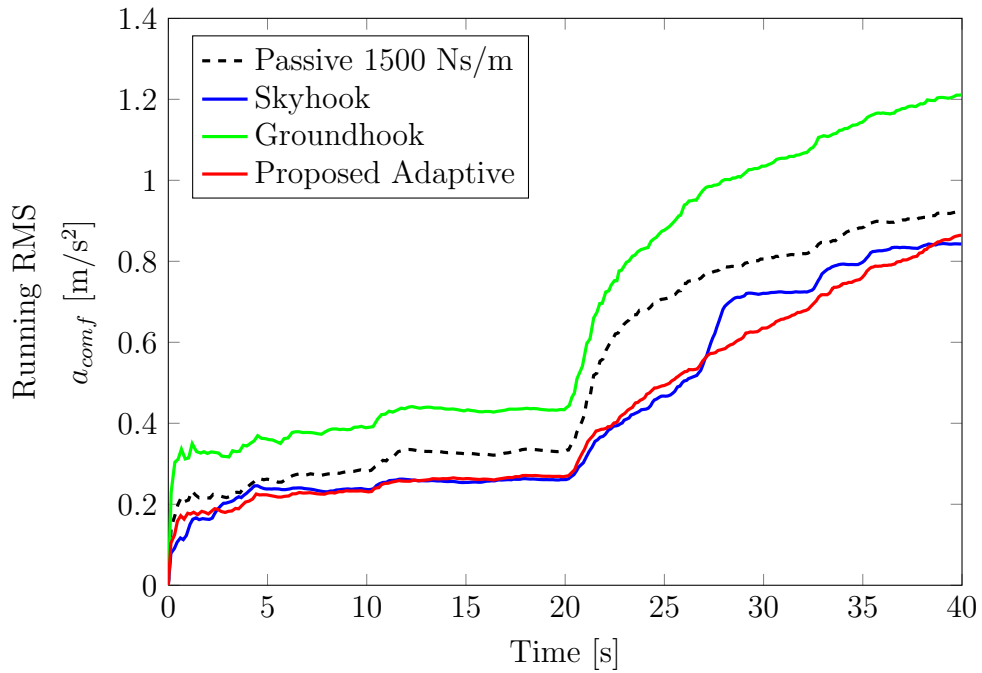
Parameter	Description	Value
m_s	Sprung mass	493 kg
m_u	Unsprung mass	62 kg
k_p	Spring stiffness	35 600 N/m
k_t	Tire stiffness	277 000 N/m

Figure 4.9 shows the simulation results for a transitional road input, where initially, the road profile is smooth (type-A), but switches to rough (type-C) at $t = 20$ s, the total simulation time being 40 s. The power spectral density of the acceleration of the sprung mass in the frequency band of maximum human sensitivity is shown in Figure 4.9a as an index of comfort. It is seen that over the expected result of skyhook controller being better and groundhook controller being worse than a passive system in improving comfort, the proposed adaptive algorithm shows a performance ranging from close to slightly better than the skyhook. A peak is discernible in the 1-2 Hz region which is clearly the resonant frequency of the sprung mass. The new controller seems to do a quite good job in reducing this peak as well. To quantitatively visualize the effect on comfort over time, the running RMS of comfort weighted acceleration is plotted in Figure 4.9b. It can be clearly observed here the adaptive controller offers a comfortable ride in both the road conditions.

It might occur to the reader that the difference in the performance of skyhook and proposed controller is not significant enough. However, the actual strength of adaptive controller can be seen in Figure 4.9c, which compares the running RMS of the tire force with different controllers. While the skyhook controller leads to exceedingly high dynamic tire force, the adaptive controller shows handling as good as that of the groundhook controller, which, however, is not good in providing comfort. Hence, the true efficacy of the proposed adaptive controller is providing a better compromise between comfort and handling than a passive system. The core of this controller are the adaptation parameters and Figure 4.9d shows how these parameters vary for the given case of smooth to rough road conditions. The fast adaptation parameter α_f is almost zero throughout, except for a small peak at $t = 20$ s where the road type changes abruptly. The slow adaptation parameter α_s , on the other hand, is zero on smooth road as the RMS of dynamic tire force is quite low and does not violate the 6σ condition described in Section 4.4. It is when the road becomes rough that the tire force starts hitting bounds resulting in slow adaptation error e_s and thereby a positive slow adaptation parameter α_s . Since the running RMS of the dynamic tire force keeps increasing from $t = 20$ s to $t = 40$ s, so does α_s . The final weighting parameter α

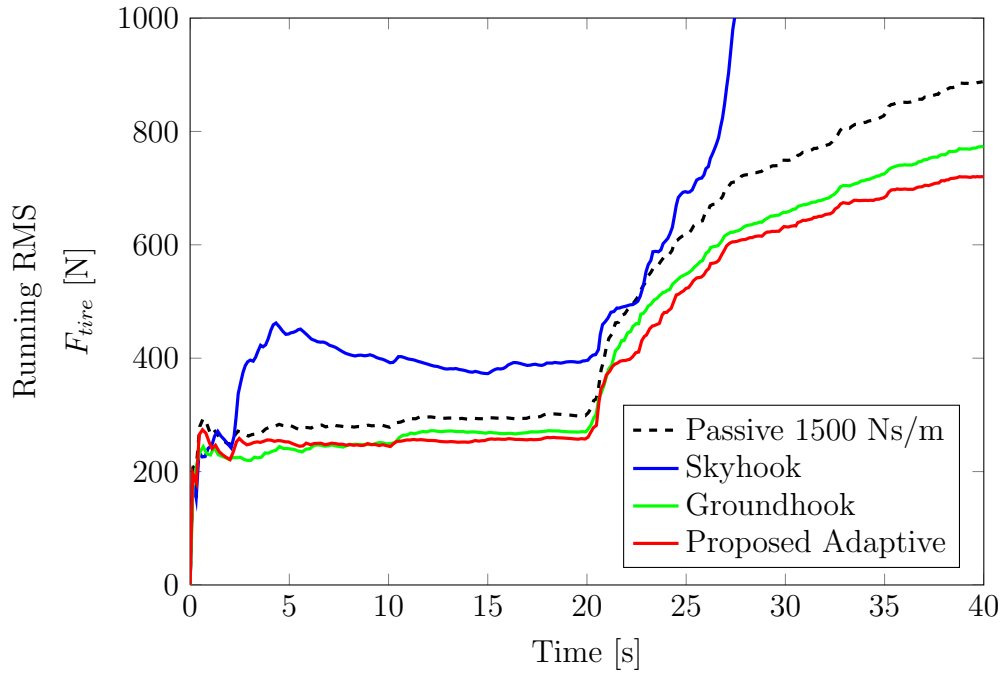


(a) Power spectral density of the acceleration of the sprung mass in the frequency band of maximum human sensitivity

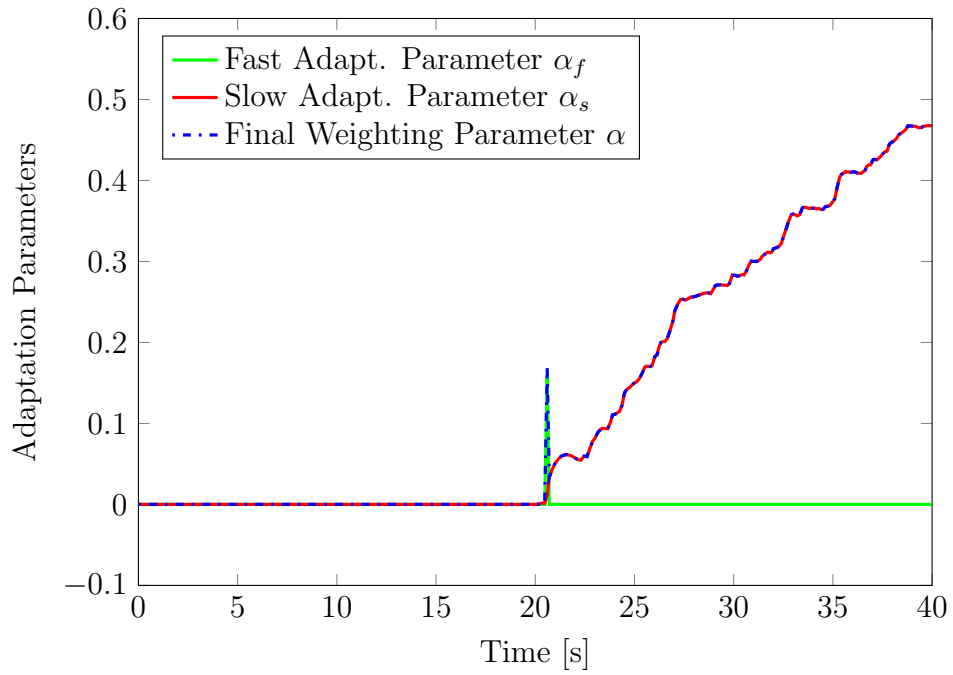


(b) Running RMS of comfort weighted acceleration of the sprung mass

Figure 4.9: Simulation results for a transition from type-A road to type-C road at 15 m/s (cont.)



(c) Running RMS of the dynamic tire force



(d) Variation of adaptation parameters with time

Figure 4.9: Simulation results for a transition from type-A road to type-C road at 15 m/s

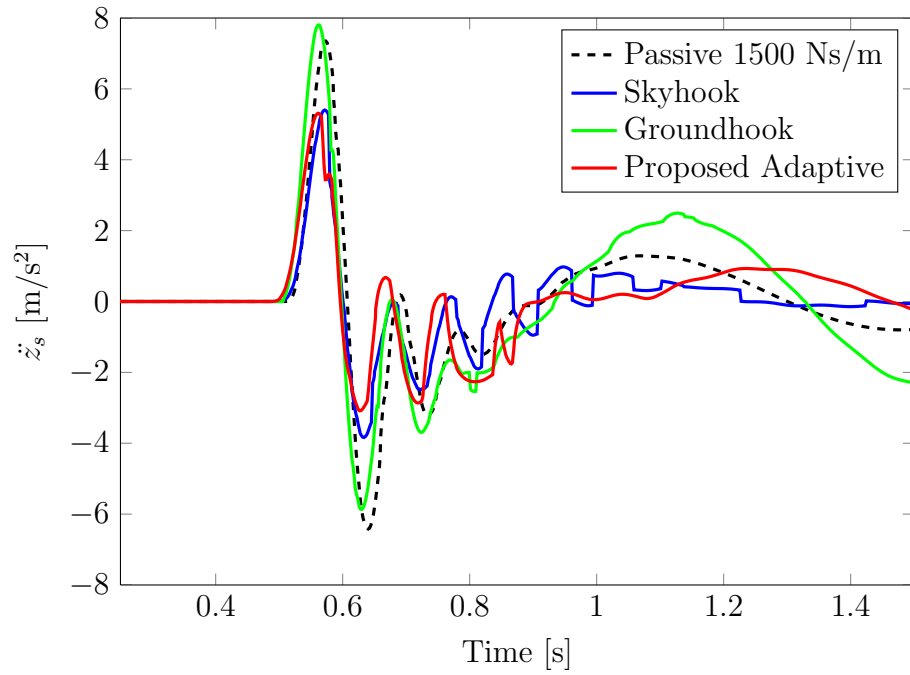
being the sum of the slow and fast adaptation parameters is almost the same as α_s in this case.

As mentioned before, the modeled quarter car system was also simulated with a bump as the road input. Figure 4.10 shows the results for a bump of height 6 cm, width 1.5 m and vehicle speed 10 m/s; quite similar to that shown in Figure 2.11. The bump starts at $t = 0.5$ s. Since a bump is a transient event, the instantaneous values for chassis acceleration and tire force are generally of interest (and significance) than their RMS values. The variation of the acceleration of the sprung mass with time is plotted in Figure 4.10a for the same four controllers in action as described before. Again, with the proposed adaptive controller, the comfort is seen to be better than the passive system and very close to the skyhook controller in terms of peak in sprung mass' acceleration. The adaptive controller also manages to reduce the oscillations in \ddot{z}_s a few moments after crossing the bump, unlike other controllers. This is due to its ability to change the weighting parameter online.

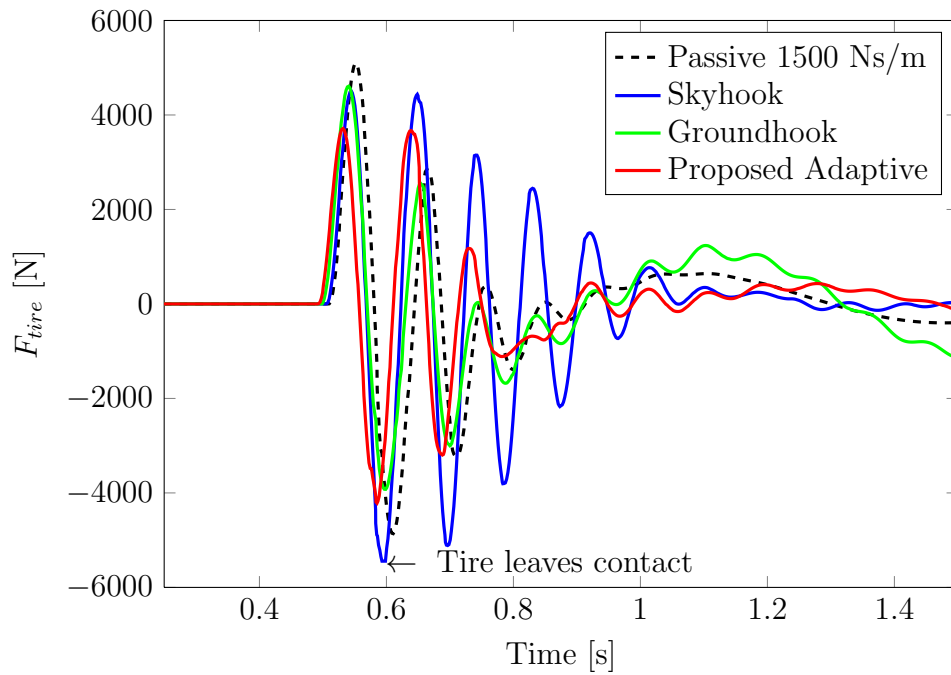
Even after providing a comfortable pass over the bump, the proposed adaptive controller does not lead to high fluctuations in dynamic tire force like those with skyhook controller. This is quite crucial during normal driving conditions. When a vehicle passes over a bump at medium to high speeds, the tire might leave contact with the ground as observed in the results in Figure 4.10b. If a driver tends to apply brakes or a steering input in this time duration, the normal force between the ground and tire would not be sufficient enough to produce a braking or cornering effect. Hence, for a controlled handling and ride safety, F_{tire} should be within bounds as is successfully done with the adaptive controller. It should be noted that a phase difference between the different plots has been intentionally added for distinctive clarity.

In the case of a bump, the fast adaptation parameter α_f plays the major role (Figure 4.10c). As the absolute value of F_{tire} crosses the threshold of 0.8 times the static tire force, the fast adaptation error e_f rises sharply as output from the heuristic function $h(u)$, which effectively generates high value of α_f . As soon as F_{tire} is brought under control, there is no critical requirement of adaptation parameters and they approach back to zero.

Now that it has been established from theoretical simulations that an efficient adaptive controller has been designed, it must be validated through actual practical implementation. However, as this is a generic controller applicable to any suspension system with an active or passive force source, and a prototype consisting of a mechatronic suspension strut with variable shunt impedance was not constructed due to impracticability on passenger vehicles, the controller can be very well be tested on a passenger vehicle with MR dampers. This will be done in the next chapter.

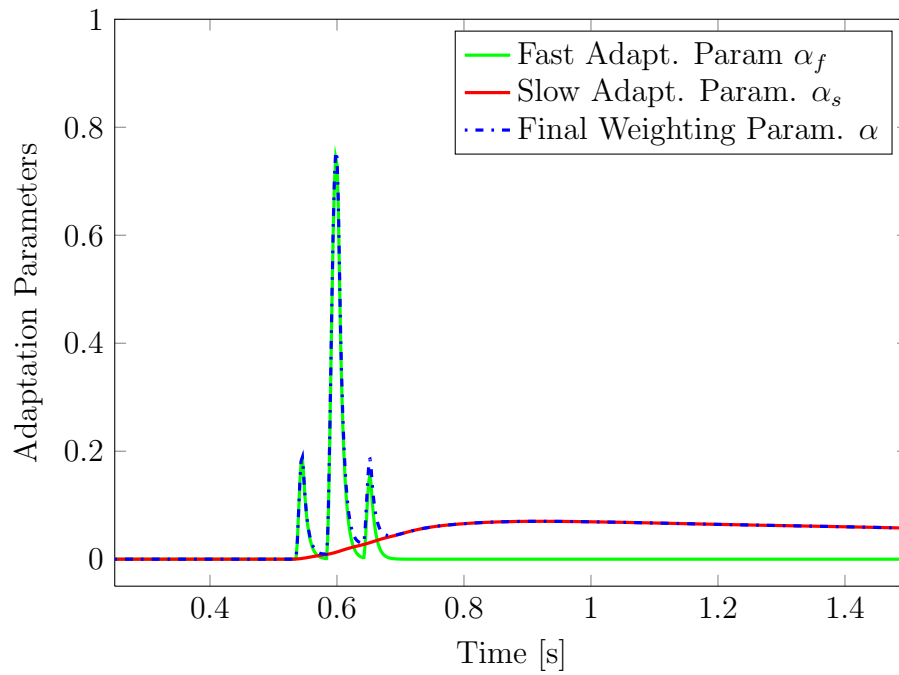


(a) Variation of acceleration of the sprung mass with time



(b) Variation of dynamic tire force with time

Figure 4.10: Simulation results for over a bump at speed 10 m/s (*cont.*)



(c) Variation of adaptation parameters with time

Figure 4.10: Simulation results for over a bump at speed 10 m/s

Chapter 5

Experimental Validation

Before discussing the performance of the controller in experiments, this chapter first describes in detail the experimental setup and implementation of theory in practice. Then the normal tire force estimator is validated and the MR damper installed in the vehicle is characterized. Finally, the proposed controller's performance is evaluated performing road tests with different controllers.

5.1 Description of the experimental setup

All the experiments in this research are performed on a fully instrumented Cadillac STS at the Mechatronic Vehicle Systems Lab., University of Waterloo. This vehicle was factory-equipped with MR dampers at all the four suspension corners, and for the purpose of this research, the front-left damper was hacked into by disconnecting the original connector and mounting a custom connector using which the current supplied to the damper can be varied as required. Since the vehicle is extensively used at the aforementioned laboratory for various research purposes, it is installed with several sensors, data acquisition boards, processor, etc. However, in this document, the hardware relevant to this research only will be described.

A six-axis inertial navigation system (Datron technology) can measure the linear acceleration and velocity of the vehicle along all three axes, i.e., longitudinal, lateral and vertical; and the three rotational movements, i.e., roll, pitch and yaw. Out of these six degree of freedoms, only heave (vertical), roll and pitch are affected by the suspension system, and hence were recorded. The vehicle is also equipped with load sensors at the wheels which can measure forces and moments along all three axes at the contact patch, and for the purpose of studying the suspension system, only the vertical tire force was recorded. To measure the suspension travel, a string potentiometer was mounted between the chassis and the suspension control-arm. A dSpace AutoBox mounted with an I/O and

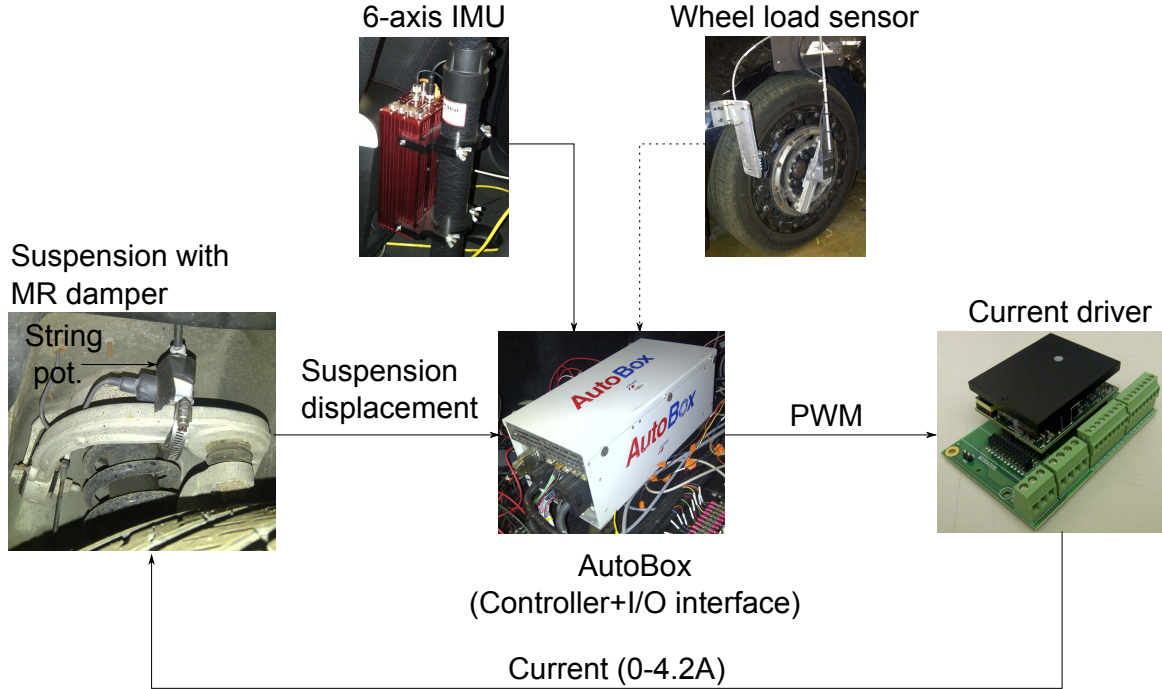


Figure 5.1: Structure of the experimental setup

a processor board is installed in the trunk of the car through which sensor data can be recorded, as well as a required PWM signal can be generated. A servo drive with current operation mode (AZ20A8DDC from Advanced Motion Controls) takes a PWM signal as input and supplies amplified current proportional to the signal's duty-cycle to the coils of MR damper. The structure of this experimental setup has been depicted in Figure 5.1. The signal from the wheel load sensor is shown with a dashed line as it is supposed to be used only for verification; the controller actually works on estimated value of tire force.

Since most of the formulations till now were performed on a quarter car model which required the acceleration of the (quarter) sprung mass, but in the experimental setup only a single IMU is mounted on the vehicle, the acceleration of the front-left corner's sprung mass can be approximated from the vertical acceleration of the total vehicle's sprung mass and roll and pitch acceleration about its center of gravity assuming small angular movements. In an slightly modified SAE coordinate system [30] where the origin is at the CoG of the sprung mass (or chassis), the corner acceleration can be given by

$$\ddot{z}_{s_{LF}} = \ddot{z}_{s_{CoG}} - X_F \ddot{\beta} - Y_L \ddot{\alpha} \quad (5.1)$$

where Y_L and X_L are respectively the distances along the Y-axis and X-axis from the CoG of the chassis to the front-left tire contact patch as shown in Figure 5.2.

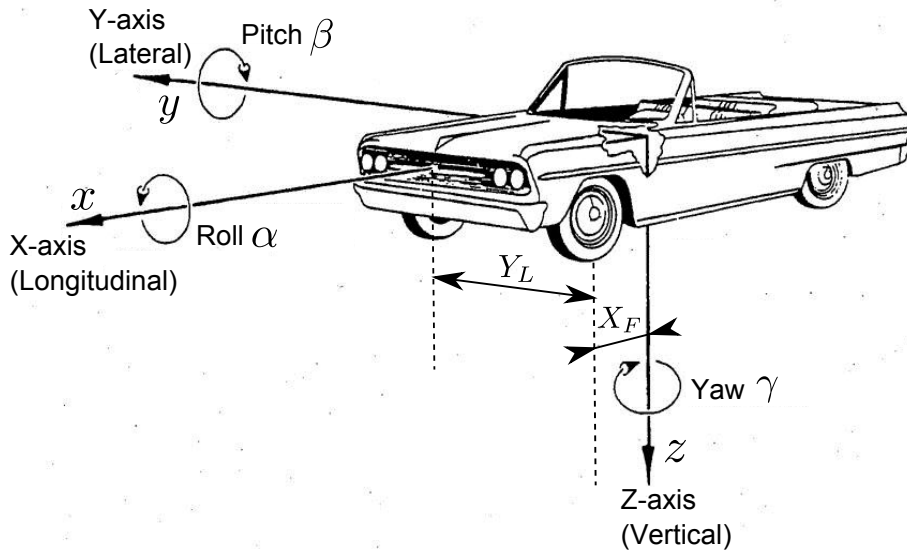
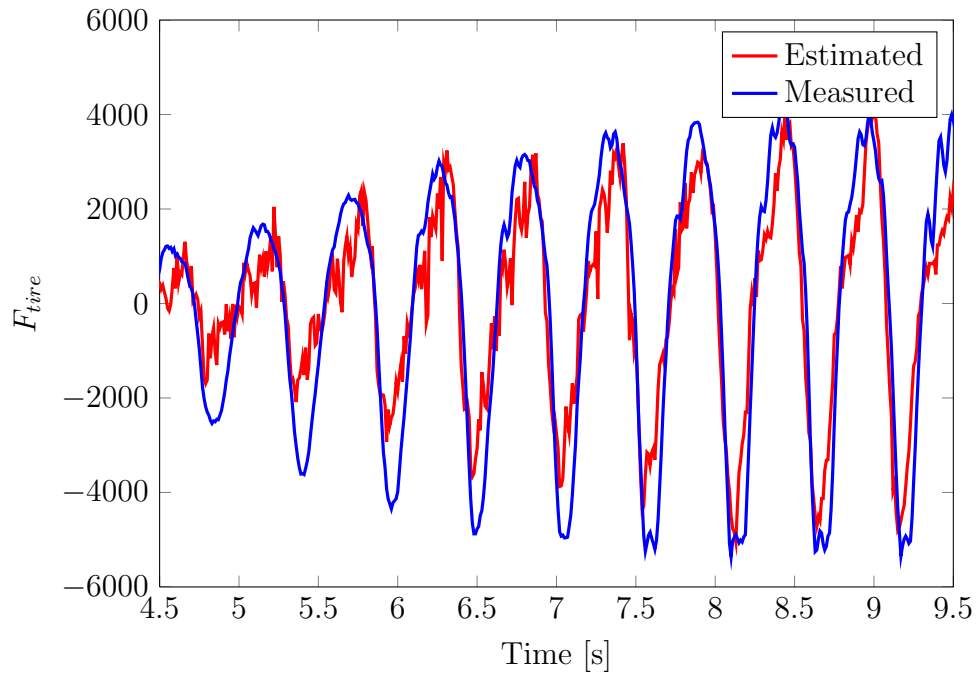


Figure 5.2: SAE Coordinate system for vehicle dynamics. Image adapted from [30] and then modified

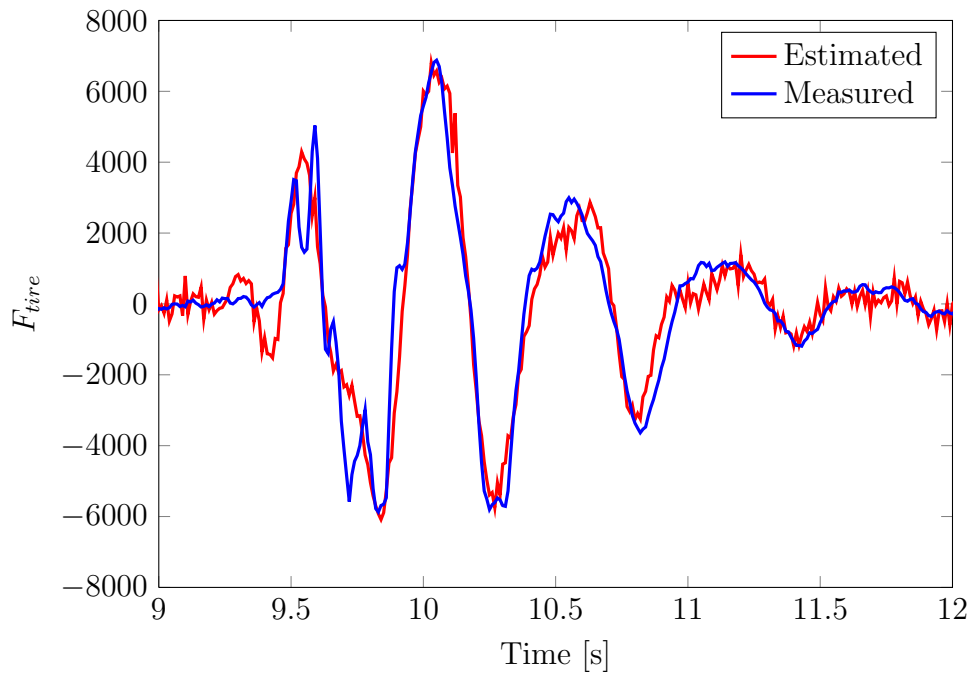
5.2 Validation of the estimator

The first test to be performed on the setup was to verify that the estimator for dynamic tire force mentioned in Section 4.3 gives practically useful results. Since the vehicle is equipped with highly sophisticated wheel load sensors, the exact normal force at the contact patch can be measured. By obtaining the static tire force when the vehicle is stationary, the dynamic tire force can easily be calculated by subtracting the former from every future measurement and then compared with the estimated values.

To obtain large but slow variations in F_{tire} for easy comparison, two types of vehicle runs were done. One was harsh pitching maneuvers in a straight line (periodic accelerating and braking) and second was driving over a speed bump at 40 km/h. The results from the two runs are shown in Figure 5.3, where it can be seen that the estimated F_{tire} follows the measured one. The difference in the two values can be attributed to factors like over-simplified model (quarter-car) and interaction of the other three wheels. A better method would be to use a sophisticated estimator which takes into account a complex model for the vehicle and inherent non-linearities, like Extended Kalman Filter (EKF). Nonetheless, the estimated value is good enough for the proof of concept of the adaptive controller in the following sections.



(a) Harsh pitching maneuvers



(b) Speed bump

Figure 5.3: Measured and estimated vertical tire force

5.3 Modeling the characteristics of an MR damper

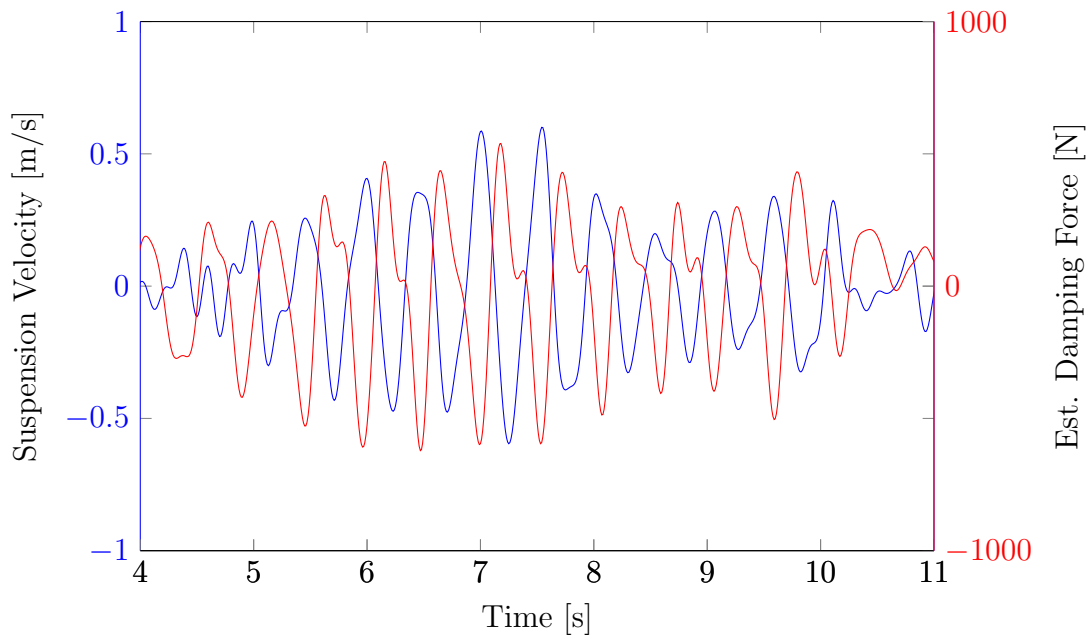
Before implementing any controller on the Cadillac STS, it is first necessary to have a characterization of the MR damper installed in it, which would comprise of a relation between the input current, the suspension rattle speed and the produced damping force. This would modify the controller such that it outputs a current i [A] instead of a damping force F_d [N], which is actually how it can be implemented on the vehicle.

The characterization of the MR damper was done on the vehicle itself without separately testing it. For different currents through the damper ranging from 0 A to 4.2 A, harsh pitching maneuvers in a straight line were performed for each current to obtain large variations in suspension speed. The damping force was estimated from the equation of motion of the unsprung mass (which makes it somewhat independent from the dynamics of the other three corners).

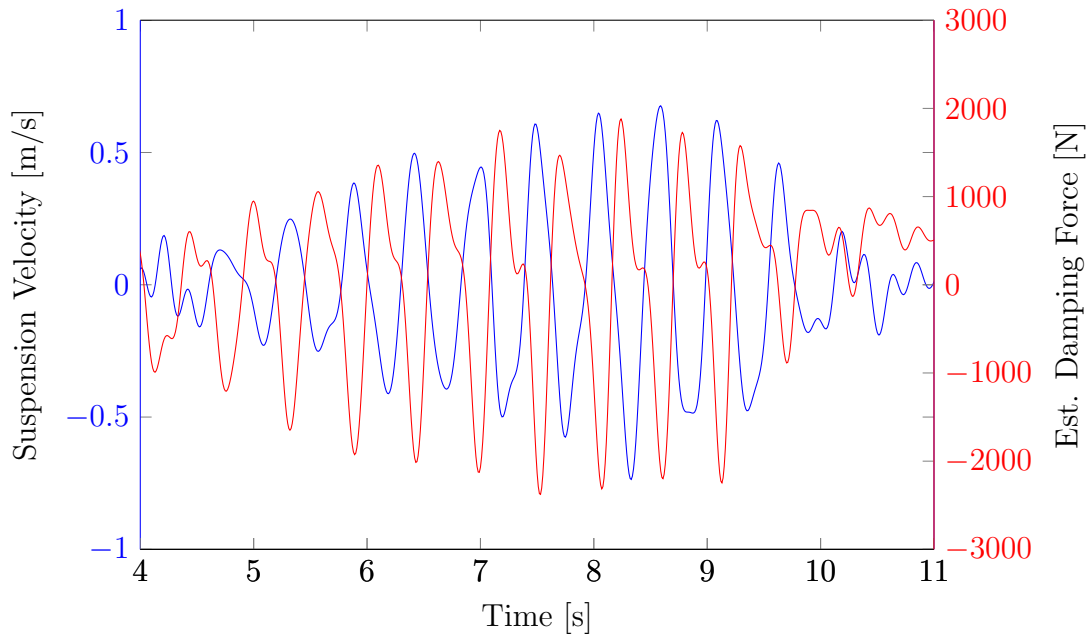
$$F_d = -m_u \ddot{z}_u + k_p(z_s - z_u) - k_t(z_u - z_r) \quad (5.2)$$

Some exemplary results from the tests are shown in Figure 5.4 for current value of 1.26 A and 3.36 A where both suspension velocity and damping force are plotted together using two y-axes for easy comparison. The two have opposite signs as expected from the fact that damping force always opposes relative velocity. Another feature to be noted is that the magnitude of the ratio of damping force to suspension velocity is higher for lower velocities. This implies that the damping coefficient is not constant at a given current. In other words, the damper is not a linear device. It can also be clearly observed that for the same suspension velocity, higher current produces more damping force, which is again expected from an MR damper. To obtain the final characteristic of the damper, the local extremum (peak) values of suspension velocity and damping force were considered for each current value and a smooth, shape-preserving curve was fit through the data points. Figure 5.4a and 5.4b show the obtained relation as a two and three dimensional map respectively.

However, for implementing in a controller, an inverse mapping is required which gives a current value for a given damping force and suspension speed. The inverse mapping obtained from the damper characteristic is depicted in Figure 5.7. If the required damping force is in the same direction as the suspension velocity, or if the required damping force is less than what is achievable by the minimum current (zero) at a given suspension velocity, the mapping outputs zero current. The maximum current has been limited at 4.2 A, so if an arbitrarily high damping force is required at a very low suspension velocity, the current output is 4.2 A.



(a) Current $i = 1.26$ A



(b) Current $i = 3.36$ A

Figure 5.4: Suspension velocity and estimated damping force for a given current and harsh pitching maneuvers

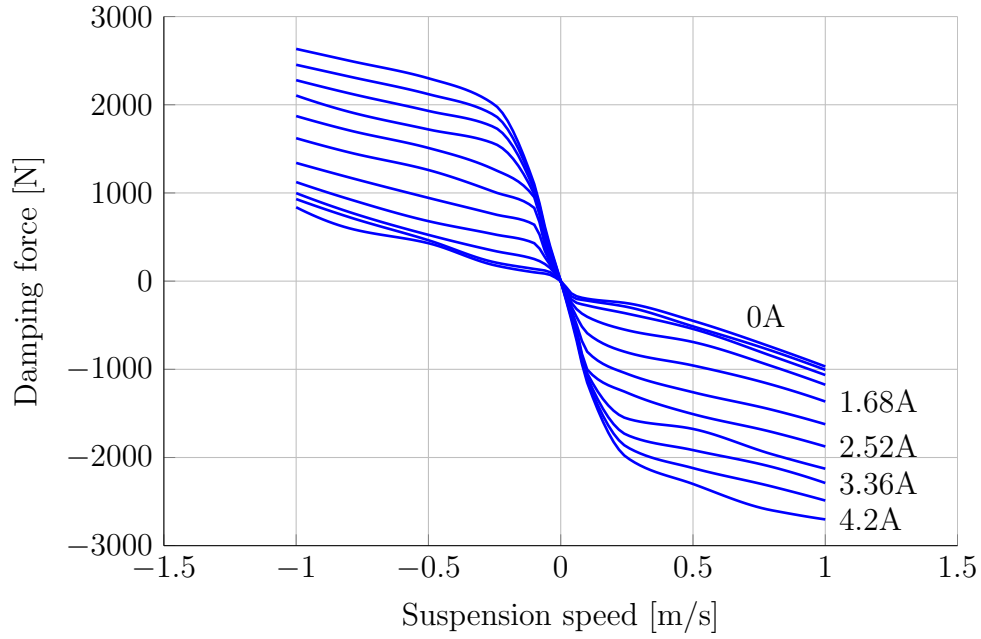


Figure 5.5: Characteristics of the MR damper (obtained after a smooth curve-fit) showing damping force as a function of suspension velocity at different currents

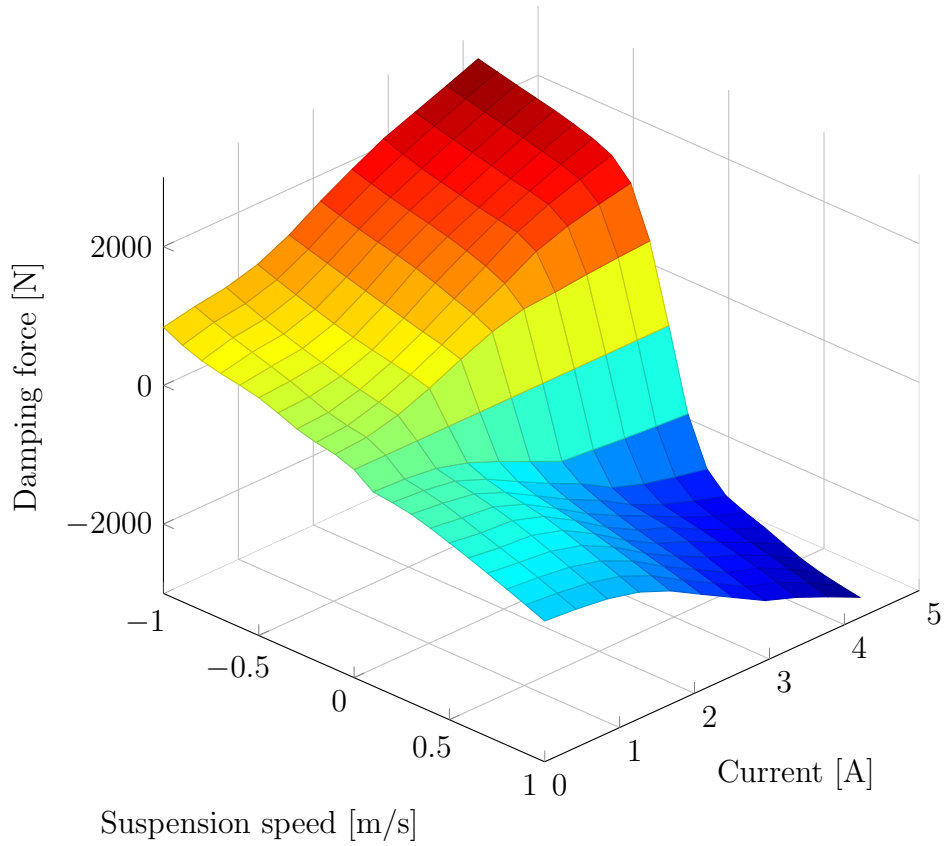


Figure 5.6: Characteristics of the MR damper as a 3D map

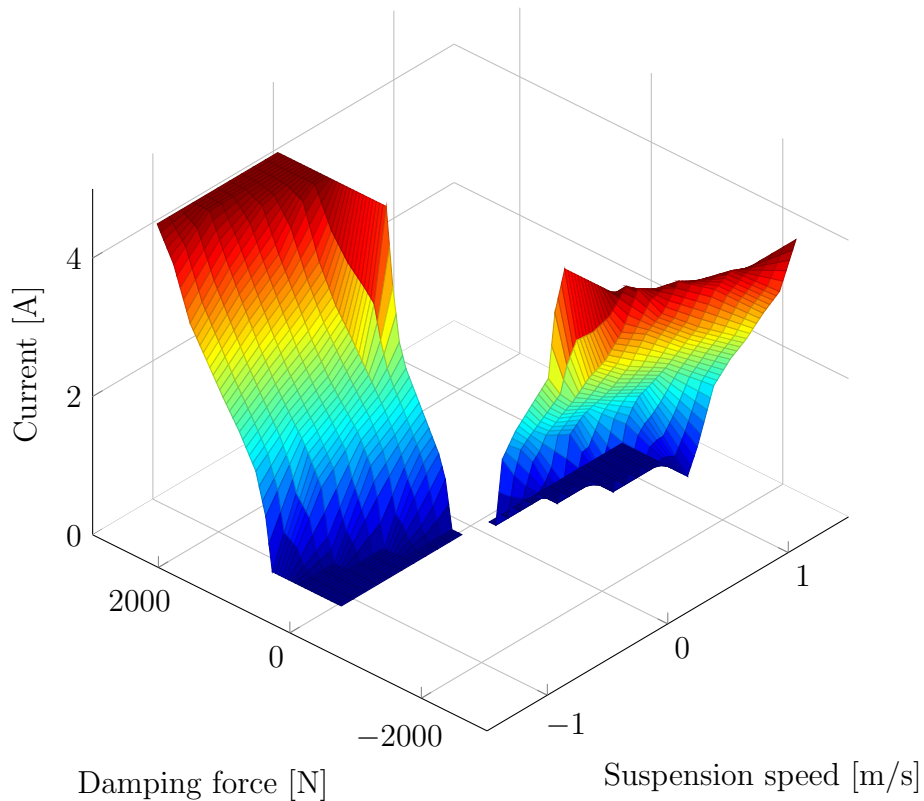


Figure 5.7: Inverse mapping from MR damper characteristics

5.4 Implementation of controllers and comparison of results

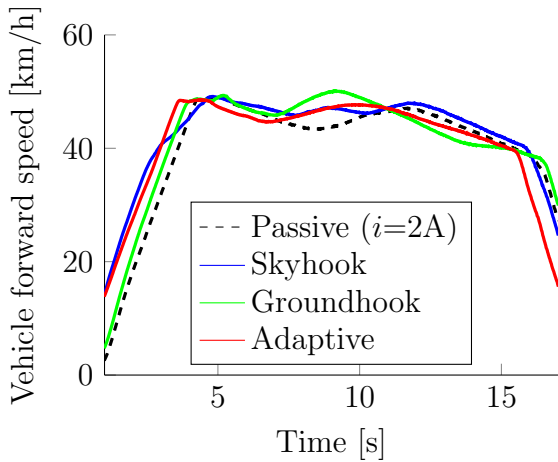
With the damper characteristics at hand and the estimator validated, the controllers could actually be implemented on the vehicle. Similar to the simulations, tests were performed on a track with smooth to rough (gravel) profile transition at a forward speed of 45 km/h, and over a speed bump at 40 km/h. The test conditions are shown in Figure 5.8, in the form of photographs of the roads and forward velocity of the vehicle (obtained from the IMU) for the four runs. Figure 5.10a is a satellite image of the the test track (obtained from Google Maps), which actually is Region of Waterloo Emergency Services Training Area [19]. The smooth road and gravel area are distinguishable due to color contrast. It was tried to keep the vehicle speed as constant as possible around 45 km/h, but slight variations (Figure 5.8c) could not be avoided in that rough ride. Due to limited length of this patch of road, the test results have been cropped to span $t=1$ s to $t=17$ s, duration during which the controllers were actually in action. Figure 5.8b shows the bump on ring road, UW, which was used for testing purposes. It was easier to keep the speed almost

constant at 40 km/h as shown in Figure 5.8d while driving over it, as the test duration was quite short and the road was otherwise smooth. The same criteria of PSD of the acceleration of the sprung mass (front-left corner in this case) and running RMS of the dynamic tire force is used for comparing the performance of different controllers, just as in simulations. To emulate a passive damper, a constant current of 2 A was supplied to the MR damper.

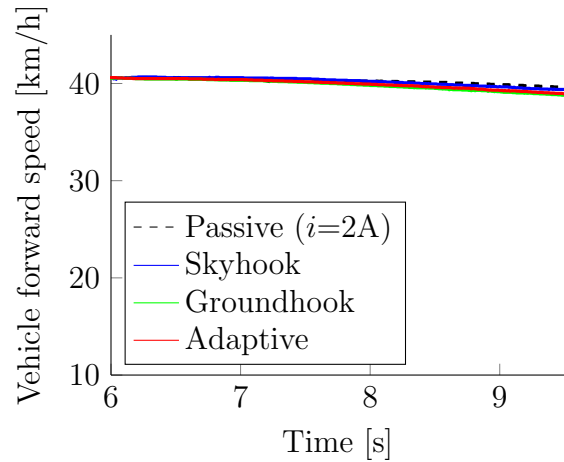


(a) Satellite image of the test track showing smooth and rough profiles [19]

(b) Image of the bump over which vehicle was tested



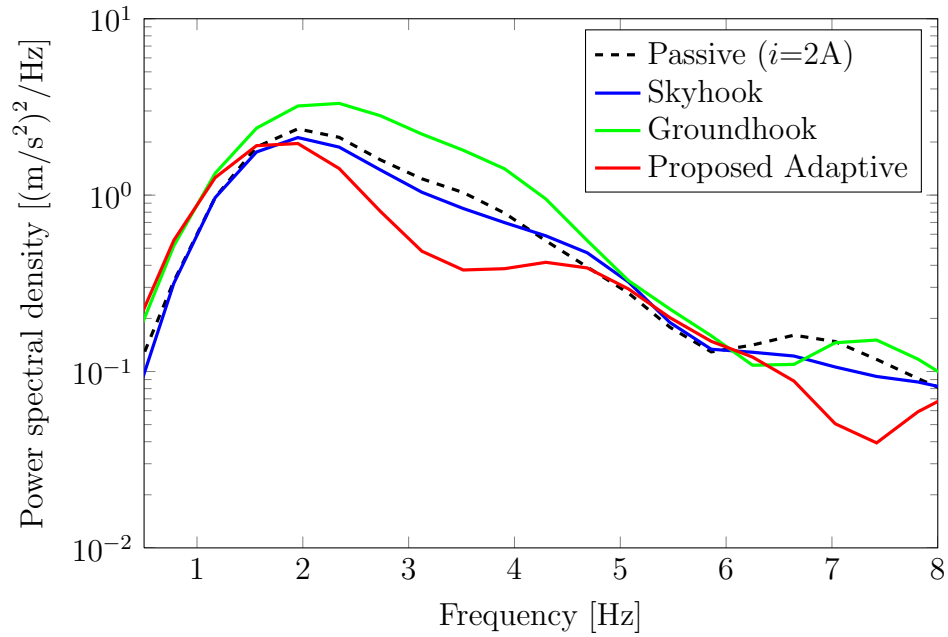
(c) Forward velocity of the vehicle for the four runs on test track



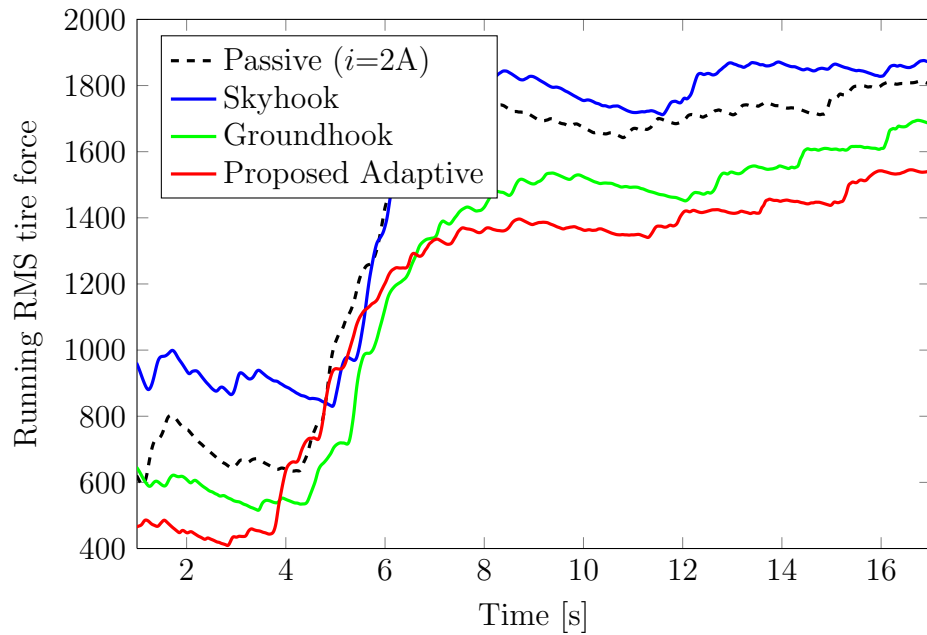
(d) Forward velocity of the vehicle for the four runs on bump

Figure 5.8: Experimental conditions

Figures 5.9a, 5.9b and 5.9c show the results for the smooth to gravel transitional track. The PSD of the sprung mass acceleration with the proposed adaptive controller was obtained to be lower than the passive and skyhook for most of the frequencies between 2-8 Hz, implying greater comfort. Groundhook controller is the worst in providing comfort. The

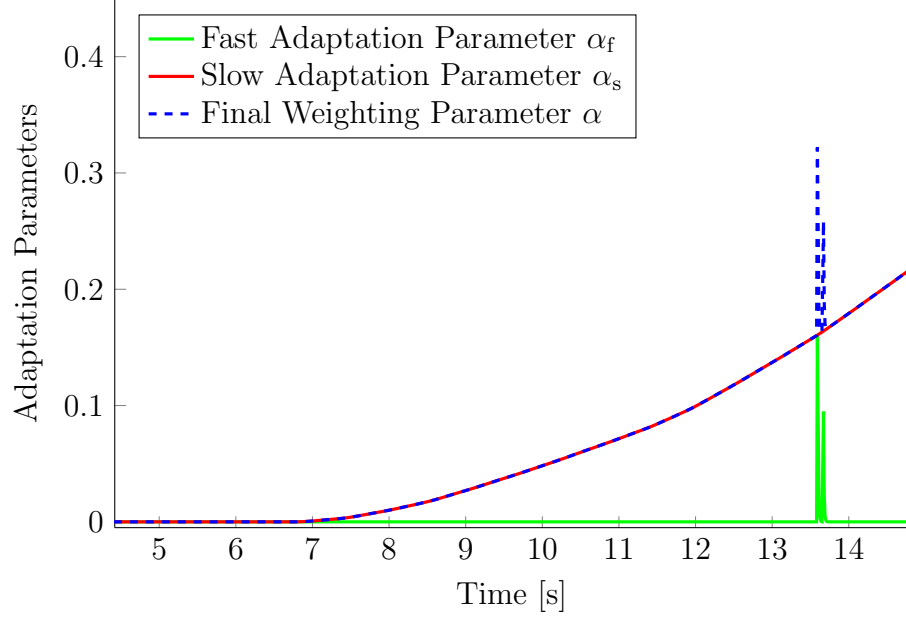


(a) PSD of the acceleration of the corner



(b) Running RMS of the dynamic tire force

Figure 5.9: Test results for a transition from smooth to rough (gravel) road at 45 km/h
(*cont.*)

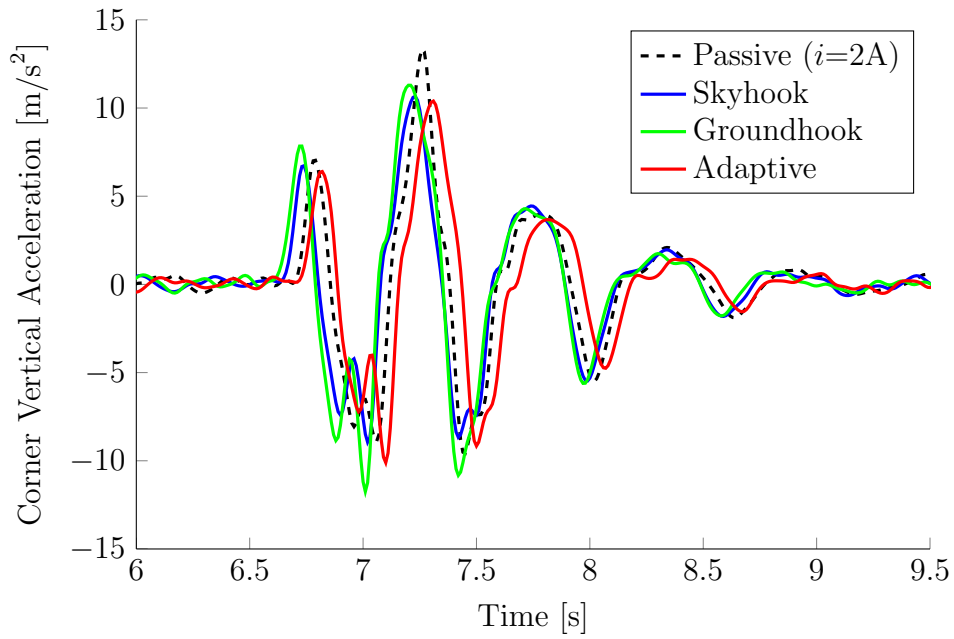


(c) Variation of adaptation parameters with time

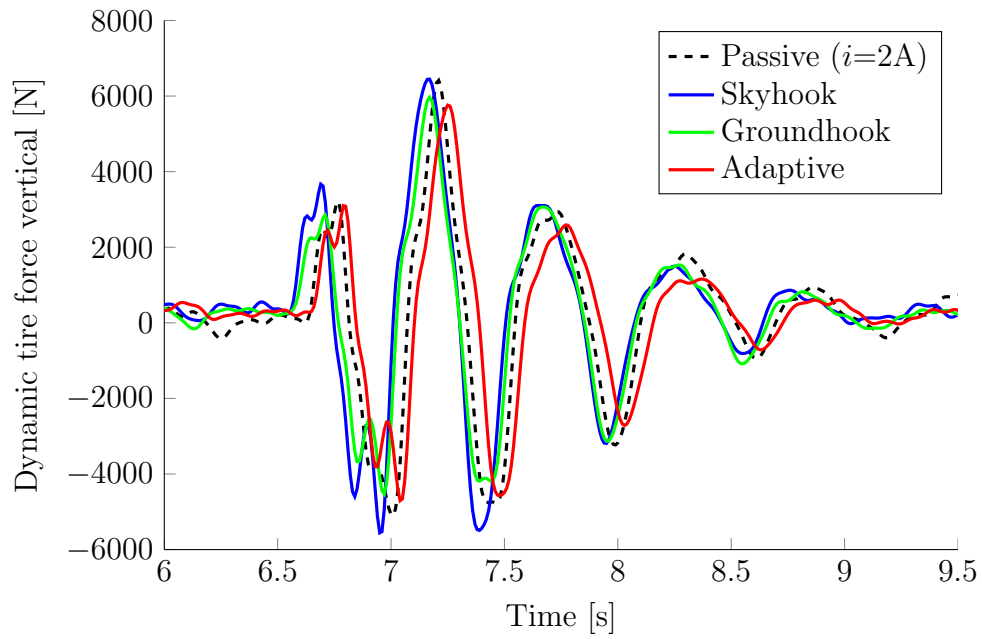
Figure 5.9: Test results for a transition from smooth to rough (gravel) road at 45 km/h

adaptive controller also shows better handling compared with passive and groundhook controller in terms of the running RMS of the tire force, while skyhook controller is worst in controlling dynamic tire force. Similar to the trend seen in the simulation results, the final weighting parameter α constitutes mostly of slow adaptation parameter α_s which increases gradually to account for the rough road and hence higher tire force. A peak seen in the fast adaptation parameter α_f was probably due to a rock in the gravel area.

Results from a test by running the vehicle over a bump at 40 km/h are presented in Figures 5.10a, 5.10b, 5.10c and 5.10d. A slight phase delay has been added in the first two plots for distinctive clarity. The peak value of corner's vertical acceleration with adaptive controller is almost equal to that obtained from skyhook controller, which is more comfortable than the passive suspension. The proposed controller also shows slightly less peak in the dynamic tire force compared with the groundhook controller, and substantially better than the passive suspension. Hence, overall, the adaptive controller gives a performance with less compromise between comfort and handling. Since the bump was on a relatively smooth road, there is no variation in the slow adaptation parameter α_s . The fast adaptation parameter α_f , however, has huge peaks during the time span of the bump. It is clipped at its highest value of one to obtain the final weighting parameter α . The variation of current with time can be seen in Figure 5.10d. Although there is no direct relation between α and the supplied current because the current depends on the required damping

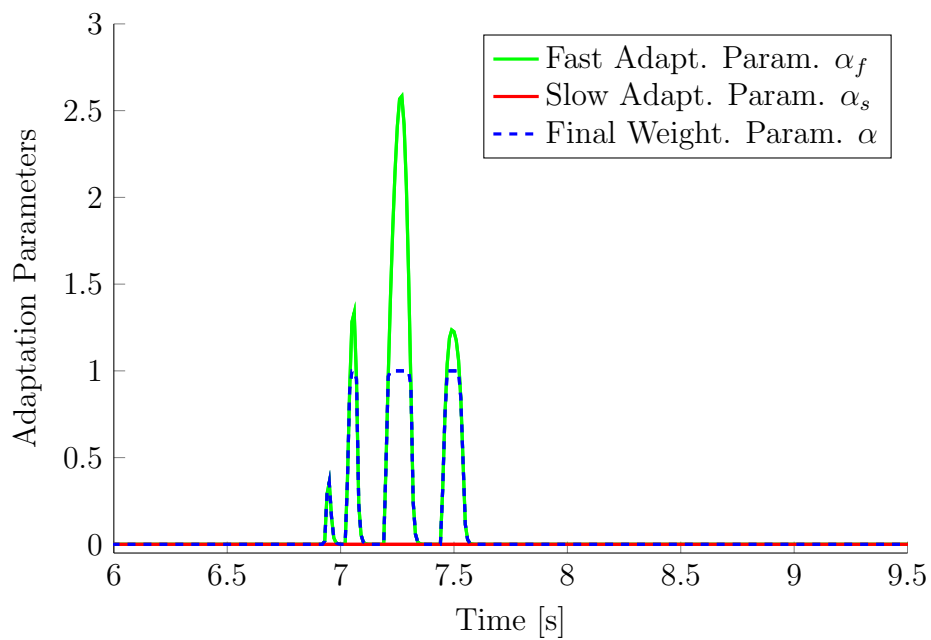


(a) Variation of acceleration of the corner with time

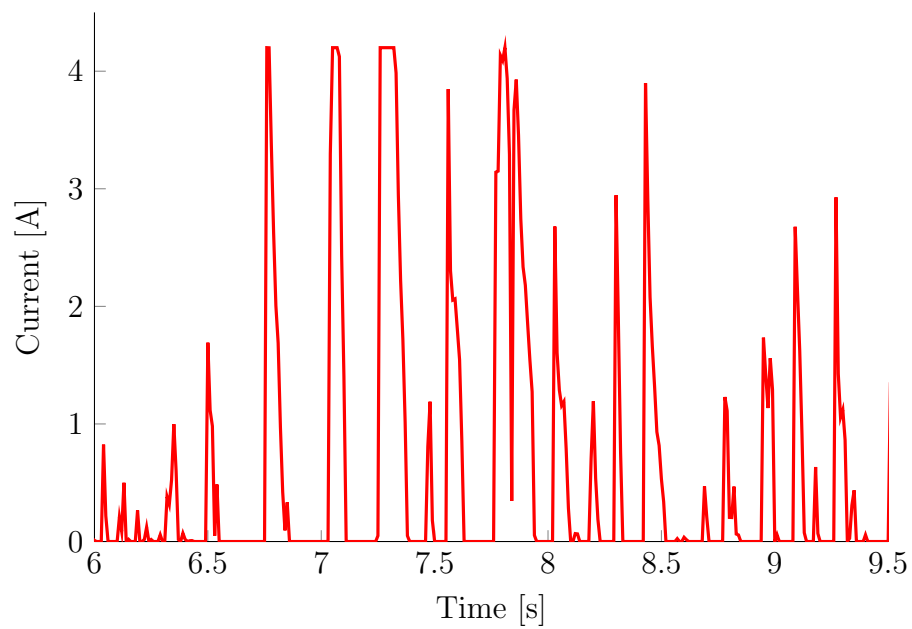


(b) Variation of dynamic tire force with time

Figure 5.10: Test results for over a bump at speed 40 km/h (*cont.*)



(c) Variation of adaptation parameters with time



(d) Variation of current with time

Figure 5.10: Test results for over a bump at speed 40 km/h

force as well as the suspension speed, however, it is somewhat intuitive that reducing the dynamic tire force would require more damping, and hence, more current. Therefore, some saturated current peaks can be seen concurrent with the peaks in α .

Table 5.1: Summary of test results comparing different controllers

	Passive	Skyhook	Groundhook	Adaptive
Smooth to rough road				
$\ddot{z}_{s,RMS}$ ($t=1$ s to $t=17$ s) [m/s ²]	1.76	1.67	1.860	1.65
% change in $\ddot{z}_{s,RMS}$	-	-5.00%	5.74%	-6.14%
$F_{tire,RMS}$ ($t=1$ s to $t=17$ s) [N]	1806	1871	1686	1543
% change in $F_{tire,RMS}$	-	3.6%	-6.64%	-14.56%
Bump profile				
$\ddot{z}_{s,RMS}$ ($t=6$ s to $t=9.5$ s) [m/s ²]	3.6319	3.4246	3.9171	3.1534
% change in $\ddot{z}_{s,RMS}$	-	-5.71%	7.85%	-7.75%
$F_{tire,RMS}$ ($t=6$ s to $t=9.5$ s) [N]	2034	2169	1902	1825
% change in $F_{tire,RMS}$	-	6.66%	-6.49%	-10.27%

A summary of the test results has been presented in Table 5.1. RMS values are calculated over the time duration of interest, i.e., the time during which the controllers were actively involved and the test conditions (basically vehicle’s forward speed) were consistent throughout the four runs. For the first scenario of smooth/rough road patch, this time is 16 s while for the bump, it is much shorter at 3.5 s. Assuming the performance with passive system as the baseline, percentage changes in RMS values are calculated for the three controllers. It can be seen that the adaptive controller improves comfort by 6-7% and handling by 10-15%. Although the improvement in comfort by skyhook controller is also of the same order, it worsens the handling by almost the same amount. Similar is the case with groundhook controller, where it degrades comfort by almost the same amount by which it improves handling, which is around 6%.

This concludes the crux of this work. The next chapter will summarize the conclusions which can be derived from this research and recommendations for future work.

Chapter 6

Conclusions and Future Work

An ideal inerter offers some improvement in suspension performance, but depends on the configuration in which it is connected to spring(s) and a damper. Different designs of mechanical circuits demonstrate different amount of improvement. Apart from the circuit design, the static stiffness of the suspension system plays a major role in deciding the end result. For softer stiffnesses like those in passenger cars, there exists a configuration consisting of an extra spring in series with a parallel arrangement of a damper and an inerter where the values of these components can be optimized so as to obtain simultaneous decrement in the acceleration of the sprung mass (better comfort) and the dynamic tire force (better handling and safety). For stiffer systems which are characteristic of sports cars, a series combination of a second spring, damper and an inerter in parallel with the main spring should be able to provide better handling as well as comfort. The exact amount by which the suspension performance improves depends on the parameters of the quarter car model like the sprung mass, the unsprung mass and the tire stiffness. but the numbers generally lie in the range of 5-10% (compared to a system with a single damper optimized for the same criterion).

Since a passive suspension with multiple springs, inerters and dampers becomes quite complex and bulky for practical and economic implementation, one potential solution is to use a linear motor with a shunt impedance consisting of multiple inductors, capacitors and resistors; the mechanical-electrical analogy promises the exact same results. This offers many potential advantages like low weight for complex circuits, scope of adaptive suspension system by using variable impedance and an appropriate control algorithm, and power regeneration. However, obtaining an ideal linear motor with no internal resistance and inductance is certainly impossible. Even if a real linear motor is used, it is impractical because of its huge cost and weight and low energy density. Alternately, a cheaper rotary motor with higher energy density can be used with a mechanism like a ball-screw and nut to convert the linear motion of the suspension to the motor's rotary motion. However, the

inertia of the rotor and impedance of its coils have a huge effect on the optimization results previously obtained for an ideal, mechanical case. It was observed that the design was not practically beneficial anymore for low static stiffness suspensions of passenger cars but for suspensions with higher stiffness, this design showed quite good results.

An adaptive control algorithm which makes the best compromise between comfort and handling on-the-run was worth development, whether to be used on a mechatronic strut with variable impedance or a suspension with simple MR damper. Hence, a controller was designed for active/semi-active suspension systems which had a weighting parameter $\alpha \in [0, 1]$ such that at one end ($\alpha = 0$), the controller outputs a force which provides maximum comfort while at the other end ($\alpha = 1$), it is purely handling oriented. For semi-active systems, the force is set to be zero whenever it violates the passivity constraint, i.e., power needs to be injected. The weighting parameter α is adjusted online depending on the value of the dynamic tire force, both RMS and absolute. The controller is practically economical to implement as it only uses sensors to measure the acceleration of the sprung mass and the suspension travel. All other variables of interest are estimated from these two measurements. Simulations were performed for a smooth to rough transitional road profile and a bump as input from the ground. While the skyhook controller led to very high dynamic tire force and the groundhook controller was not good in providing comfort, the proposed adaptive controller demonstrated a performance better than the passive system for both the criteria and both driving scenarios.

Experimental validation was done on one corner (front-left) of a fully instrumented Cadillac STS equipped with MR dampers. First the estimator for the dynamic tire force was tested and was found to provide values practically comparable with the actual force measured by a sophisticated wheel load sensor. Then, the MR damper was characterized as a 3-dimensional map relating suspension speed, input current and damping force, which was also estimated. Finally, the proposed adaptive controller was implemented, along with skyhook, groundhook and emulated passive (constant current), and tested on road conditions quite similar to those in simulations: at 45 km/h on a road with smooth to rough transition and over a road bump at 40 km/h. For both the cases, the controller could adapt itself to the driving conditions and provided ride comfort and handling better or similar to the skyhook and groundhook controller respectively.

After the proof of concept on a single corner of the vehicle, it would be worthwhile to implement the controller on all four corners of the vehicle. For better results, the controller structure would need to be modified for a 7-dof full-car model (like the one shown in Figure 6.1) from a 2-dof quarter-car one. As the sprung mass in this model will have three degrees of freedom, i.e., roll, pitch and vertical heave, the controller can also be modified to take into account roll and pitch stability of the vehicle during harsh cornering

and accelerating (or decelerating) maneuvers respectively. More sophisticated estimator like EKF can also be incorporated in the controller for better results.

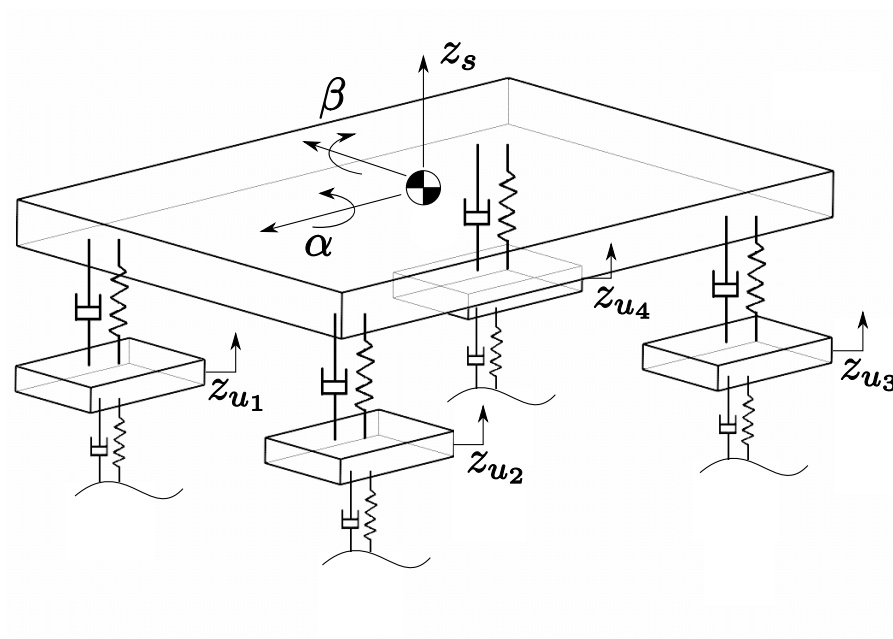


Figure 6.1: Seven degree of freedom full car model

References

- [1] ISO 2631-1:1997. Mechanical vibration and shock-evaluation of human exposure to whole-body vibration. *International Organization for Standardization, Geneva, Switzerland, Tech. Rep.*, 1997.
- [2] ISO 8608:1995. Mechanical vibration-road surface profiles: Reporting of measured data. *International Organization for Standardization, Geneva, Switzerland, Tech. Rep.*, 1995.
- [3] W.B. Adams. *English Pleasure Carriages*. C. Knight & co., 1837.
- [4] M. Biglarbegan, W. Melek, and F. Golnaraghi. A novel neuro-fuzzy controller to enhance the performance of vehicle semi-active suspension systems. *Vehicle System Dynamics*, 46(8):691–711, 2008.
- [5] BMW. Dynamic Drive. http://www.bmw.com/com/en/newvehicles/6series/coupe/2007/allfacts/engine_dynamicdrive.html.
- [6] BMW. 7-Series. <http://www.caranddriver.com/photos-08q4/231910/2009-bmw-7-series-suspension-controls-photo-231927>, 2009.
- [7] H. Bolandhemmat, C. M. Clark, and F. Golnaraghi. Development of a systematic and practical methodology for the design of vehicles semi-active suspension control system. *Vehicle System Dynamics*, 48(5):567–585, 2010.
- [8] Bose Corporation. Bose Suspension System. http://www.bose.com/controller?url=/automotive/bose_suspension/the_system.jsp.
- [9] R. Bott and R. J. Duffin. Impedance synthesis without use of transformers. *Journal of Applied Physics*, 20(8):816–816, 1949.
- [10] O. Brune. Synthesis of a finite two-terminal network whose drivingpoint impedance is a prescribed function of frequency. *Journal of Mathematical Physics*, 10:191–236, 1931.

- [11] BWI Group. Magneride. <http://www.bwigroup.com/en/pshow.php?pid=22>.
- [12] M.Z.Q. Chen, C. Papageorgiou, F. Scheibe, Fu cheng Wang, and M.C. Smith. The missing mechanical circuit element. *Circuits and Systems Magazine, IEEE*, 9(1):10–26, quarter 2009.
- [13] Daimler AG. Active Body Control. <http://www.cubiccapacity.com/wp-content/uploads/2008/12/prescan2.JPG>.
- [14] S. Darlington. Synthesis of reactance 4-poles which produce prescribed insertion loss characteristics. *Journal of Mathematical Physics*, 10:257–353, 1931.
- [15] J. De Jesus Lozoya-Santos, R. Morales-Menendez, J.C. Tudn-Martnez, O. Sename, L. Dugard, and R. Ramirez-Mendoza. Control strategies for an automotive suspension with an mr damper. volume 18, pages 1820–1825, 2011.
- [16] F1-Technical. J-Dampers in Formula One. <http://www.f1technical.net/features/10586>.
- [17] I. J. Fialho and G. J. Balas. Design of nonlinear controllers for active vehicle suspensions using parameter-varying control synthesis. *Vehicle System Dynamics*, 33(5):351–370, 2000.
- [18] F. A. Firestone. A new analogy between mechanical and electrical systems. *The Journal of the Acoustical Society of America*, 4(3):249–267, 1933.
- [19] Google Maps. Region of Waterloo Emergency Services Training Area Satellite Image. <http://www.maps.google.com>.
- [20] B.L.J. Gysen, T.P.J. van der Sande, J.J.H. Paulides, and E.A. Lomonova. Efficiency of a regenerative direct-drive electromagnetic active suspension. *Vehicular Technology, IEEE Transactions on*, 60(4):1384–1393, may 2011.
- [21] J K Hedrick and T Butsuen. Invariant properties of automotive suspensions. *Proceedings of the Institution of Mechanical Engineers, Part D: Journal of Automobile Engineering*, 204(1):21–27, 1990.
- [22] W.D. Jones. Easy ride: Bose corp. uses speaker technology to give cars adaptive suspension. *Spectrum, IEEE*, 42(5):12–14, may 2005.
- [23] Dean Karnopp. Theoretical limiations in active vehicle suspensions. *Vehicle System Dynamics*, 15(1):41–54, 1986.

- [24] Dean Karnopp. How significant are transfer function relations and invariant points for a quarter car suspension model? *Vehicle System Dynamics*, 47(4):457–464, 2009.
- [25] Guido Koch, KlausJ. Diepold, and Boris Lohmann. Multi-objective road adaptive control of an active suspension system. In Heinz Ulbrich and Lucas Ginzinger, editors, *Motion and Vibration Control*, pages 189–200. Springer Netherlands, 2009.
- [26] Zhongjie Li, Zachary Brindak, and Lei Zuo. Modeling of an electromagnetic vibration energy harvester with motion magnification. *ASME Conference Proceedings*, 2011(54938):285–293, 2011.
- [27] H. Liu, K. Nonami, and T. Hagiwara. Active following fuzzy output feedback sliding mode control of real-vehicle semi-active suspensions. *Journal of Sound and Vibration*, 314(1-2):39–52, 2008.
- [28] Racer. Spring rate. <http://www.racer.nl/tutorial/suspensions.htm#suspspring>.
- [29] S. Rakheja and S. Sankar. Vibration and shock isolation performance of a semi-active 'on-off' damper. In *American Society of Mechanical Engineers (Paper)*, 1985.
- [30] SAE. Sign convention for vehicle crash testing. *Society of Automotive Engineers, US*, 1994.
- [31] Brian Scully, Lei Zuo, Jurgen Shestani, and Yu Zhou. Design and characterization of an electromagnetic energy harvester for vehicle suspensions. *ASME Conference Proceedings*, 2009(43833):1007–1016, 2009.
- [32] Y. Shen, M. F. Golnaraghi, and G. R. Heppler. Semi-active vibration control schemes for suspension systems using magnetorheological dampers. *JVC/Journal of Vibration and Control*, 12(1):3–24, 2006.
- [33] Malcolm C. Smith and Fu-Cheng Wang. Performance benefits in passive vehicle suspensions employing inerters. *Vehicle System Dynamics*, 42(4):235–257, 2004.
- [34] Malcolm Clive SMITH. Force-controlling mechanical device. Patent, 01 2008. US 7316303.
- [35] M.C. Smith. Synthesis of mechanical networks: the inerter. *Automatic Control, IEEE Transactions on*, 47(10):1648 – 1662, oct 2002.
- [36] M. Strassberger and J. Guldner. Bmw's dynamic drive: an active stabilizer bar system. *Control Systems, IEEE*, 24(4):28 – 29, 107, aug. 2004.

- [37] H. E. Tseng and J. K. Hedrick. Semi-active control laws - optimal and sub-optimal. *Vehicle System Dynamics*, 23(7):545–569, 1994.
- [38] M. Valek, M. Novk, Z. ika, and O. Vaculn. Extended ground-hook - new concept of semi-active control of truck’s suspension. *Vehicle System Dynamics*, 27(5-6):289–303, 1997.
- [39] P. J. T. Venhovens. Development and implementation of adaptive semi-active suspension control. *Vehicle System Dynamics*, 23(3):211–235, 1994.
- [40] F.-C. Wang and H.-A. Chan. Vehicle suspensions with a mechatronic network strut. *Vehicle System Dynamics*, 49(5):811–830, 2011. cited By (since 1996) 2.
- [41] Fu-Cheng Wang and Hsiang-An Chan. Mechatronic suspension design and its applications to vehicle suspension control. In *Decision and Control, 2008. CDC 2008. 47th IEEE Conference on*, pages 3769 –3774, dec. 2008.
- [42] J.Y. Wong. *Theory of Ground Vehicles*. John Wiley & Sons, 2008.
- [43] ZF Friedrichshafen AG. Continuous Damping Control. http://www.zf.com/corporate/en/products/product_range/cars/cars_cdc.shtml.